Bahar BİRSÖZ

M.S. Thesis In Chemistry

January - 2007

SYNTHESIS AND CHARACTERIZATION OF METAL BOROPHOSPHATE-BOROARSENATE COMPOUNDS

by

Bahar BİRSÖZ

January 2007

SYNTHESIS AND CHARACTERIZATION OF METAL BOROPHOSPHATE-BOROARSENATE COMPOUNDS

by

Bahar BİRSÖZ

A thesis submitted to

the Graduate Institute of Sciences and Engineering

of

Fatih University

in partial fulfillment of the requirements for the degree of

Master of Science

in

Chemistry

January 2007

Istanbul, Turkey

..

APPROVAL PAGE

I certify that this thesis satisfies all the requirements as a thesis for the degree of Master of Science.

Assist. Prof. Dr. Metin TÜLÜ
Head of Department

This is to certify that I have read this thesis and that in my opinion it is fully adequate, in scope and quality, as a thesis for the degree of Master of Science.

Assist. Prof. Dr. Abdülhadi BAYKAL
Supervisor

Examining Committee Members

Assoc.Prof. Dr. Ayhan BOZKURT ……..

Assist. Prof. Dr. Abdülhadi BAYKAL ……..

Assist. Prof. Dr. Omar ALAGHA ……..

It is approved that this thesis has been written in compliance with the formatting rules laid down by the Graduate Institute of Sciences and Engineering.

Assist. Prof. Dr. Nurullah ARSLAN

Director

**SYNTHESIS AND CHARACTERIZATION
OF
METAL BOROPHOSPHATE-BOROARSENATE COMPOUNDS**

Bahar BİRSÖZ

M. S. Thesis - Chemistry
January 2007

Supervisor: Assist. Prof. Dr. Abdülhadi BAYKAL

ABSTRACT

The solid state, hydrothermal, micro-wave assisted methods (autoclave and glass ampoule) were used in the synthesis of transition metal borophosphate and boroarsenate compounds. The products were investigated by XRD, FTIR, ICP, TGA, ESR and SEM methods. The solid state reactions of several boron compounds with a phosphating / arsenating agent has been studied in the range 500 – 1200 ^{o}C.

$Fe_2[BP_3O_{12}]$ was synthesized successfully by solid state method and found to be isostructural with $Ba_3[BP_3O_{12}]$ which crystallize in the orthorhombic system. The unit cell parameters were found to be as a= 8.0805 and c= 7.4244 Å.

$(NH_4)_xM_{((3-x)/2)}(H_2O)_2[BP_2O_8].(1-x)H_2O$ (x = 0.5), where M = Mn and Co which is isostructural with the reported $NH_4Cd(H_2O)_2(BP_2O_8).0.72H_2O$, $LiCd(H_2O)_2[BP_2O_8].H_2O$, $Fe(H_2O)_2BP_2O_8.H_2O$, $Sc(H_2O)_2[BP_2O_8].H_2O$ was also synthesized successfully by hydrothermal method and indexed in the hexagonal crystal system. The unit cell

parameters were found to be as a=9.5104, c=15.7108 Å and a=9.4920, c=15.5820 Å respectively.

Using hydrothermal method $(H)_{0.5}Co_{1.25}(H_2O)_{1.5}[BP_2O_8].H_2O$ compound was also prepared successfully and indexed depending on the unit cell parameters given in the literature.

Na–M-As–B–O containing compound where M = Mn, Co, Zn and Al–As–B–O containing compound was tried to be synthesized. But their crystal structure investigation and characterization studies were not successful due to the powder form of products.

All the compounds prepared have been investigated by FTIR spectroscopy and the assignment of the functional BO_3, BO_4, AsO_4 and PO_4 groups were done.

Keywords: Borophosphate Compounds, Boroarsenate Compounds, Transition Metal Borophosphate Compounds, FTIR and X-ray Powder Diffraction, Hydrothermal Method, Micro-wave Method, Solid State Synthesis.

METAL BOROFOSFAT VE BOROARSENAT BİLEŞİKLERİNİN SENTEZİ VE KARAKTERİZASYONU

Bahar BİRSÖZ

Yüksek Lisans Tezi - Kimya
Ocak 2007

Tez Yöneticisi: Yrd. Doç. Dr. Abdülhadi BAYKAL

ÖZ

Geçiş metal borofosfat ve boroarsenat bileşiklerinin sentezi; katı hal, hidrotermal (otoklav ve cam ampül) ve mikrodalga metodları kullanılarak gerçekleştirilmiştir. Ürünlerin karakterizasyonu XRD, FTIR, ICP, TGA, ESR ve SEM metotları kullanılarak yapılmıştır. Bazı bor bileşiklerinin fosfatlama ve arsenatlama araçları ile gerçekleştirilen katı hal reaksiyonları 500 – 1200 ^{o}C arasında gerçekleştirilmiştir.

Bu çalışmada $Fe_2[BP_3O_{12}]$ başarıyla sentezlenmiş ve ortorombik yapıda kristallenen $Ba_3[BP_3O_{12}]$ ile aynı yapıda olduğu ispatlanmıştır. Birim hücre parametreleri a= 8.0805 and c= 7.4244 Å olarak hesaplanmıştır.

$NH_4Cd(H_2O)_2(BP_2O_8).0.72H_2O$, $LiCd(H_2O)_2[BP_2O_8].H_2O$, $(H)_{0.5}Co_{1.25}(H_2O)_{1.5}[BP_2O_8].H_2O$, $Fe(H_2O)_2BP_2O_8.H_2O$, $Sc(H_2O)_2[BP_2O_8].H_2O$ ile aynı yapıda olan $(NH_4)_xM_{((3-x)/2)}(H_2O)_2[BP_2O_8].(1-x)H_2O$ (x = 0.5), M = Mn ve Co sentezi de hidrotermal metotla kullanılarak gerçekleştirilmiş ve hegzagonal kristal yapısına gore

indekslenmiştir. Birim hücre parametreleri; sırasıyla, a=9.5104, c=15.7108 Å ve a=9.4920, c=15.5820 Å olarak hesaplanmıştır.

Hidrotermal metot yöntemiyle $(H)_{0.5}Co_{1.25}(H_2O)_{1.5}[BP_2O_8].H_2O$ bileşiği başarıyla sentezlenmiş ve birim hücre parametreleri kullanılarak indekslenmiştir.

Na–M-As–B–O içeren (M = Mn, Co, Zn) ve Al–As–B–O içeren bileşiklerin sentezi çalışılmıştır. Fakat ürünün toz olmasından dolayı kristal yapısının araştırmaları ve karakterizasyon çalışmaları başarılı olmamıştır.

Elde edilen bütün bileşiklerin araştırması FTIR spektroskopisi kullanılarak BO_3, BO_4, AsO_4 ve PO_4 fonksiyonel gruplarının analizi yapılmıştır.

Anahtar Kelimeler: Borofosfat Bileşikleri, Boroarsenat Bileşikleri, Geçiş Metal Borofosfat Bileşikleri, FTIR ve X-ışınları Toz Difraktomu, Hidrotermal Sentez, Mikrodalga Sentez, Katı Hal Sentez

Dedicated to my parents.

ACKNOWLEDGEMENT

I would like to express my gratitude to my supervisor Assist. Prof. Dr. Abdülhadi BAYKAL whose help, stimulating suggestions and encouragement helped me during the course of research and writing of this thesis.

I also want to express my thanks to Asst. Prof. Dr. Muhammed S. TOPRAK for his help during SEM, TGA, ICP analysis of my compounds in Royal Institute of Technology in Sweden, Prof. Dr. Mehmet SOMER from KOÇ University for his help during XRD measurements and Prof. Dr. Bekir AKTAŞ from Gebze Institute of Technology for ESR measurements.

I express my thanks and appreciation to my family for their understanding, motivation and patience. Lastly, but in no sense the least, I am very grateful to all colleagues and friends in Fatih University for their suggestions and helpful discussions also special thanks to Nermin KASAPOĞLU and Mehmet ŞENEL, who made me stay at the university a memorable and valuable experience.

TABLE OF CONTENTS

LIST OF FIGURES

LIST OF TABLES

CHAPTER 1

INTRODUCTION

1.1 THE CHEMISTRY OF BORON

The boron atom has the electron configuration: $1s^2$, $2s^2$, $2p^1$ and is placed in Group III of the Periodic Classification. The chief oxidation state of boron is +3 and the element normally combines with oxygen (of electron configuration $1s^2$, $2s^2$, $2p^4$) to form three triangular-planar bonds by sp^2 orbital hybridization. The boron-oxygen radius ratio is 0.20 and from spatial considerations alone, boron would be expected to occur in three- or fourfold coordination. The transition to tetrahedral sp^3 orbital hybridization is facilitated by the easy acceptance of an electron-pair from a base into the low-energy fourth orbital of the boron valence shell.

The elemental form of boron is unstable in nature; boron is found combined with oxygen in a wide variety of hydrated alkali and alkaline earth-borate salts and borosilicates. Boric acid, derived from weathered rocks or volcanic activity, is eventually incorporated into marine sediments. Even though the most abundant boron-containing mineral is the borosilicate toumaline, deposited during granitic crystallization, the bulk of commercial boron is obtained from minerals concentrated by the evaporation of salt lakes [1].

An important use of boron is to make boron steel or boron carbide control rods for nuclear reactors. Boron has a very high cross-section for capturing neutrons. Control rods made of boron steel or boron carbide may be lowered into a reactor to absorb neutrons and thus slow the reactor down. Boron carbide is also used as an abrasive. Boron is used to make impact resistant steel, as it increases the hardenability of steel [2]. The fifth element in the periodic table, boron, is receiving quite a bit of attention in the world of medicine for the treatment of tumors. Boron is an element

that can be irradiated with neutrons to release high-energy alpha particles and gamma rays that can destroy tumor cells.

Boron has been used as far back in history as early Egypt. Mummification was a regular practice for the burial of the deceased. Mummification depended upon an ore known as natron, which contained borates as well as some other common salts. Natron was a highly prized substance and was very expensive. Boron was also used for welding in China and glassmaking in ancient Rome. Boron minerals were discovered in Southern California about 1869.

Boron likes to combine with oxygen to form several different compounds. One element over from boron is carbon which, like boron, also likes to combine with oxygen to form compounds such as carbon dioxide. However, carbon also likes to combine with hydrogen to form hydrocarbons for fuels such as gasoline. In nature there is no known combination of boron and hydrogen. In 1910, Alfred Stock, began working on combining boron and hydrogen to make boron-hydrides and he succeeded. However, these compounds were very expensive and very reactive. It was not until the U.S. Army began research on boron-hydrides as a possible rocket fuel that this research proved to be useful. This research continued until 1948 when the research facility was washed out with carbon tetrachloride, not realizing that carbon tetrachloride and decaborane form an explosive mixture similar to nitroglycerine and the plant was blown away. Current stockpiles of pentaborane (B_5H_9) and decaborane ($B_{10}H_{18}$) are being destroyed because these compounds are powerful central nervous system toxins.

Boron is being used today for the treatment of tumors. Boron has two isotopes, boron-10 and boron-11 (Figure 1.1). Boron-10 is the only light element with an extremely high propensity to bind with a slow moving neutron. These slow neutrons are referred to as thermal neutrons. When boron-10 picks up this thermal neutron it becomes a high-energy boron-11. This boron-11 nucleus is quite unstable, so it fissions or blows up releasing two heavy particles, a lithium-7 nucleus and a helium-4 nucleus plus a gamma photon. The heavy lithium-7 and helium-4 nuclei exit at a very high speed making them very deadly to the cell they originated in. If researchers could selectively incorporate boron-10 into cancer cells, they could then irradiate the patient with thermal neutrons. The destruction of tissue would be localized to only the

cancerous cells, since they are the only ones that contain boron-10. The BNC (boron neutron capture) would kill the targeted tumor cells and the body could heal itself, replacing the dead tumor tissue with normal tissue (Figure 1.2). The attractive part of this treatment is that the length of travel of the lithium and helium ions produced from BNC is only about one cell thick. Due to their weight and energy, they virtually tear the cell to pieces, but the damage ends there.

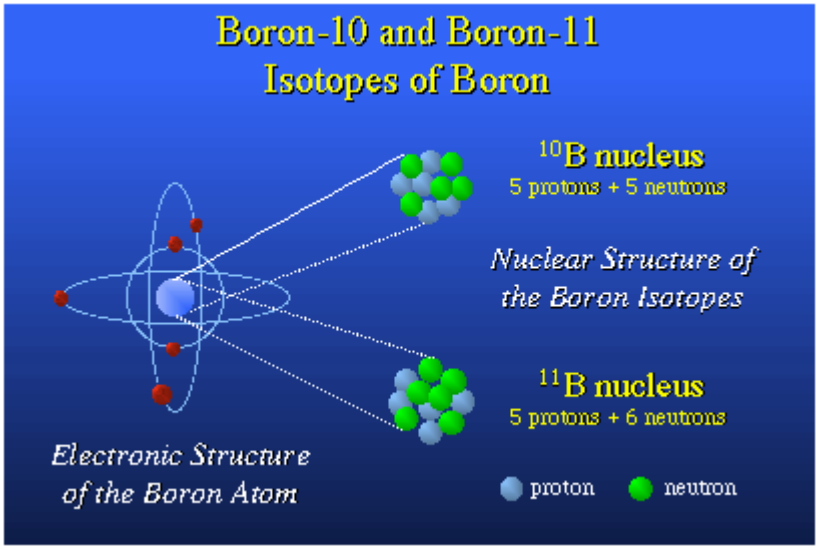

Figure 1.1 Electronic structure of the boron atom [3].

This therapy is being studied as a treatment for glioblastoma multiform, a very deadly brain cancer. Researchers are also looking at BNCT for treatment of lung and prostate cancer (Figure 1.3) [3].

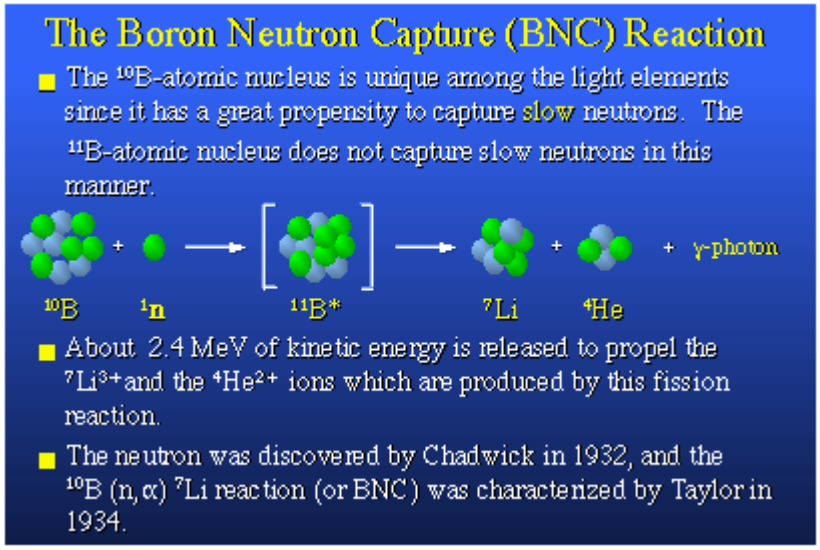

Figure 1.2 Boron neutron capture reaction [3].

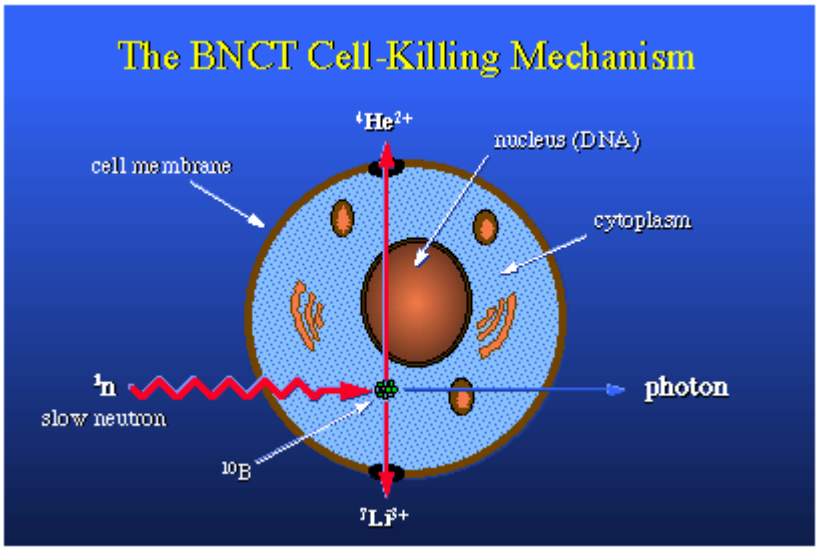

Figure 1.3 BNCT cell-killing mechanism [3].

1.1.1 Boron Oxygen Chemistry

Boron, a non-metallic element of low general abundance's, has little in common with the other elements of Group III. Being the most electronegative element of the group, it resembles in general the non-metals, particularly silicon, far more than aluminum and the metals of A and B subgroups. Boron, like silicon, occurs in nature exclusively as oxy-compounds, particularly hydroxyborates of calcium and sodium with the formula of; $Na_2B_2O_5(OH)_4.8H_2O$ (borax). The borate ion, $[B(OH)_4]^{1-}$, is found in ocean [4].

In borates based exclusively on BO_3 coordination groups there would be a simple relation between the O : B ratio and the number of O atoms shared by each BO_3 group, assuming these to be equivalent and each bonded to 2B atoms as shown in Table 1.1.

Table 1.1 Different types of borates [5].

O:B ratio		Number of O atoms shared
3	Orthoborate: discrete BO_3^{3-} ions	0
2½	Pyroborates: discrete $B_2O_5^{4-}$ ions	1
2	Metaborates: cyclic or chain ions	2
1½	Boron trioxide	3

All of the above four possibilities are realized in compounds in which B exclusively 3-coordinated (n = 3), but there are two factors which complicate the oxygen chemistry of boron. First, there is tetrahedral coordination of B in many oxy-compounds, either exclusively or admixed with 3-coordination in the same compound. Therefore, there is no simple relation between O : B ratios and the structures of borates. Second, there are many hydroxyborates containing OH bonded to B as part of 3- or 4-coordination group.

To explain the bonding chemistry and to classify the structures of other solid borate compounds the following statements are considered [1].

1) **a)** In borates, boron is observed to exist in threefold (tri-angular- planar) and four-fold (tetrahedral) coordination by oxygen.

   b) The ratio of tetrahedral boron to total boron is equivalent to the ratio of cation charge to total boron. The postulates are exact for the majority of hydrated borates; a few high-temperatures phases are exceptions.

2) The crystalline borates are monomeric or polymeric. The existence of monomers, dimers, trimers, tetramers, pentamers, and polydimensional networks (including glasses) has been indicated.

3) In the higher crystalline polyborates, the basic structure is a six-atom ring with alternate boron oxygen atoms (Figure 1.4). Structures for the vast majority of the higher crystalline polyborates appear to have the configuration as an integral part of the polymer. Also, the predominant polymeric species in dilute borate solutions is a trimer probably consistent with the ring structure below;

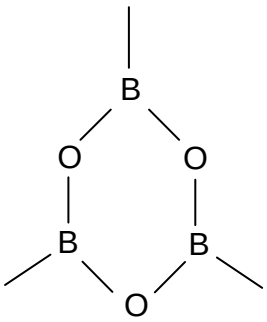

Figure 1.4 Structure with six-atom ring with alternate boron and oxygen atoms [1].

   a) The rings may contain zero, one, two or possibly three tetrahedral boron atoms. Rings with one or two tetrahedral borons are particularly common under hydrating conditions and appear to have some special chemical stability.

   b) The trimeric rings may be broken at the tetrahedral boron atoms to form higher polyanions, for example, the tetramer and pentamer.

   c) The resultant polyanions may be linked by shared oxygen atoms to form chains, sheets, or three-dimensional networks.

4) Miscellaneous borates, including some rare or synthetic species, have their structural equivalent in other chemical systems, which are analogs of the carbonates and silicates. A few gaseous borate species uniquely exhibit twofold boron-oxygen coordination [1,5,6].

Compounds containing monomeric triangular, BO_3 units are rare-earth orthoborates $M^{III}BO_3$. Binuclear trigonal planar units are found in the pyroborates $[B_2O_5]^{4-}$. Trinuclear cyclic units occur in the metaborates, $[B_3O_6]^{3-}$. Monomeric tetrahedral $[BO_4]^{5-}$ units are found in the Zr-type compounds and in the minerals.
Units containing B in planar BO_3 coordination, units of containing B in tetrahedral BO_4 coordination and units containing B in both BO_3 and BO_4 coordination are given in the following section [1].

1.2 THE CHEMISTRY OF BOROPHOSPHATES

The crystal chemistry of borophosphates exhibits a larger variety, compared with purely tetrahedral structures, because boron can be either three (trigonal-planar) or four (tetrahedral) coordinated by oxygen, and that the BO_3 and PO_4 tetrahedra share corners and build infinite chain and network. A first approach to the development of a structural chemistry of borophosphates was done based on linking principles of the primary building units following the general line of silicate crystal chemistry [7-8]. The studies on the synthesis and structural characterization of metal borophosphates show that borophosphates have a rich structural chemistry with a large variety in their anionic $[B_xPyOz]^{n-}$ structural building blocks [9].

The crystal structures of borophosphates are first divided into anhydrous and hydrated phases. Further gradings are based on the (molar) B:P ratios [7]. The anion groups in these compounds should be large enough to separate active ions, in order to reduce the concentration quenching behavior caused by the ion-ion interactions. Therefore, the work of exploring and investigating new earth compounds consisting of large anion groups such as BO_3, PO_4, or BO_4 must be significance [10].

Today, the structural chemistry of borophosphate anions already extends from isolated species, oligomers, rings, and chains to layers and frameworks. The existing minority of compounds containing isolated borate besides isolated phosphate structural units are regarded as borophosphates as well, although they actually have to be classified as borate-phosphates. But this distinction is not pursued any further. Hydrated borophosphates with a molar ratio B:P>1 have the chain anions contain boron in a 3-

fold and in a tetrahedral coordination. BO_3 groups are exclusively linked to borate species. Terminal (non-bridging) oxygen positions of the BO_3 groups are always protonated. All the corners of BO_4 tetrahedra share common corners with neighboring units within the chains. The crystal structure of $K_3[B_5PO_{10}(OH)_3]$ (B:P=5) contains a central tetrahedral borate chain which is loop-branched by single $BO_2(OH)$ and $PO_3(OH)$ groups with the sequence B ── B ── P along the chain. Hydrated borophosphates with a molar ratio B:P=1 and B:P<1 are exclusively built of borate and phosphate tetrahedra and do not contain boron in a triangul planar coordination [7].

Borophosphate compounds with 3D tetrahedral open-framework structures are difficult to synthesize. Sevov reported first metal borophosphate ($CoB_2P_3O_{12}(OH).C_2H_{10}N_2$) with an open framework structure [11]. Bontchev reported a few organically templated vanadium borophosphates with cluster anions [12-13]. The first tetrahedral framework structural borophosphate compounds are $K[ZnBP_2O_8]$ and A[ZnBP$_2$O8] (A=NH_4^+, Rb^+, Cs^+] published by Kniep's group [14].

The crystal structure of α-$Zn_3[BPO_7]$ (≡$Zn_3[(BO_3)(PO_4)]$) contains isolated planar BO_3 groups and PO_4 tetrahedra. Trigonal planar borate groups sharing one common oxygen atom with a phosphate tetrahedron as well as isolated phosphate tetrahedral are present in the crystal structure of $Co_5[BP_3O_{14}]$ (≡$Co_5[(BPO_6)(PO_4)_2]$) [7].

1.2.1 The Synthesis of Borophosphates

Borophosphates can be synthesized under mild hydrothermal conditions using common starting materials. Other less frequently used preparation methods are high temperature (solid state) and microwave methods [7]. One of the reason of the preparing new compound combining both borate and phosphate groups is the best known materials with optical and electro-optical applications are either borates or phosphates such as BBO (β-BaB_2O_4), KDP (KH_2PO_4), etc. [14]. $NH_4Cd(H_2O)_2(BP_2O_8).0.72H_2O$ [15], $\{(NH_4)_{0.5}Co_{1.25}\}(H_2O)_2(BP_2O_8).0.5H_2O$ [16], $LiCd(H_2O)_2[BP_2O_8].H_2O$ [17], $(H)_{0.5}M_{1.25}(H_2O)_{1.5}[BP_2O_8].H_2O$ (M = Co(II) and Mn(II)) [14] , $LiBaB_9O_{15}$, $BaBPO_5$ [18] are the examples of compounds that were synthesized by hydrothermal method. $CaBPO_5$ was synthesized by high temperature method [19].

1.2.2 The Importance of Borophosphates

There has been intense research activity in the area of inorganic open-framework materials in the past few years. These materials are of technological importance as shape-selective catalysts and ion exchange materials and are widely used in various industrial and technological processes. BPO_4 itself is a catalyst used industrially for many reactions including hydration, dehydration, alkylation, and oligomerization [14]. BPO_4 itself is a good catalyst (100% conversion) for the decomposition of CCl_2F_2 (Freon 12) which is a known killer of the ozone layer [20-22]. BPO_4 is, therefore, a very promising catalyst for fluorine-containing compounds because of its durability towards fluorine due to its nonmetalic character [23]. Thus, considerable efforts have been made towards the design and synthesis of open-framework borophosphates [24-31] but only a few such structures have been found to date [32-33]. Substitution of some oxygen atoms with fluorine led to the first fluoro-boro-phosphate $(C_2H_{10}N_2)[BPO_4F_2]$, a compound with infinite chains of $[BPO_4F_2]$ separated by the protonated organic templates [34].

In addition to these applications, borophosphate compounds are also used in polymer chemistry. The Zaidi's study is an attempt to improve the performance of the sullfonated polyether-ether ketone / polybenzimidazole (SPEEK/PBI) blend membranes by introducing the inorganic proton conducting material, BPO_4. According to Zaidi's study BPO_4 under certain conditions reveals the properties of a proton conductor and have a proton conductivity 6×10^{-2} S/cm at room temperature under full humidification. Another interesting feature of BPO_4 is that it can retain water at high temperature. The composite membranes were prepared from SPEEK/PBI blend suspension and boron phosphate, and their conductivity was monitored by impedance spectroscopy as a function of PBI content for the blend and BPO_4 loading for composite membranes respectively [35].

1.3 ARSENATES

Arsenate (AsO_4^{3-}) is a predominant species of As in toxic waters, sediments, and hydrothermal fluids. With the exception of weathered profiles containing As sulfides (or As substituted pyrites), the low natural abundances of arsenate does not allow its formation as a pure mineral, and hence As commonly occurs as adsorbed species on sediment or soil minerals such as Fe- and Al-oxyhydroxides. As is a labile element and that changing redox conditions, solution pH, and the presence of organic ligands in the environment modify the adsorbed arsenate speciation, solubility, and dispersion. Vibrational spectroscopy is particularly useful for the examination of in situ coordination of arsenate [36]. Arsenate is a tetrahedral molecule and exhibits four fundamental vibrations, an A_1 (symmetric stretch, υ_1), an E (symmetric bendig υ_2), and two F vibrations (asymmetric stretching & bending, υ_3 & υ_4, respectively). The vibrations E and F are doubly and triply degenerate modes, respectively. Metal complexation of protonates AsO_4^{3-} does not significantly change the AsO_4^{3-} group frequencies [37]. While the vibrational spectroscopy has been widely used in examining the AsO_4^{3-} coordination chemistry, insufficient knowledge on the correlation of AsO_4^{3-} molecular structure and its vibrational spectra impeded the complete spectral interpretation [36].

1.3.1 Arsenate Compounds and Their Applications

Chromated copper arsenate (CCA) is a wood preservative used for timber treatment, in use since 1930's. It is a mix of copper chromate and copper arsenate. It preserves the wood from rotting due to insects and microbes. It is also known under trade name Tanalith. The chromium acts as a bactericide, the copper acts as fungicide, and the arsenate acts as insecticide [38].

Lead arsenate and calcium arsenate are arsenical pesticides used on apple, blueberry, and potato crops [39].

The main uses of arsenicals, as components of pesticides and herbicides, have been banned in many countries. Arsenicals are also used in leather pigments. Chromated copper, sodium, and zinc arsenates are used in antifungal wood

preservatives, and in some places, arsanilic acid is added to farm animal feed as a growth stimulant. Metallic arsenic is used in electronics and as a metal alloy, and sodium arsenite has been included in drugs for treating leukemia and other diseases. Arsenic is also used in lead crystal glass manufacturing, contributing to atmospheric emissions and the generation of highly toxic wastes [40].

1.3.2 Boroarsenates

Framework materials have been extensively studied due to their important applications in areas as diverse as cation exchangers, catalysts, and nonlinear optical materials. Oxotetrahedral frameworks are the most prevalent structures, as exemplified by the large number of zeolite, aluminophosphate, and zincophosphate structures [41-43]. Recently, significant developments of oxotetrahedral frameworks have been made with the synthesis of a generation of structures containing less common units, for example, BO_4, FeO_4, and NiO_4 tetrahedra; these normally occur in association with the more traditional species of SiO_4, AlO_4, and PO_4 [44,45]. In some framework structures, tetrahedra may terminate in oxygen or a protonated oxygen, for example, $NaZnSiO_3OH$ [46] and the dumortierite analogues, $CoCo_6(OH)_3(AsO_4)(AsO_3OH)$ [47]. The quest for structural diversity in framework materials has also led to the use of borate units, with their three- or four-coordinate linking abilities [48-50]. These borate groups in combination with group 15 oxotetrahedra, such as PO_4, can produce building blocks isoelectronic with silicates and lead to analogous structures, for example, the quartz analogue BPO_4 [51], mixed isolated borate and phosphate units, [52-53] chain structures, [54-55] and fully three-dimensional frameworks [7]. In contrast, the area of boroarsenate chemistry has been relatively poorly explored, with very few known examples in the current literature. The minerals Teruggite [$Ca_4Mg(B_6(OH)_6O_8(AsO_3))_2(H_2O)_{14}$] and Cahnite [$Ca_2$-$BAsO_4(OH)_4$], which contains discrete $B(O,OH)_4$ and $As(OH)_4$ tetrahedra, are known, as are a few dense boroarsenates, prepared at high temperature, including $Ba(BAsO_5)$, $Pb(BAsO_5)$, and Pb_6-$AsO_4(B(AsO_4)_4)$. The combination of the unique framework forming behaviors of arsenate (AsO_4-$n(OH)n$) and (fluoro)borate (BO_3, BO_4, BO_3F) has not been studied in any detail up to now. Investigation of these arsenate species provides an opportunity to develop completely new framework types, quite distinct from borophosphates, that can coordinate to anionic species through the proton of the OH unit or hydrogen bond within channels [56,57].

1.4 SYNTHESIS METHODS

1.4.1 Hydrothermal Methods

Hydrothermal method involves heating the reactants in water/steam at high pressures and temperatures. The water has two functions, as a pressure-transmitting medium and a solvent. The method is quite simple; reactants and water are placed inside a teflon – lined cylinderic autoclave (bomb) (home made) (Figure 1.5) which is either sealed or connected to an external pressure control or glass ampoule. The autoclave is then placed in an oven, usually, at a temperature in the range 100 – 500^{o}C.

Hydrothermal route is one of the most used ones, owing to its economics and the high degree of compositional control [55]. In addition, the hydrothermal synthesis requires neither extremely high processing temperature nor sophisticated processing [58].

Hydrothermal synthesis methods have a wide range of applications such as zeolite synthesis (e.g. aluminosilicate) and single crystal synthesis (e.g. quartz) [59].

In addition to these advantages, hydrothermal method requires long period for most of the compound synthesis.

The major difference between hydrothermal processing and the other technologies is that there is no need for high-technologies is that there is no need for high temperature calcination. This eliminates the need for milling. Powders are formed directly from solution by taking advantage of the complex reactions which take place in high-temperature water. By controlling these reactions, it is possible to produce anhydrous crystalline powders with controlled particle size, controlled stoichiometry, and in some cases controlled particle shape [60].

Figure 1.5 Autoclave used in hydrothermal process.

1.4.1.1 What Happens in a Hydrothermal Autoclave?

To understand the behavior of any dense fluid at high pressure, it is first necessary to know how it behaves under various conditions of pressure, volume, and temperature.

The Figure 1.6 below shows the pressure-temperature behaviour of water contained in autoclaves filled to various percentages of fullness. The line A-C is the vapor pressure curve, along which liquid and gas coexist. C is the critical point for water: 374 ^{o}C, 220 bar. At this critical point, the density of both the gas and liquid is 0.32 g/cc.

If an autoclave at room temperature is filled to 80% of its free volume and then heated, the pressure inside will rise as indicated by the vapor pressure curve. The density of the liquid water decreases and the density of water vapor increases as the temperature rises, as shown (at constant pressure) in the Figure 1.7, causing the liquid level in the autoclave to rise until the autoclave is entirely filled with liquid water at 250 ^{o}C. At this point (B in the graph belove), the pressure in the autoclave departs from the vapor pressure curve to rise along curve B-D. The density of the water will be 0.80 g/cc under these conditions. Thus, when the pressure and temperature are such that only

liquid or as is present in the autoclave, the density of the fluid is identical to the initial percent fill divided by 100.

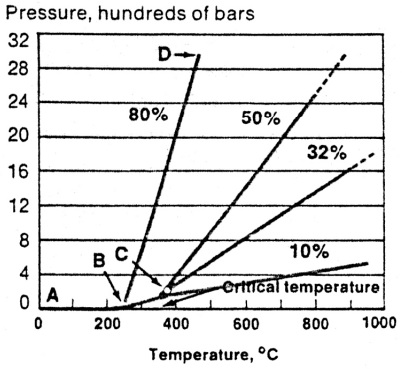

Figure 1.6 Pressure-temperature behavior of water [59].

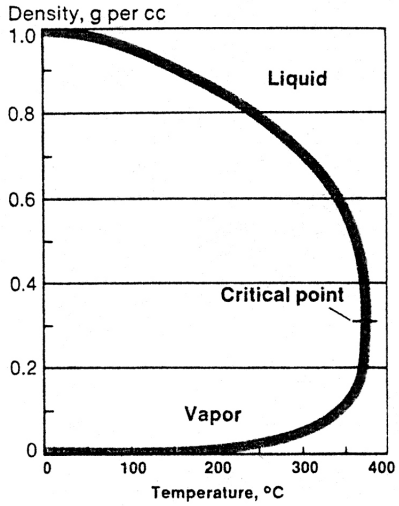

Figure 1.7 Density-temperature behavior of water [59].

Above the critical point, a liquid cannot exist, so that the fluid in the autoclave will be, by definition, a gas. But no discontinuity occurs when the fluid passes through the critical point.

In any autoclave filled more than 32% with water, the liquid will expand to fill the autoclave at some temperature below the critical temperature. The higher the percentage of fill, the lower the temperature at which the autoclave becomes filled with

liquid. If the autoclave is filled initially to 32%, the liquid level remains unchanged as the temperature rises. The liquid-vapor meniscus disappears at the critical temperature and classical critical-point phenomena, such as opalescence, occur. When the autoclave is filled initialy to less than 32%, the liquid level drops as the temperature increases because liquid is lost, the autoclave boils dry, at temperatures below the critical temperature [59].

1.4.2 Microwave Synthesis

In the electromagnetic spectrum, the microwave radiation region is located between infrared radiation and radio waves. Microwaves have wavelengths of 1mm-1m, corresponding to frequencies between 0.3 and 300 GHz [61].

Up to date, a large number of phosphate and arsenate compounds were prepared by solid-state reaction (high temperature) or hydrothermal process with long period [62]. Since the reactions are completed in short time periods (usually between 10-30 min) by applying microwave irradiation, micro-wave assisted synthesis reactions have also been used for phosphate containing materials as well as many inorganic materials in recent years [63-64].

Microwave-assisted synthesis is generally much faster, cleaner, and more economical than the conventional methods. A variety of materials such as carbides, nitrides, complex oxides, silicates, zeolites, apatite, etc. have been synthesized using microwaves. Many of these are of industrial and technological importance [65].

In recent years, much progress has been made in the synthesis of materials by hydrothermal and microwave methods. Conventional techniques, such as solid-state reaction at high temperatures, or photochemical, catalytic, ultrasonic and high pressure reactions are used stimulate chemical reactions that proceed slowly under ambient conditions [66, 67].

On the other hand, the use of controlled microwave energy for ceramic processing, drying and for melting silica, alumina and aluminosilicate gels have been reported [68].

The basic idea for a microwave-assisted preparation of borophosphates and boroarsenates is consistent with the observation of the high microwave susceptibilities of those phosphate, arsenate and borate hydrates [64, 65, 69, 70].

Microwave processing of materials is fundamentally different from conventional processing in its heat mechanism. In a microwave oven, heat is generated within the sample itself by the interaction of microwaves with the material. In conventional heating, heat is generated by heating elements and then transferred to the sample surfaces [71]. After the solution reaches the point of spontaneous combustion, it begins burning and becomes solid which burns at a temperature over 1000 °C. The combustion is not finished until all the flammable substances are all burned up and become loose substances. The whole process takes only a few minutes to yield powders of ferrite.

Preparation of phosphates and phosphate containing materials generally involves long reaction times and high temperatures in conventional methods. But phosphates are not susceptible to microwaves and therefore it is difficult to use microwaves for the preparation of phosphates except when one of the other reactants is a susceptor. However, recently it has been found that crystalline $NaH_2PO_4.2H_2O$ is a good microwave susceptor. When $Na_2H_2PO_4.2H_2O$ is irradiated by microwaves, heating occurs initially due to the presence of water of crystallization [64].

1.4.3 Solid State Reaction or Shake ‘n Bake Methods

When the solid compounds are employed to react with the each other at high temperatures, this does not necessarily imply that all components are still in the solid state at the temperatures required for the reaction to occur. A liquid phase (melt) or even gaseous intermediates may be involved to provide mass transport. An enormous amount of mixing of atoms or ions between particles is therefore required, either by solid state counter diffusion or by liquid or gas phase transport, in order to bring together atoms of the different elements, and in the correct ratio, to form the desired product [72].

The oldest, simplest and still most widely used method of preparing multicomponent solid materials is by direct reaction of solid components at high temperatures. Since solids do not react with each other at room temperature - even if

thermodynamics favors product formation – high temperatures are necessary to achieve appreciable reaction rates. The advantage of solid-state reactions is the ready availability of the precursors and the low cost for powder production on the inductrial scale. Almost all the new high T_c superconductors were first prepared by solid-state reaction methods [73].

1.5 MICROPOROUS MATERIALS

Microporous materials are porous solids with pore size below 20Å [74-77]. Porous solids with pore size between 20 and 500Å are called mesoporous materials. Macroporous materials are solids with pore size larger than 500 Å. Mesoporous and macroporous materials have undergone rapid development in the past decade. A frequently used term in the field of microporous materials is molecular sieves [78] that refer to a class of porous materials that can distinguish molecules on the basis of size and shape.

Crystalline microporous materials generally have a narrow pore size distribution. This makes it possible for a microporous material to selectively allow some molecules to enter its pores and reject some other molecules that are either too large or have a shape that does not match with the shape of the pore. A number of applications involving microporous materials utilize such size and shape selectivity [79].

Zeolite molecular sieves are crystalline, highly porous materials, which belong to the class of aluminosilicates. These crystals are characterised by a three-dimensional pore system, with pores of precisely defined diameter. The corresponding crystallographic structure is formed by tetrahedras of $[AlO_4]^{5-}$ and $[SiO_4]^{4-}$ that are linked by all their corners to form channels and cages of discrete size with no two aluminum atoms sharing the same oxygen. Due to the difference in charge between the $[SiO_4]^{4-}$ and $[AlO_4]^{5-}$ tetrahedra, the net framework charge of an aluminum containing zeolite is negative and hence must be balanced by a cation, typically an alkali or alkaline earth metal cation. The adsorbed molecules are located in the cavities of the zeolites, and access to these cavities is through a pore or window whose size can be the same or smaller than the cavities. The dimension of this pore determines the size of the molecule that can be adsorbed into these structures. $[SiO_4]^{4-}$ and $[AlO_4]^{5-}$ tetrahedras are

the basic building blocks for various zeolite structures, such as zeolites A and X (Figure 1.8, Figure 1.9), the most common commercial adsorbents [80,81].

Figure 1.8 Molecular sieve type A [80,81].

Figure 1.9 Molecular sieve type X [80,81].

The class of molecular sieves has been greatly extended during the last fifteen years by the discovery of zeolite-like aluminophosphates, metalloaluminophosphates, gallophosphates, zincophosphates, titanosilicates, zincosilicates and some other phosphate-based or silica-based microporous materials. Their common feature is a three-dimensional, low-density, and open-framework structure consisting of AlO_4, PO_4 , SiO_4 or other metal-oxygen tetrahedra (MO_4), linked to each other through bridging oxygen atoms. Due to their well-defined channel and cavity systems with pore dimensions up to 15 Å, they are able to recognise and discriminate molecules with a precision of less than 1 Å, which makes them widely applicable in many industrial and research areas [82].

1.5.1 The Use of Microporous Materials

Zeolites and related microporous materials contain regularly spaced molecule-sized pores and are fascinating examples of molecular engineering. More than just aesthetically inspiring, as can be seen in Figure 1.10, these materials represent billions of dollars in commerce, as they have widespread industrial applications [83]. Because of the presence of stable Brønsted acid sites (P–OH–M, Si–OH–Al) and Lewis acid sites (framework defects MO_3^-, AlO_3^-) in the negatively charged frameworks of $MAlPO_4$, $SiAlPO_4$, $MSiO_4$ or $AlSiO_4$ molecular sieves, they are extensively used as solid acid catalysts, adsorbents and ion exchangers in various types of organic shape-

selective conversion and separation reactions in the chemical and petrochemical industries [83]. Materials of this type are used as catalysts to produce gasoline and pharmaceuticals. For medical and industrial purposes, they are employed to separate N_2, O_2, and other gases. Zeolites are also applied for air-purification purposes such as separation of CO_2 and H_2O from the air gas mixture, but the main purpose of zeolite application in this field is the separation of O_2 and N_2. Formulated in household detergents, they remove the calcium ions that make water “hard” replacing environmentally unfriendly phosphates. Zeolites and related microporous materials are also employed to sequester radioactive ions for bioremediation. Many new applications are being investigated in areas such as selective membranes, batteries, and fuel cells [83-84].

The ion exchange property is the exchange of ions held in the cavity of microporous materials with ions in the external solutions. The gas sorption is the ability of a microporous material to reversibly take in molecules into its void volume. For a material to be called microporous, it is generally necessary to demonstrate the gas sorption property [79].

The importance of microporous materials has increased recently due to their activity as hosts to a range of other species, including small clusters of semiconductors, coordination complexes or metal clusters for optical and electronic applications.

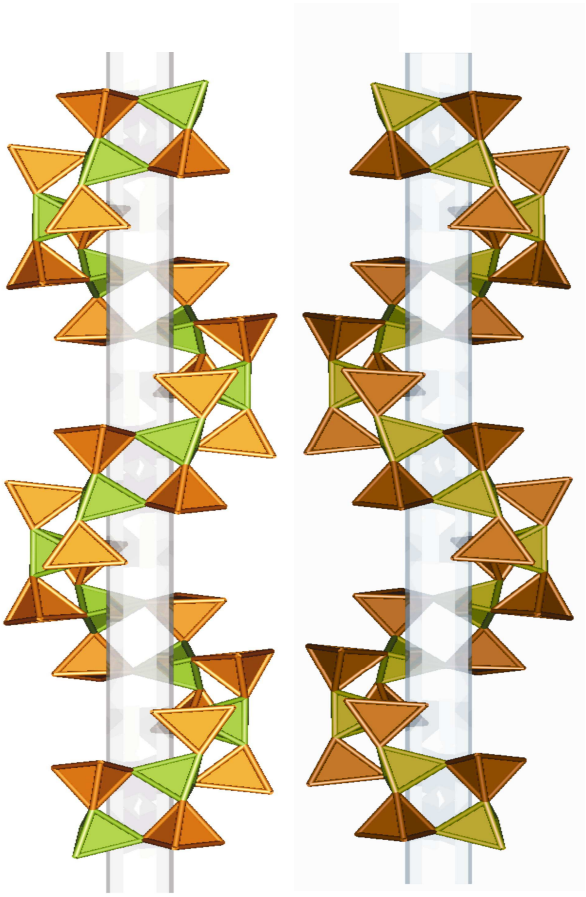

Figure 1.10 Shape of a microporous materials contain regularly spaced molecule-sized pores [83].

The ability to modify their frameworks by transition metal substitution has enabled rich compositional and structural diversities, especially in the metalloaluminophosphate system (*e.g.* M = Co, Zn, Mn *etc.*), and has expanded the importance of these materials in industrial catalysis due to the formation of redox catalytic sites ($M^{2+} \leftrightarrow M^{3+}$) [82].

As usual gaseous and fluid hydrocarbons without OH groups are non-polar, the interaction with hydrophilic zeolites like those based on high Al containing aluminosilicates is inhibited caused by their high cavity polarity. In addition, high alumina zeolites are quite unstable in the protonated form. Therefore, these processes are optimized reducint the zeolite hydrophility by tuning the Si/Al ratio and the development of low-alumina (high silica, all silica) zeolites. In this field, non aluminosilicate materials mainly based on phosphates play their dominant role in applicaton. The most important step in the specific application of zeolites is the

clarification of the fundamental processes and basic interactions taking place in the channel and cage systems related to ions and molecules accessing the zeolite cavity system. If these processes are understood, new application fields will be posseble and existing fields will be deepened and widened if zeolites with the properties needed are available. Because of their high water sorption properties zeolites are applied in science for drying purposes of organic liquids. Polarity, shape selectivity and stability of the respective zeolite and its cavity system with respect to chemical influences make them very suitable for these purposes. By the modification of these adsorption properties for specific absorption of polar aliphates like ethanol, zeolites are applicable for the removal of alcohol in drinks. Research in this field would be an important step for a softening of drins as it is assumed that alcohol e.g. in wine and beer does not influence the taste of these products if the ethanol component is only removed without any further process like heating etc. Another new research fields based on hydrothermally tailored synthesized zeolites is the storage and cracking of in vivo components like e.g. sugars as additives for food (optimized gain of food). New research on zeolite application must be done in the field of organ substitution in medicine for:

- Self controlled artificial liver (storage and conversion of hydrocarbons)
- Artificial lung (“breathing” behavior of zeolites: reversible selective adsorption of CO_2)
- Artificial heart (use of piezoelectric zeolites)
- Artificial blood (transport of hydrocarbons, body supply with O_2 and removal of CO_2 with much higher efectiveness than hemoglobin)
- Artificial kidney (in vivo membranes which allow the separation of blood and metabolic products like urea)
- Zeolites are until now only applied to regenerate artificial dialysis solutions.

Optical applications have yet been only for minor interest in zeolite research. The ion exchange capabilitiy for ions however, combined with their charge distribution within the void system and the optical transmittivity of the alumosilicate framework makes them very interesting as tunable luminescent materials and materials with non-linear optical property [81].

1.6 MAGNETIC PROPERTIES

Magnetic effects arise mainly from the electrons in a molecule because the magnetic moment of an electron is about 10^3 times that of the proton. Inorganic solids that exhibit magnetic effects other than diamagnetism, which is a property of all substances, are characterized by having unpaired electrons present. These are usually located on metal cations. Magnetic behavior is thus restricted mainly to compounds of transition metals and lanthanides, many of which possess unpaired d and f electrons, respectively. Several magnetic effects are possible. The unpaired electrons may be oriented at random on the different atoms, in which case the material possesses an overall magnetic moment and is ferromagnetic. Alternatively, they may be aligned in antiparallel fashion, giving zero overall magnetic moment and antiferromagnetic behaviour. If alignment of the spins is antiparallel but with unequal members in the two orientations, a net magnetic moment result and the behavior is ferromagnetic [81].

1.7 X-RAY POWDER DIFFRACTION (XRD)

The interaction of X-ray radiation with crystalline sample is governed by Bragg's law, which indicates a relationship among the diffraction angle (Bragg angle), X-ray wavelength, and interplanar spacing. According to Bragg's Law, the X-ray diffraction can be visualized as X-rays reflecting from a series of crystallographic planes as shown in Figure 1.11. The path differences introduced between a pair of waves traveled through the neighboring crystallographic planes are determined by the interplanar spacing. As the total path difference is equal to nλ (as n being an integer and λ being the wavelength), the constructive interference will occur and a group of diffraction peaks can be observed and give rise to X-ray powder patterns. The quantitative account of Bragg's law can be expressed as equation (1.1):

$$n\lambda = 2d_{hkl} \sin \theta \qquad (1.1)$$

where d is the interplanar spacing for a given set of *hkl*, λ is the wavelength, and θ is the Bragg angle.

The intensity of powder diffraction peaks is in principal determined by the structural factor, $\mathbf{F}_{hkl}$ as expressed in below equation (1.2), which depends on the crystal structures including relative positions of atoms in the unit cell, types of unit cells and other characteristics such as thermal motion and population parameters.

$$F_{hkl} = \sum_{i=1}^{n} g^i t^i(s) f^i(s) \exp[2\pi i (hx^i + ky^i + lz^i)] \quad (1.2)$$

where f^i (s) is the atomic scattering factor, g^i is the population factor of i^{th} atom, t^i (s) is the temperature factor, *hkl* are the Miller indices, and xyz are the fractional coordinates of i^{th} atom in the unit cell.

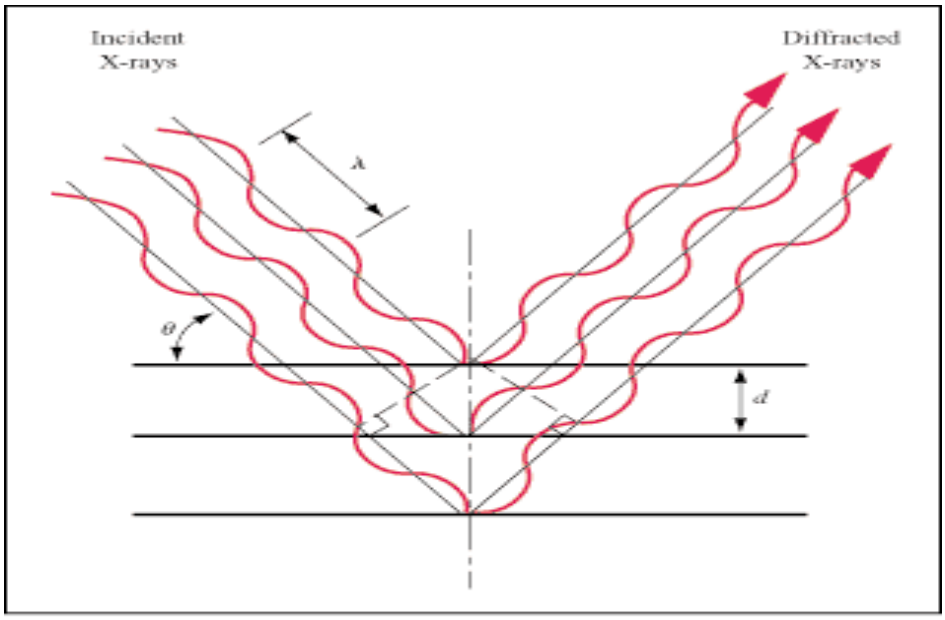

Figure 1.11 Geometrical illustrations of crystal planes and Bragg's law [85].

In addition to the primary structural factors, the intensity of diffraction is dependent on other factors, which are not only relevant to sample effects such as its shape and size, grain size and distribution *etc.*, but also with the instruments including detector, slit and / or monochromator geometry [85].

1.8 INDUCTIVELY COUPLED PLASMA EMISSION SPECTROMETRY

ICP optical emission spectrometry is based on the fact that atoms are promoted to higher electronic energy levels when heated to high temperatures. In fact, the plasma temperature is sufficient to ionize most atoms. For about three-quarters of the elements amenable to the technique, the most sensititive line arises from an ion rather than an atom. As the excited species leave the high-temperature region, the absorbed energy is released as ultraviolet and visible photons when the excited atoms decay to lower energy lecels or the ground electronic state. Useful emission lines generally occur in the region between 160 and 900 nm. Atomic and ionic emission lines are narrow, typically less than 5 pm, and their wavelengths follow well-understood selection rules [86].

1.9 PURPOSE OF THE WORK

The importance and the aim of this work will be summarized briefy in this section. Preparation of new metal borophosphate and structural investigation of these compounds are very important since these compounds were found to have very useful properties that can be applied to high technology. Besides, the synthesis and characterization studies of borophosphates, boroarsenate compounds were also studied in this work. Boroarsenate compounds have similar chemical and physical properties with that of borophosphates due to arsenic and phosphorous are in the same group in periodic table. The aim of this research is then classified as:

a) Attempts to prepare and characterize new metal borophosphate and boroarsenate compounds by Solid State, Hydrothermal and Microwave Asissted Methods.

b) Attempts to find the structures by X-ray diffraction (XRD), refine their unit cell parameters with the existing computer programs in our laboratory: Infrared (IR), Scanning Electron Microscope (SEM), Thermal Gravimetric Analysis (TGA) studies have a great deal of help in the discussion of the probable structures.

c) Quantitative analysis of the produced materials are quite difficult in some cases since they are not soluble in any solvent. However attempts to analyze these compounds have been made using Inductively Coupled Plasma. The formulas are proposed depending on these techniques.

CHAPTER 2

EXPERIMENTAL TECHNIQUES

2.1 CHEMICAL SUBSTANCES

The following substances were used in the synthesis of products: $AlCl_3.6H_2O$, As_2O_5 (synthesized in our laboratory), $Cd(OAc)_2.2H_2O$, $CoCl_2.6H_2O$, $CrCl_3.6H_2O$, $FeCl_2.4H_2O$, Fe_2O_3, H_3BO_3, $KBO_2.1.5H_2O$, K_2CO_3, KH_2PO_4, $Li_2B_4O_7$, $LiOH.H_2O$, $MnCl_2.2H_2O$, $NaBO_2.4H_2O$, $Na_2B_4O_7.12H_2O$, $Na_2HAsO_4.7H_2O$, $(NH_4)_2B_4O_7.4H_2O$, $NH_4H_2PO_4$, $(NH_4)_2HPO_4$, $ZnCl_2$, H_3AsO_4 (as prepared in our laboratory), H_3PO_4, HCl, HNO_3, (From Merck, Aldrich).

Spectroscopic KBr was used for making IR pellets. It was dried at 80^0 C for 2 hours before using.

2.2 INSTRUMENTATION

2.2.1 X-Ray Powder Diffractometer

During the characterization, three kinds of X-ray diffractometer were used. Huber JSO-DEBYEFLEX 1001 Diffractometer (Cu K_α) in KOÇ University. Philips diffractometer with PW 3020 goniometer (Cu K_α) in Royal Institute of Technology in Sweden (KTH), Rigaku diffractometer with D/max RINT-2200 (Cu K_α) in Gebze High Technology Institute.

2.2.2 Infrared Spectrophotometer (FTIR)

Mattson Satellite Infrared Spectrometer FTIR was used in the region 400-4000 cm^{-1}. Spectra of solid samples were obtained from KBr pellets using KBr / sample ratio = 100/3 (w/w).

2.2.3 Furnaces

The solid state reactions have been carried out in air with the aid of Carbolite Temperature Programmer Eurotherm 2416CG, 2416P8 furnace. Heating ranges were 300 – 2500 ^{o}C with Rh-Pt-Rh thermocouple.

Memmert Model 500 oven (heating range; 0 – 200 ^{o}C) and Ecocell MMM-Group oven (heating range; 0 – 250 ^{o}C) were used for the hydrothermal synthesis.

2.2.4 Inductively Coupled Plasma (ICP) and Nitrogen Analyzer

Inductively coupled plasma (ICP) atomic emission spectroscopy was used for the elemental analysis (B, Mn, P, Co, As, Zn) of the prepared sample using Perkin Elmer Optima 4300 DV type ICP instrument.

The nitrogen content was analyzed with a carrier gas hot reaction method (LECO, CHNS-932).

2.2.5 ESR

ESR measurements were performed using a commercial X-band (f≈ 9.7 GHz) *Bruker EMX* model spectrometer equipped with a cylindrical TE_{011} cavity. The powder sample was placed into a quartz sample holder tube, put into the cavity. ESR spectra were obtained by sweeping the magnetic field from 0 to 16 kOe. The magnetic field was calibrated using a α, α-diphenil-β-picryl hydrazyl (DPPH) sample (g= 2.0036). The field derivative of microwave power absorption, dP/dH, was registered as a function of DC magnetic field H. To obtain the intensity of microwave power absorption, P, digital integration of the EPR curves was performed by using *Bruker WinEPR* software.

2.2.6 SEM

Scanning electron microscopy (SEM) analysis was performed, in order to investigate the microstructure and morphology of the sample, using an FEI XL40 Sirion FEG Digital Scanning Microscope. Samples were coated with gold at 10 mA for 2 min. prior to SEM analysis.

2.2.7 TGA

Thermal gravimetric analysis (TGA) was used to assess the thermal decomposition behavior of the sample using a NETZCH STA 409 system.

2.3 EXPERIMENTAL PROCEDURE

Hydrothermal synthesis had been used to synthesize new borophosphate / boroarsenate compounds using different chemicals and various compositions of reactants. To perform hydrothermal reactions, the calculated amounts of starting materials were put into a 50 mL beaker. Then water (15 mL) and concentrated HCl, concentrated HNO_3 or concentrated H_3PO_4 (5 mL) was added in order to dissolve the solid mixture completely in a minimum amount of solution.

After dissolving the mixture completely in order to obtain concentrated solution, the volume of the solution was reduced to 20 mL by evaporation at 85 ^oC. After obtaining clear and concentrated solution, it was put in a Teflon coated autoclave (TF, home made, 20 mL) (degree of filling 60 %), closed very tightly, and heated at 160 ^oC in an oven for several days (Table 2.1). After the heating process, the autoclave was taken from the oven and opened after cooling to room temperature. In order to take its solid part, it was filtered by Whatman-1 and washed with hot distilled water and ethanol. The precipitate was put in an oven at 80 ^oC for drying about 2 hours. After the drying process, FTIR spectra and X-ray powder diffraction patterns of the sample were recorded.

As it is explained above, Teflon coated autoclave was used in order to obtain the solid inorganic product (Figure 2.1). On the other hand, sealed glass ampoule (Amp) (vol. 10-12 mL, degree of filling 25-30%) was also used instead of Teflon autoclave (Figure 2.2). To perform hydrothermal reactions, the starting materials and solvent were put into the glass ampoule. The glass ampoule was sealed and heated at 160 ^oC in an oven again for several days (3-15 days).

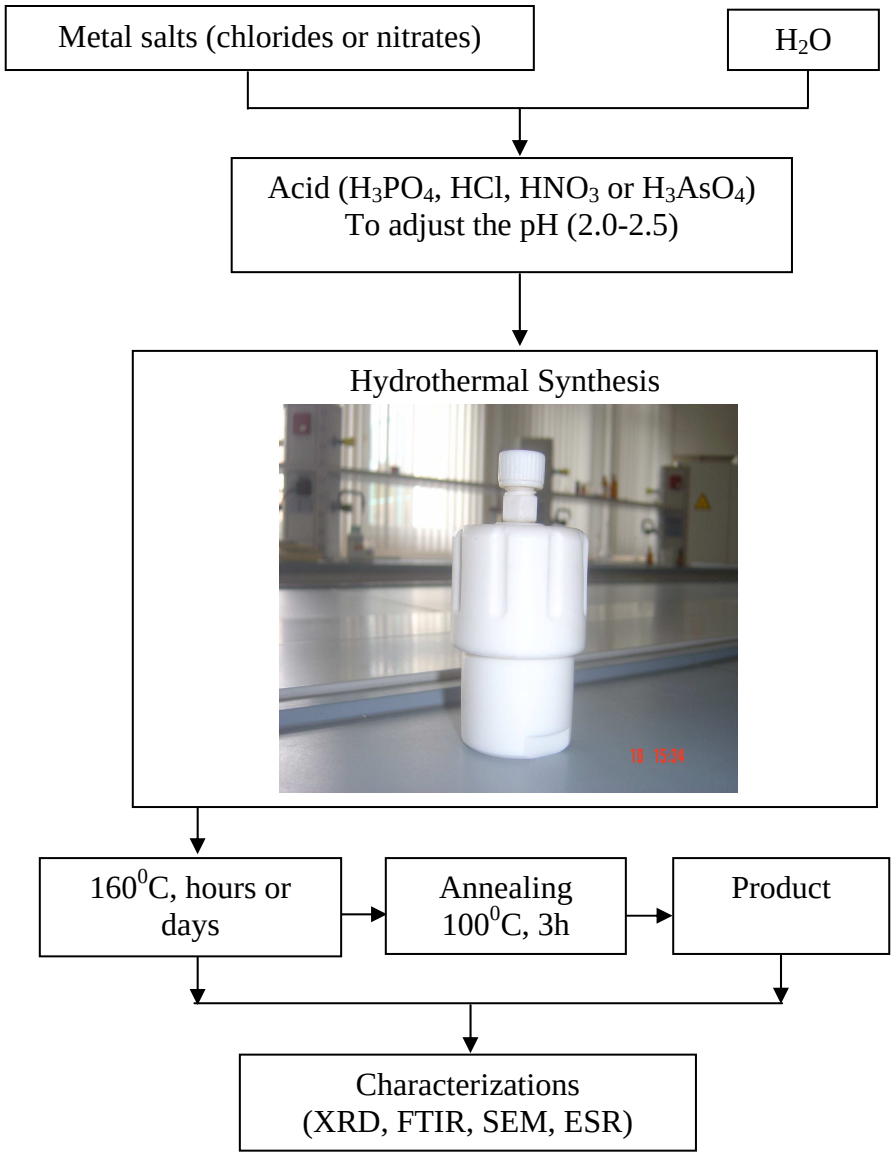

Figure 2.1 Flow chart of hydrothermal procedure using teflon autoclave.

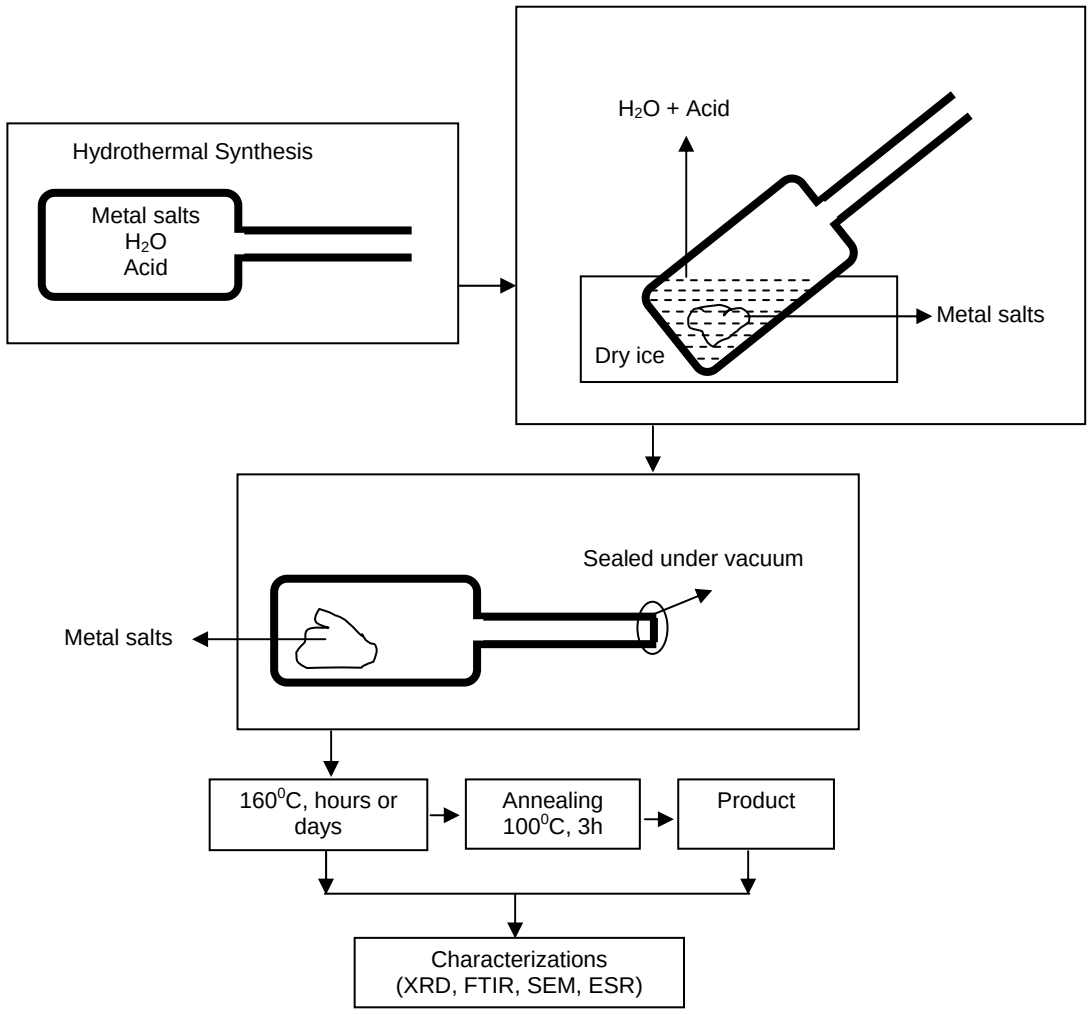

Figure 2.2 Flow chart of hydrothermal procedure using glass ampoule.

2.3.1 Synthesis of $(NH_4)_{0.5}Co_{1.25}(H_2O)_2[BP_2O_8].0.5H_2O$

The procedure which was explained in Sec. 2.3 was applied for the synthesis of $(NH_4)_{0.5}Co_{1.25}(H_2O)_2[BP_2O_8].0.5H_2O$. The experimental details are given in below table (Table 2.1).

Table 2.1 Experimental conditions for $(NH_4)_{0.5}Co_{1.25}(H_2O)_2[BP_2O_8].0.5H_2O$.

$(NH_4)_{0.5}Co_{1.25}(H_2O)_2[BP_2O_8].0.5H_2O$						
Exp. No	**Starting Materials (g)**			**TF/Amp**	**Solvent**	**Duration (day)**
	$CoCl_2.6H_2O$	**$(NH_4)_2B_4O_7.4H_2O$**	**$(NH_4)_2HPO_4$**			
20	0.238	0.487	0.792	Amp	HCl/H_2O	15
26	0.476	0.974	1.584	TF	HNO_3/H_2O	7
38	6.77	1.758	7.55	TF	H_3PO_4/H_2O	7
38a	6.77	1.758	7.55	TF	H_3PO_4/H_2O	15

2.3.2 Synthesis of $(NH_4)_{0.5}Mn_{1.25}(H_2O)_2[BP_2O_8].0.5H_2O$

The procedure which was explained in Sec. 2.3 was applied for the synthesis of $(NH_4)Mn(H_2O)_2[BP_2O_8].H_2O$. The experimental details are given in below table (Table 2.2).

Table 2.2 Experimental conditions for $(NH_4)_{0.5}Mn_{1.25}(H_2O)_2[BP_2O_8].0.5H_2O$.

$(NH_4)_{0.5}Mn_{1.25}(H_2O)_2[BP_2O_8].0.5H_2O$						
Exp. No	**Starting Materials (g)**			**TF/Amp**	**Solvent**	**Duration (day)**
	$MnCl_2.2H_2O$	**H_3BO_3**	**$(NH_4)_2HPO_4$**			
35	4.876	0.744	2.384	TF	HCl/H_2O	7
35h	4.876	0.744	2.384	TF	HCl/H_2O	15

	$MnCl_2.2H_2O$	**$(NH_4)_2B_4O_7.4H_2O$**	**$(NH_4)_2HPO_4$**			
40	6.769	1.758	7.55	TF	H_3PO_4/H_2O	15

2.3.3 Synthesis of $NaMn(H_2O)_2[BAs_2O_8].H_2O$

Hydrothermal synthesis of $NaMn(H_2O)_2[BAs_2O_8].H_2O$ was carried out with starting materials of $MnCl_2.2H_2O$, $Na_2B_4O_7.12H_2O$ and $Na_2HAsO_4.7H_2O$ (Table 2.3). All experiments were done in Amp and HCl/H_2O mixture was used as solvent.

Table 2.3 Experimental conditions for $NaMn(H_2O)_2[BAs_2O_8].H_2O$.

$NaMn(H_2O)_2[BAs_2O_8].H_2O$				
Exp. No	**Starting Materials (g)**			**Duration (day)**
	$MnCl_2.2H_2O$	**$Na_2B_4O_7.12H_2O$**	**$Na_2HAsO_4.7H_2O$**	
73	0.322	0.383	2.184	7
73a	0.322	0.383	2.184	15

2.3.4 Synthesis of $NaCo(H_2O)_2[BAs_2O_8].H_2O$

$NaCo(H_2O)_2[BAs_2O_8].H_2O$ was tried to be synthesized with $CoCl_2.6H_2O$, $Na_2B_4O_7.12H_2O$ and $Na_2HAsO_4.7H_2O$ in stoichiometric amounts as given in Table 2.4. The reaction was performed in Amp and HCl/ H_2O mixture was used as solvent.

Table 2.4 Experimental conditions for $NaCo(H_2O)_2[BAs_2O_8].H_2O$.

$NaCo(H_2O)_2[BAs_2O_8].H_2O$					
Exp. No	**Starting Materials (g)**			**TF/Amp**	**Duration (day)**
	$CoCl_2.6H_2O$	**$Na_2B_4O_7.12H_2O$**	**$Na_2HAsO_4.7H_2O$**		
61	0.744	2.115	5.616	TF	15
61a	0.5	1	0.9	TF	15
71	0.237	0.708	1.87	Amp	7
71a	0.237	0.708	1.87	Amp	15
71b	0.237	0.708	1.87	TF	21

2.3.5 Synthesis of $NaZn(H_2O)_2[BAs_2O_8].H_2O$

The procedure which was explained in Sec. 2.3 was applied for the synthesis of $NaZn(H_2O)_2[BAs_2O_8].H_2O$. HCl/H_2O mixture was used as solvent for all experiments (Table 2.5).

Table 2.5 Experimental conditions for $NaZn(H_2O)_2[BAs_2O_8].H_2O$.

$NaZn(H_2O)_2[BAs_2O_8].H_2O$					
Exp. No	**Starting Materials (g)**			**TF/Amp**	**Duration (day)**
	$ZnCl_2$	**$Na_2B_4O_7.12H_2O$**	**$Na_2HAsO_4.7H_2O$**		
64	0.35	0.491	2.805	TF	15
64a	0.35	0.491	2.805	TF	7
72	0.273 g	0.383	2.184	Amp	15
72a	0.2726	0.383	1.87	Amp	15
72b	0.2726	0.383	1.87	TF	15

2.3.6 Synthesis of $(H)_{0.5}Co_{1.25}(H_2O)_{1.5}[BP_2O_8].H_2O$

The synthesis of $(H)_{0.5}Co_{1.25}(H_2O)_{1.5}[BP_2O_8].H_2O$ was carried out by hydrothermal method starting from mixtures of $CoCl_2.6H_2O$, H_3BO_3 and $(NH_4)_2HPO_4$ (Table 2.6).

Table 2.6 Experimental conditions for $(H)_{0.5}Co_{1.25}(H_2O)_{1.5}[BP_2O_8].H_2O$.

$(H)_{0.5}Co_{1.25}(H_2O)_{1.5}[BP_2O_8].H_2O$						
Exp. No	**Starting Materials (g)**			**TF/Amp**	**Solvent**	**Duration (day)**
	$CoCl_2.6H_2O$	**H_3BO_3**	**$(NH_4)_2HPO_4$**			
37	6.770	1.758	7.550	TF	H_3PO_4/H_2O	15

2.3.7 Synthesis of $LiMn(H_2O)_2[BP_2O_8].H_2O$

The procedure which was explained in Sec. 2.3 was applied for the synthesis of $LiMn(H_2O)_2[BP_2O_8].H_2O$. All experiments were done in TF (Table 2.7).

Table 2.7 Experimental conditions for $LiMn(H_2O)_2[BP_2O_8].H_2O$.

$LiMn(H_2O)_2[BP_2O_8].H_2O$					
Exp. No	**Starting Materials (g)**			**Solvent**	**Duration (day)**
	$MnCl_2.2H_2O$	**$Li_2B_4O_7$**	**$(NH_4)_2HPO_4$**		
70	0.5	1.584	0.974	H_3PO_4/H_2O	7
70a	0.6	1.584	0.974	H_3PO_4/H_2O	7
70b	0.7	1.584	0.974	H_3PO_4/H_2O	7
	$MnCl_2.2H_2O$	**$LiOH.H_2O$**	**H_3BO_3**		
59	0.476	5.042	1.568	H_3PO_4/H_2O	7
59a	0.476	5.042	1.568	H_3PO_4/H_2O	15

2.3.8 Synthesis of $LiCd(H_2O)_2[BAs_2O_8].H_2O$

$LiCd(H_2O)_2[BAs_2O_8].H_2O$ was tried to be synthesized with $Cd(OAc)_2.2H_2O$, $LiOH.H_2O$ and H_3BO_3 in stoichiometric amounts as given in Table 2.8. All experiments were done in TF and H_3AsO_4/H_2O mixture was used as solvent.

Table 2.8 Experimental conditions for $LiCd(H_2O)_2[BAs_2O_8].H_2O$.

$LiCd(H_2O)_2[BAs_2O_8].H_2O$				
Exp. No	**Starting Materials (g)**			**Duration (day)**
	$Cd(OAc)_2.2H_2O$	**$LiOH.H_2O$**	**H_3BO_3**	
75	0.603	5.042	1.568	6
75a	1	4	1.568	6

2.3.9 Synthesis of $Cr(H_2O)_2[BP_2O_8].H_2O$

The procedure which was explained in Sec. 2.3 was applied for the synthesis of $Cr(H_2O)_2[BP_2O_8].H_2O$. All experiments were done in TF and H_3PO_4/H_2O mixture was used as solvent (Table 2.9).

Table 2.9 Experimental conditions for $Cr(H_2O)_2[BP_2O_8].H_2O$.

$Cr(H_2O)_2[BP_2O_8].H_2O$				
Exp. No	**Starting Materials (g)**			**Duration (day)**
	$CrCl_3.6H_2O$	**H_3BO_3**	**$(NH_4)_2HPO_4$**	
50	5.675	1.758	0	7
51	5.675	1.76	7.55	7

2.3.10 Synthesis of $Fe(H_2O)_2[BP_2O_8].H_2O$

$Fe(H_2O)_2[BP_2O_8].H_2O$ was tried to be synthesized with $FeCl_2.4H_2O$, H_3BO_3 and $(NH_4)_2HPO_4$ in stoichiometric amounts as given in Table 2.10. The reaction was performed in TF and H_3PO_4/H_2O mixture was used as solvent.

Table 2.10 Experimental conditions for $Fe(H_2O)_2[BP_2O_8].H_2O$.

$Fe(H_2O)_2[BP_2O_8].H_2O$				
Exp. No	**Starting Materials (g)**			**Duration (day)**
	$FeCl_2.4H_2O$	**H_3BO_3**	**$(NH_4)_2HPO_4$**	
53	5.675	1.76	7.55	7

2.3.11 Synthesis of $Al(H_2O)_2[BP_2O_8].H_2O$

$Al(H_2O)_2[BP_2O_8].H_2O$ was tried to be synthesized with $AlCl_3.6H_2O$, H_3BO_3 and $(NH_4)_2HPO_4$ in stoichiometric amounts as given in Table 2.11. All experiments were done in TF.

Table 2.11 Experimental conditions for $Al(H_2O)_2[BP_2O_8].H_2O$.

$Al(H_2O)_2[BP_2O_8].H_2O$					
Exp. No	**Starting Materials (g)**			**Solvent**	**Duration (day)**
	$AlCl_3.6H_2O$	**H_3BO_3**	**$(NH_4)_2HPO_4$**		
56	5.675	1.76	7.55	H_3PO_4/H_2O	7

2.3.12 Synthesis of $Al(H_2O)_2[BAs_2O_8].H_2O$

The procedure which was explained in Sec. 2.3 was applied for the synthesis of $Al(H_2O)_2[BAs_2O_8].H_2O$. All experiments were done in TF.

Table 2.12 Experimental conditions for $Al(H_2O)_2[BAs_2O_8].H_2O$.

$Al(H_2O)_2[BAs_2O_8].H_2O$				
Exp. No	**Starting Materials (g)**		**Solvent**	**Duration (day)**
	$AlCl_3.6H_2O$	**H_3BO_3**		
65a	2.993	2	H_3AsO_4/H_2O	3
65b	2.993	2	H_3AsO_4/H_2O	6
65b.1	Product 65b annealed at 80 ^oC			

2.3.13 Synthesis of $Fe_2BP_3O_{12}$

The reactants Fe_2O_3, H_3BO_3 and $NH_4H_2PO_4$ were heated at temperature given in Table 2.13. The expected chemical reactions will be as the following:

$$Fe_2O_3(s) + H_3BO_3(s) + 3\ NH_4H_2PO_4(s) \longrightarrow Fe_2BP_3O_{12}(s) + 3\ NH_3(g) + 5\ H_2O(g)$$

Table 2.13 Experimental conditions for the solid state synthesis of $Fe_2BP_3O_{12}$.

$Fe_2BP_3O_{12}$				
Exp. No	**Starting Materials (g)**			**Temperature & Duration**
	Fe_2O_3	**H_3BO_3**	**$NH_4H_2PO_4$**	
48	1	0.5	2.15	180 ^oC / 12 hrs - 1000 ^oC / 5 hrs
48-1	Exp.48 was heated at 1000 ^oC for 5 hrs			
48-2	Exp.48-1 was heated at 1000 ^oC for 5 hrs			
48-3	Exp.48-2 was heated at 1000 ^oC for 5 hrs			

2.3.14 Synthesis of $K_5B_2P_3O_{13}$

2.3.14.1 Hydrothermal Reactions

The procedure which was explained in Sec. 2.3 was applied for the synthesis of $K_5B_2P_3O_{13}$. All experiments were done in TF.

Table 2.14 Experimental conditions for the hydrothermal synthesis $K_5B_2P_3O_{13}$.

$K_5B_2P_3O_{13}$				
Exp. No	**Starting Materials (g)**		**Solvent**	**Duration (day)**
	$KBO_2.1.5H_2O$	**KH_2PO_4**		
67	4	5	H_2O	11
67a	9.61	12	H_2O	11

2.3.14.2 Solid State Reactions

In order to perform high temperature reaction, the stoichiometric amounts of reactants were weighed and ground well in an agate mortar. The mixture was heated to 750 ^{o}C in porcelein crucible. After the heating procedure, the FTIR spectrum and X-Ray diffraction pattern were recorded. The expected chemical reaction will be as the following:

$$5K_2CO_3\,(s) + 4H_3BO_3\,(s) + 6(NH_4)_2HPO_4\,(s) \xrightarrow{750\ ^{o}C} 2K_5B_2P_3O_{13}(s) + 5CO_2(g) + 12NH_3(g) + 15H_2O(g)$$

Table 2.15 Experimental conditions for the solid state synthesis $K_5B_2P_3O_{13}$.

$K_5B_2P_3O_{13}$				
Exp. No	**Starting Materials (g)**			**Temperature & Duration**
	K_2CO_3	**H_3BO_3**	**$(NH_4)_2HPO_4$**	
46a	0.2175	0.1	0.5	750 ^{o}C / 5 hrs

2.3.15 Synthesis of $Na_5(B_2As_3O_{13})$

2.3.15.1 Hydrothermal Reactions

The procedure which was explained in Sec. 2.3 was applied for the synthesis of $Na_5(B_2As_3O_{13})$. All experiments were done in TF and only H_2O was used as solvent (Table 2.16). The expected chemical reaction will be as the following:

$$4NaBO_2.4H_2O\,(s) + 3/2As_2O_5\,(s) + 3Na_2HAsO_4.7H_2O\,(s) \xrightarrow{180\ ^{o}C} 2Na_5(B_2As_3O_{13})\,(s) + 77/2\ H_2O(g)$$

Table 2.16 Experimental conditions for the hydrothermal synthesis of $Na_5(B_2As_3O_{13})$.

$Na_5(B_2As_3O_{13})$				
Exp. No	**Starting Materials (g)**			**Duration (day)**
	$NaBO_2.4H_2O$	**$Na_2HAsO_4.7H_2O$**	**As_2O_5**	
3	1.13	2.39	1.5	6
4	2.71	5.74	3.55	6
6	1.81	3.83	2.36	6

2.3.15.2 Microwave-Assisted Synthesis

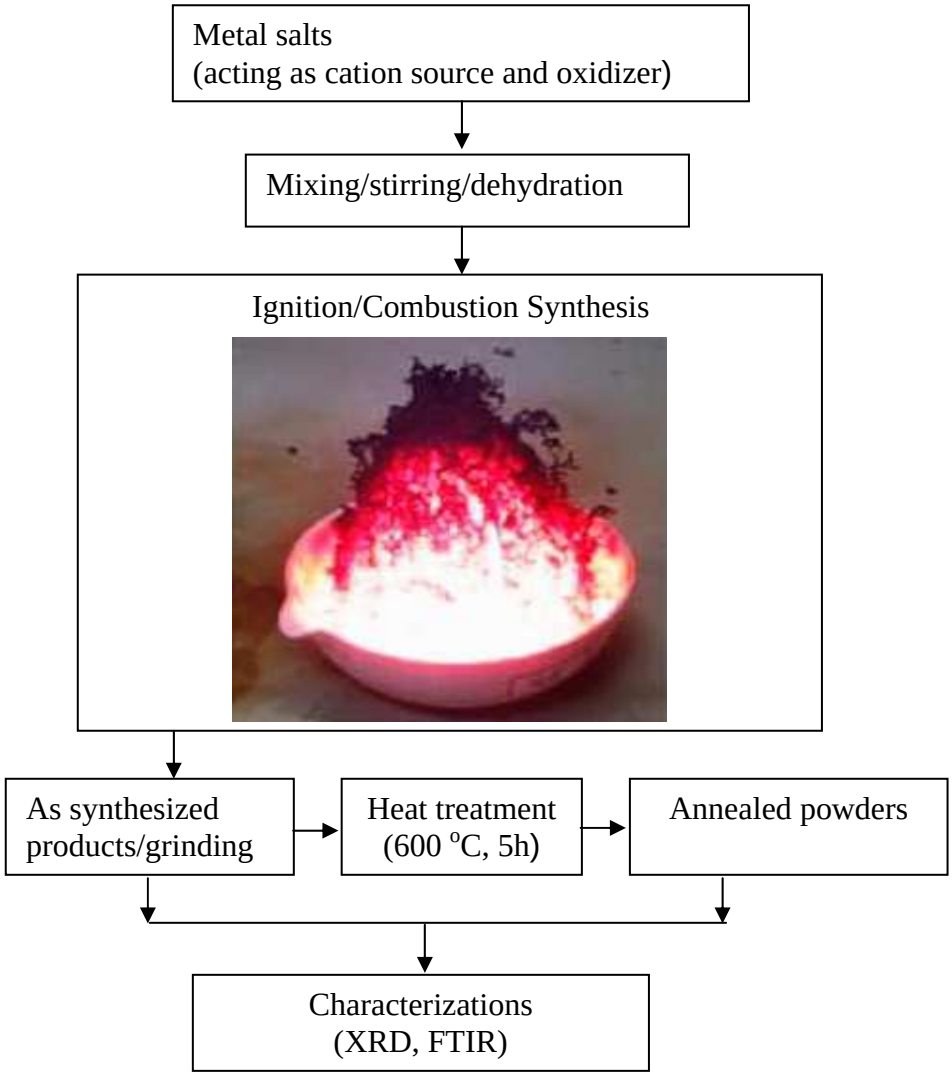

Figure 2.3 Flow chart of microwave synthesis.

The crucible containing the solid solution was introduced into microwave oven. Initially, the solid solution undergoes dehydration followed by decomposition with the evolution of large amounts of gases H_2O. After the solid solution reaches the point of spontaneous combustion, it begins burning and releases lots of heat, vaporizes all the water instantly and becomes solid burning at a high temperature.

Table 2.17 summarizes the experimental conditions of Exp.2.

Table 2.17 Experimental conditions for the microwave-assisted synthesis of $Na_5(B_2As_3O_{13})$.

$Na_5(B_2As_3O_{13})$				
Exp. No	**Starting Materials (g)**			**Duration (min.)**
	$NaBO_2.4H_2O$	**$Na_2HAsO_4.7H_2O$**	**As_2O_5**	
2	0.132	0.558	0	~ 5

CHAPTER 3

RESULTS AND DISCUSSIONS

3.1 NH_4–Co-P–B–O-H CONTAINING COMPOUND

When HCl was used as solvent to dissolve the reactant (Exp.20), product was NH_4CoPO_4. The FTIR spectrum and XRD powder pattern of product of Exp.20 were given in Figure 3.1 and Figure 3.2 respectively. The presence of NH_4^+ peak was marked with an arrow in Figure 3.1. All the peaks in the XRD powder pattern match well with the NH_4CoPO_4 (JCPDS Card No: 18-0402). Qualitatively, the presence of Co, NH_4^+ and P in the product was confirmed.

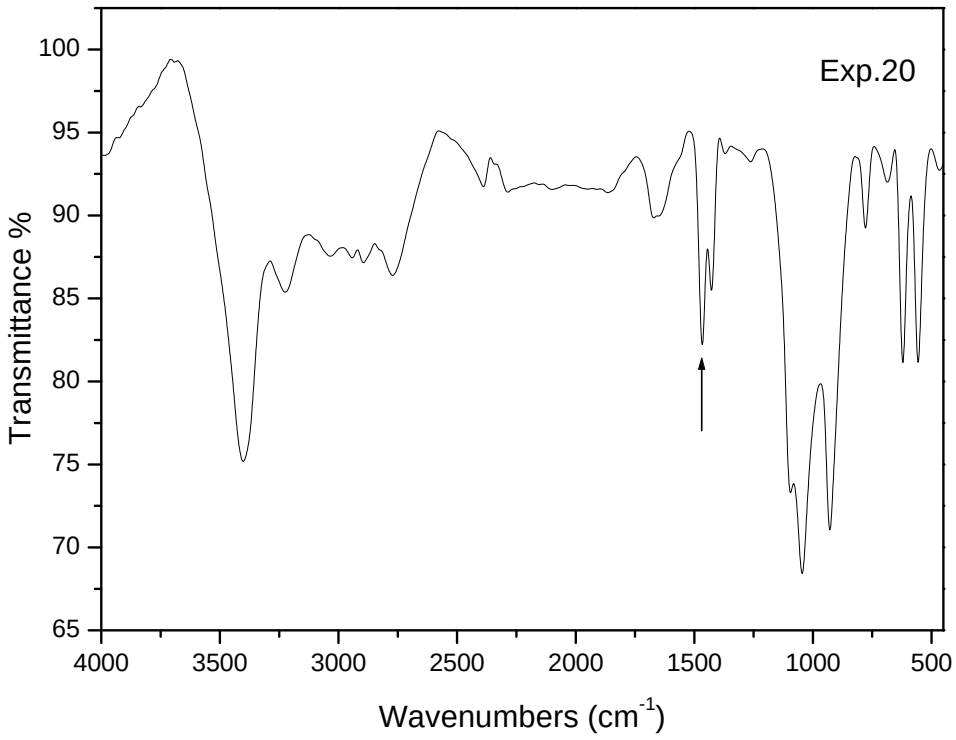

Figure 3.1 The FTIR spectrum of the product of Exp.20.

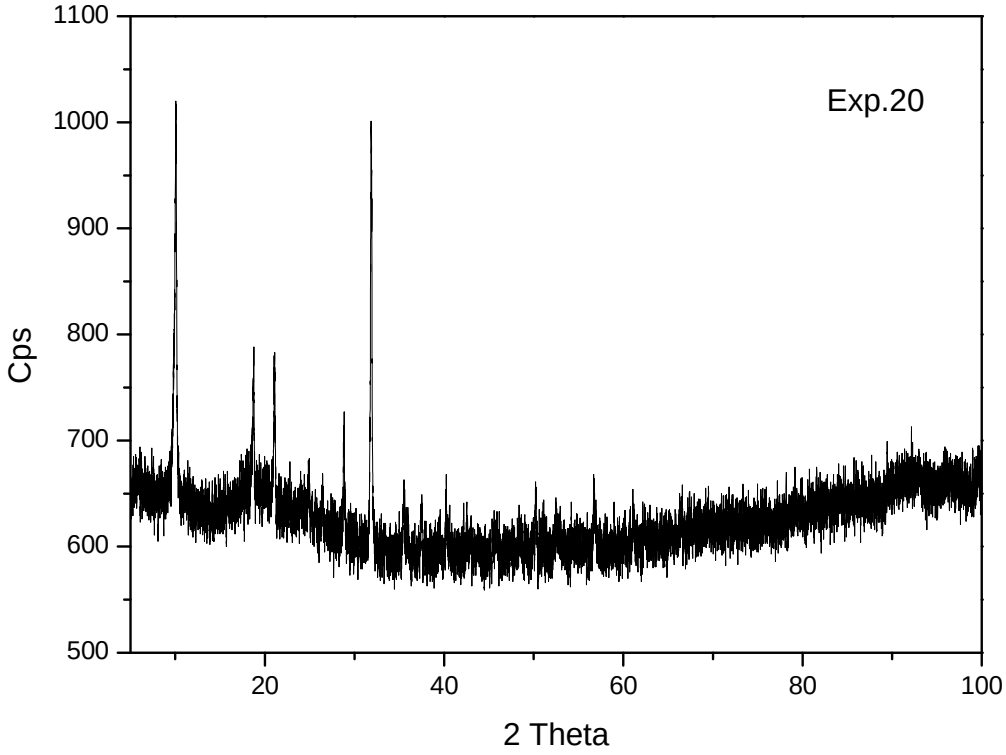

Figure 3.2 The XRD powder pattern of the product of Exp.20.

When HNO_3 and H_3PO_4 were used as solvent, purple colored new compound; $(NH_4)_xCo_{(3-x)/2)}$ $(H_2O)_2(BP_2O_8)(1-x)H_2O$ (x=0.5), was synthesized. The experimental details of this synthesis are given in section 2.3.1. The results of these three experiments (Exp.26, 38 and 38a) were same which was $(NH_4)_xCo_{(3-x)/2)}$ $(H_2O)_2(BP_2O_8)(1-x)H_2O$ (x=0.5). This shows that it is not important whether HNO_3 or H_3PO_4 is used as solvent. The powder XRD data of the product was indexed by Checkcell program in the hexagonal crystal system with the unit cell parameters a = 9.4920(±0.0002), c= 15.5820(±0.0003) (Table 3.1). This titled compound was synthesized before by Schafer et al. in 2001 [16] as single crystal. Our cell parameters are in good agreement with Schafer's study.

In order to check the reproducibility of the product, two additional experiments were done (Exp.38 and Exp.38a). Their XRD powder patterns (Exp.38 and Exp.38a) were given in Figure 3.3.

Table 3.1 The X-ray powder diffraction data of Exp.26.

Intensity	2Th(obs)	2Th(Calc)	d	h	k	l
32	10.750	10.754	8.182	0	1	0
74	12.160	12.163	7.263	0	1	1
63	15.720	15.658	5.679	0	1	2
23	18.630	18.681	4.719	1	1	0
45	19.600	19.537	4.521	1	1	1
15	21.720	21.604	4.084	0	2	0
64	22.470	22.352	3.955	0	2	1
100	24.490	24.467	3.630	0	2	2
20	25.150	25.279	3.554	0	1	4
71	27.610	27.654	3.226	0	2	3
37	28.770	28.709	3.088	1	2	0
68	29.430	29.287	3.030	1	2	1
36	30.600	30.656	2.945	0	1	5
30	31.050	30.961	2.875	1	2	2
22	31.500	31.619	2.837	0	2	4
41	32.700	32.654	2.746	0	3	0
27	33.610	33.584	2.662	1	2	3
55	34.250	34.399	2.630	1	1	5
14	34.680	34.675	2.573	0	3	2
32	37.120	37.065	2.418	0	3	3
27	37.760	37.884	2.388	2	2	0
36	39.950	39.932	2.254	1	3	1
21	41.350	41.223	2.176	1	3	2
9	41.750	41.818	2.152	2	2	3
5	41.980	42.017	2.152	0	1	7
7	43.400	43.305	2.081	1	3	3
37	44.470	44.429	2.034	0	4	1
15	47.410	47.544	1.917	0	4	3
14	48.080	48.159	1.891	2	2	5
15	48.500	48.590	1.874	2	3	1
8	49.440	49.496	1.840	1	3	5
23	50.060	50.148	1.823	0	4	4
13	53.330	53.357	1.716	0	4	5
18	54.200	54.088	1.692	0	1	9
12	57.060	57.034	1.611	2	3	5
12	57.060	57.034	1.611	2	3	5
12	57.240	57.221	1.600	0	5	2
13	60.590	60.635	1.525	2	3	6
23	62.960	62.919	1.474	1	4	6

14	63.620	63.510	1.459	0	3	9
9	66.030	66.033	1.413	0	4	8
9	67.410	67.356	1.387	0	5	6
6	70.250	70.224	1.337	0	2	11
6	70.650	70.691	1.333	3	4	2
8	73.640	73.565	1.280	1	3	10
11	73.880	73.822	1.280	0	1	12

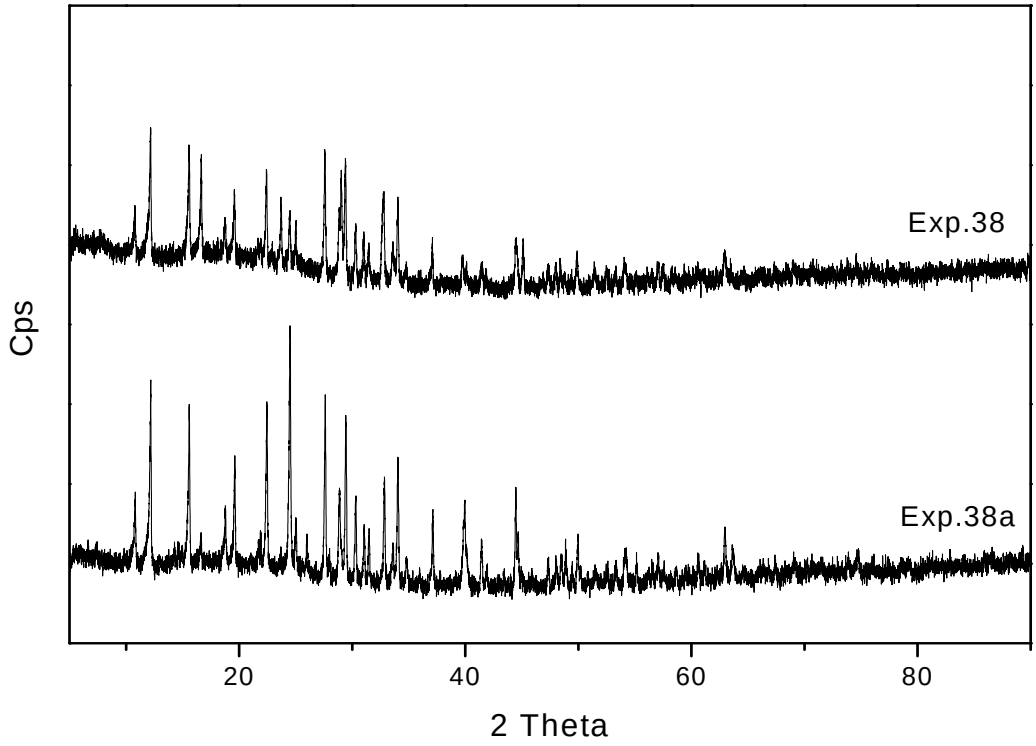

Figure 3.3 The comparison of XRD powder patterns of the products of Exp.38, 38a.

The products of the experiments containing NH_4, Co, P, B and O are summarized in Table 3.2.

Table 3.2 Products of Exp.26, 38, 38a.

Exp. No	Product
26	$(NH_4)_{0.5}Co_{1.25}(H_2O)_2[BP_2O_8].0.5H_2O$
38	$(NH_4)_{0.5}Co_{1.25}(H_2O)_2[BP_2O_8].0.5H_2O$
38a	$(NH_4)_{0.5}Co_{1.25}(H_2O)_2[BP_2O_8].0.5H_2O$

FTIR studies exhibit the presence of water and lack of hydroxyl bands are common in most of the hydrothermally synthesized borophosphate compounds. The bands at 3238, 3041, 2845 and 1436 cm^{-1} correspond to the stretching and bending vibrations of N-H groups demonstrating the presence of NH_4^+ in these compounds [87]. The bands in the region 1066-524 cm^{-1} can be assigned to the asymmetric stretching and bending vibrations of PO_4, BO_4 and B-O-P groups (Figure 3.4). An unambiguous peak assignment of the modes in the lower range could not be made.

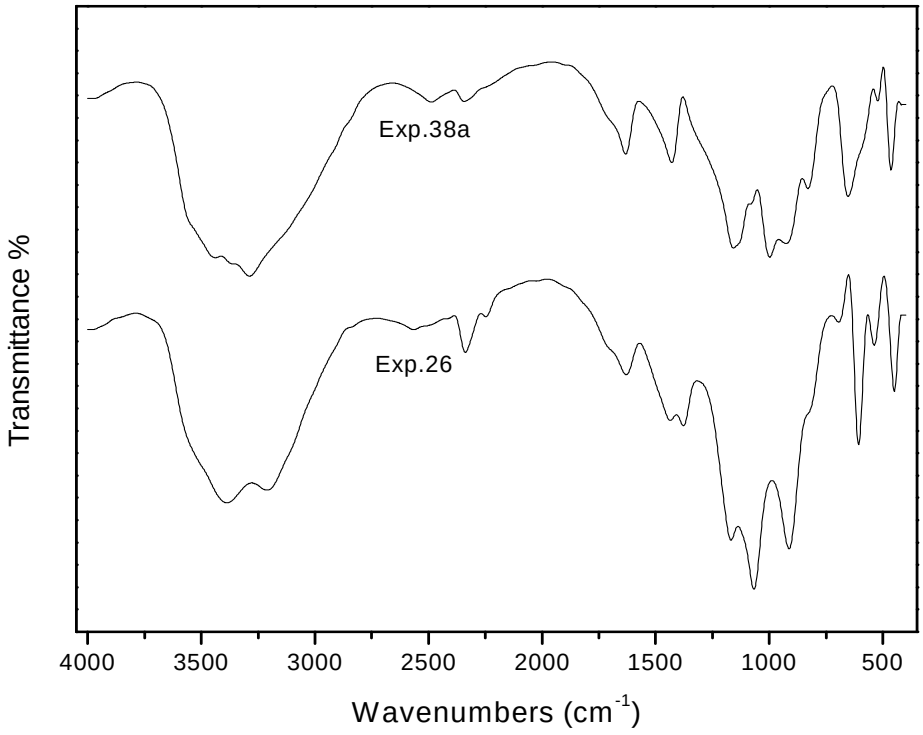

Figure 3.4 The comparison of FTIR spectra of the products of Exp.26, 38a.

The ICP results of Exp.38a are summarized in Table 3.3. In order to perform ICP analysis the sample was dissolved in aqua regia.

Table 3.3 ICP results of $(NH_4)_xCo_{((3-x)/2)}(H_2O)_2[BP_2O_8].(1-x)H_2O$ (x = 0.5).

	Cobalt %	**Boron %**	**Phosphorous %**
Theoretical	17.50	3.22	18.70
Experimental	16.30	3.30	17.9

As it can be seen from the below figure (Figure 3.5), the XRD powder pattern of Exp.26 and Exp.38a are matching very well. But the crystallinity of Exp.26 is higher than that of Exp.38a.

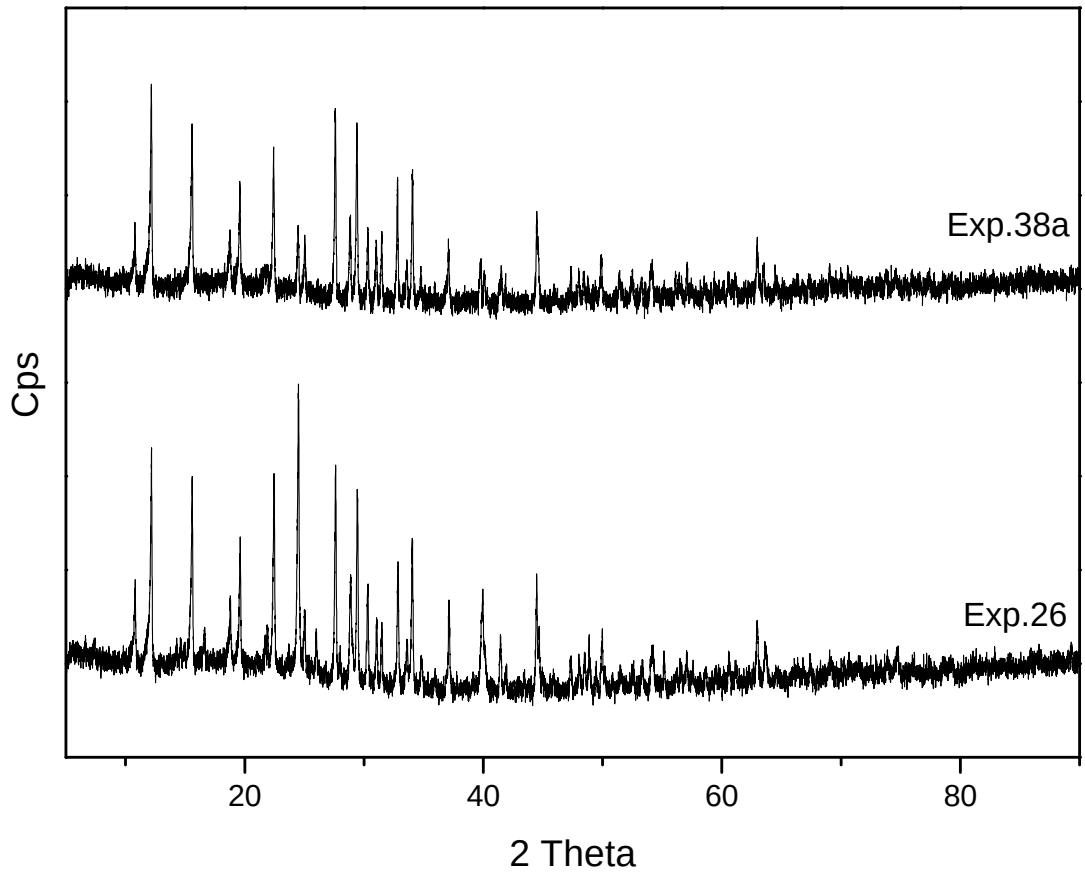

Figure 3.5 The comparison of XRD powder patterns of the products of Exp.26, 38a.

3.2 NH_4–Mn-P–B–O-H CONTAINING COMPOUND

For the synthesis of $(NH_4)_{0.5}Mn_{1.25}(H_2O)_2[BP_2O_8].0.5H_2O$ compound, three experiments were done at different conditions as given in section 2.3.2. The products of the experiments are given in below table (Table 3.4).

Table 3.4 Products of Exp.35, 35h, 40.

Exp. No	Product
35	$(NH_4)_{0.5}Mn_{1.25}(H_2O)_2[BP_2O_8].0.5H_2O$
35h	$(NH_4)_{0.5}Mn_{1.25}(H_2O)_2[BP_2O_8].0.5H_2O$
40	$(NH_4)_{0.5}Mn_{1.25}(H_2O)_2[BP_2O_8].0.5H_2O$

ICP results of Exp.35 performed to reveal its chemical composition. The results are listed in Table 3.5. In order to perform ICP analysis the sample was dissolved in aqua regia. Composition calculations based on these values confirm the composition of the title compound with x = 0.5, $(NH_4)_{0.5}Mn_{1.25}(H_2O)_2[BP_2O_8]\cdot 0.5H_2O$.

Table 3.5 Elemental and ICP results of $(NH_4)_{0.5}Mn_{1.25}(H_2O)_2[BP_2O_8].0.5H_2O$.

	Manganese %	Boron %	Nitrogen %	Phosphorous %
Theoretical	21.2	3.4	2.2	19.1
Experimental	20.9	3.5	1.9	20.1

The obtained powder product (Exp.35) was analyzed by XRD to reveal its crystalline contents and crystal structure. XRD pattern, given in Figure 3.6, was indexed by TREOR program in hexagonal crystal system with the unit cell parameters of a = 9.510(±2) Å, c = 15.710(±1) Å, Z = 6 and the space group $P6_5$ (No.176). According to the crystal model done by Kniep et al. [88], the condensation of PO_4 and BO_4 tetrahedra through common vertices leads to tetrahedral ribbons $^{1/\alpha}[BP_2O_8]^{3-}$, which are arranged around 6_1 screw axes to form helices. The spiral ribbons are built from four rings of tetrahedra in which the BO_4 and PO_4 groups alternate. Each BO_4 tetrahedron also belongs to the adjacent four-ring of tetrahedra along the ribbon, in such a way that all vertices of the BO_4 groups participate in bridging functions with PO_4 tetrahedra as shown in Kniep et al. [16, 89].

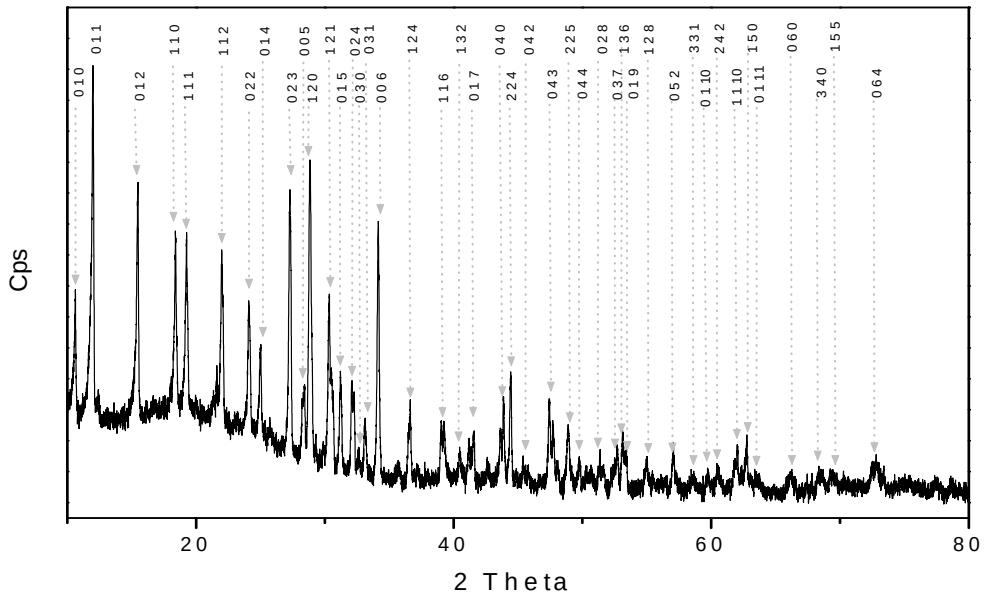

Figure 3.6 The XRD powder pattern of the product of Exp.35.

In order to check the reproducibility of Exp.35, another experiment (Exp.40) was done and the same product was obtained. The comparison of their XRD powder patterns are given in below figure (Figure. 3.7). Due to the low crystallinity of product of Exp.35h, its XRD pattern is not given in Figure 3.7.

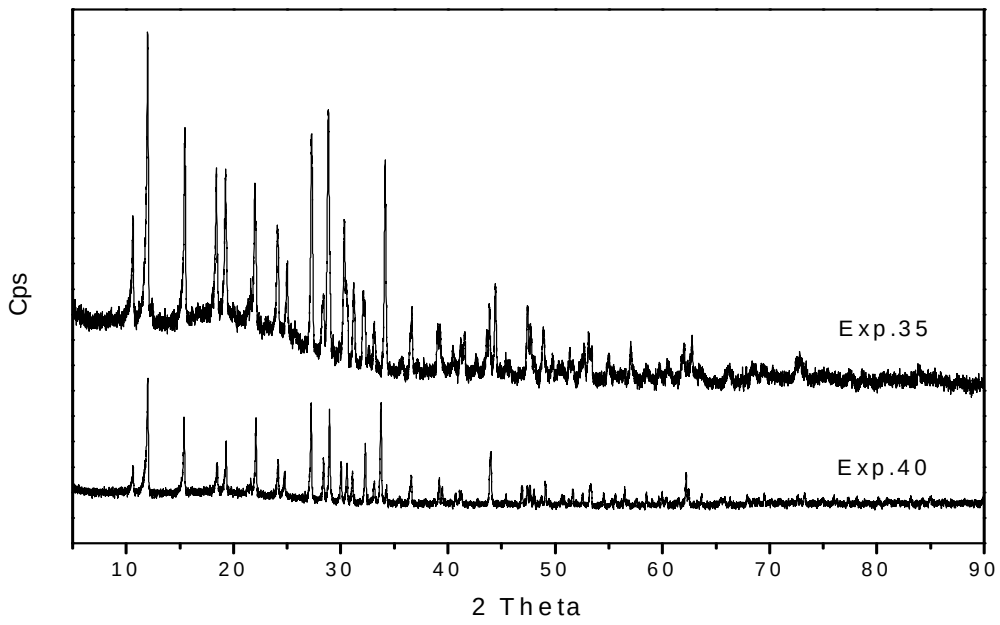

Figure 3.7 The comparison of XRD powder patterns of the products of Exp.35, 40.

The indexed results of Exp.35; $(NH_4)_{0.5}Mn_{1.25}(H_2O)_2[BP_2O_8].0.5H_2O$, is given in Table 3.6.

Table 3.6 The X-ray powder diffraction data of Exp 35.

Intensity	2Th(obs)	2Th(Calc)	d-spacing	h	k	l
36	10.600	10.733	8,32	0	1	0
100	12.080	12.123	7,37	0	1	1
66	15.620	15.576	5,72	0	1	2
50	18.510	18.645	4,818	1	1	0
48	19.380	19.488	4,604	1	1	1
47	21.950	21.831	4,037	1	1	2
35	24.290	24.385	3,689	0	2	2
25	25.110	25.098	3,558	0	1	4
73	27.430	27.532	3,266	0	2	3
18	28.450	28.381	3,139	0	0	5
79	28.740	28.653	3,092	1	2	0
8	29.130	29.222	2,987	1	2	1
46	30.430	30.423	2,944	0	1	5
28	31.400	31.450	2,863	0	2	4
26	32.500	32.589	2,742	0	3	0
16	33.190	33.097	2,702	0	3	1
71	34.250	34.216	2,623	0	0	6
24	36.760	36.811	2,451	1	2	4
17	39.310	39.246	2,293	1	1	6
7	41.210	41.119	2,19	1	3	2
16	41.620	41.675	2,171	0	1	7
24	43.870	43.937	2,062	0	4	0
32	44.530	44.508	2,037	2	2	4
8	45.490	45.503	1,996	0	4	2
24	47.460	47.404	1,915	0	4	3
23	47.880	47.942	1,904	2	2	5
9	49.920	49.971	1,831	0	4	4
13	51.470	51.514	1,777	0	2	8
13	52.690	52.629	1,735	0	3	7
17	53.200	53.166	1,722	1	3	6
13	53.650	53.625	1,722	0	1	9
11	55.180	55.261	1,668	1	2	8
15	57.060	57.083	1,613	0	5	2
6	58.550	58.476	1,577	3	3	1
7	59.830	59.886	1,546	0	1	10
9	60.560	60.598	1,53	2	4	2
12	62.180	62.177	1,494	1	1	10

15	62.790	62.762	1,479	1 5 0
8	66.320	66.374	1,409	0 1 11
8	68.310	68.271	1,38	0 6 0
7	69.360	69.346	1,387	3 4 0
5	70.260	70.276	1,338	1 5 5
10	72.950	72.945	1,297	0 6 4

The FTIR spectrum of the product of Exp.35 is given in Figure 3.8, which showed that two water bands at 3354 and 3558 cm^{-1} that can be assigned to water molecules occupying different positions in the structure. The band at 3558 cm^{-1} is due to hydrogen bonding between the hydrated molecules and the other at 3354 cm^{-1} shows the bond between anion and coordinated water. The absence of band for P-O-P (at around 740 cm^{-1}) is in agreement with the postulate by Kniep et al. [7] claiming the absence of P-O-P linking in borophosphate compounds. The stretching modes of a free PO_4^{3-} anion with T_d symmetry has four internal modes of vibrations [90-93], υ_3 (PO_4) = 1107, 1024 cm^{-1}, υ_1 (PO_4) = 954, υ_4 (PO_4) = 576, and υ_2 = 482 cm^{-1} that are also observed in the IR spectrum of the product. The presence of peaks in the FTIR spectra of the product between 850-1200 cm^{-1} proves B-O stretching of BO_4 units [94]. FTIR spectrum of the product confirms the presence of O-H and N-H vibrations by the following absorption bands with assignments: O-H stretching 3482 cm^{-1}, υ_3 (N-H) (3267 cm^{-1}), O-H deformation (1643 cm^{-1}), and υ_4 (N-H) (1448 cm^{-1}). These assignments verify the presence of NH_4^+ ion which is necessary for the charge balance together with the manganese present in mixed states, as already is assumed by the product color alone.

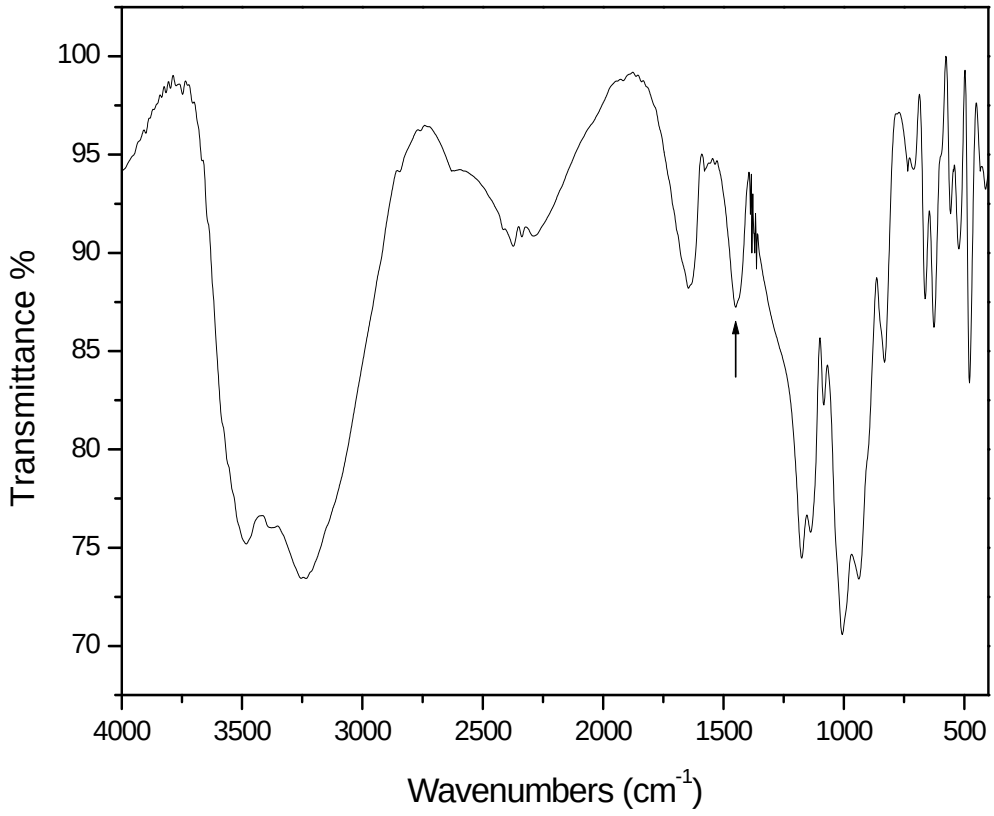

Figure 3.8 The FTIR spectrum of the product of Exp.35.

3.2.1 ESR Measurements on Experiment 35

Since EPR is able to detect paramagnetically isolated species and gives information about the coordination of isolated sites, it can be used to detect Mn^{2+} and Mn^{4+}, where as Mn^{3+} is usually not detected due to complete splitting of energy levels (no ground-state degeneracy) [95, 96]. Figure 3.9 shows the EPR spectrum of Exp. 35 showing a typical signal of Mn^{2+}. EPR measurements have been carried out by varying external magnetic field. A strong and broad microwave resonance absorption signal which shows the collective behavior of magnetic spins without hyperfine splittings (with approximately isotropic Lande factor g= 2.040; which is close to g-value of the free electron 2.0023, and peak-to-peak line width = 515 G) at X-band is observed at room temperature as seen in the Figure 3.9. A value of about 2 for g is commonly expected from an S state ion like Mn^{2+} (S=5/2) [97].

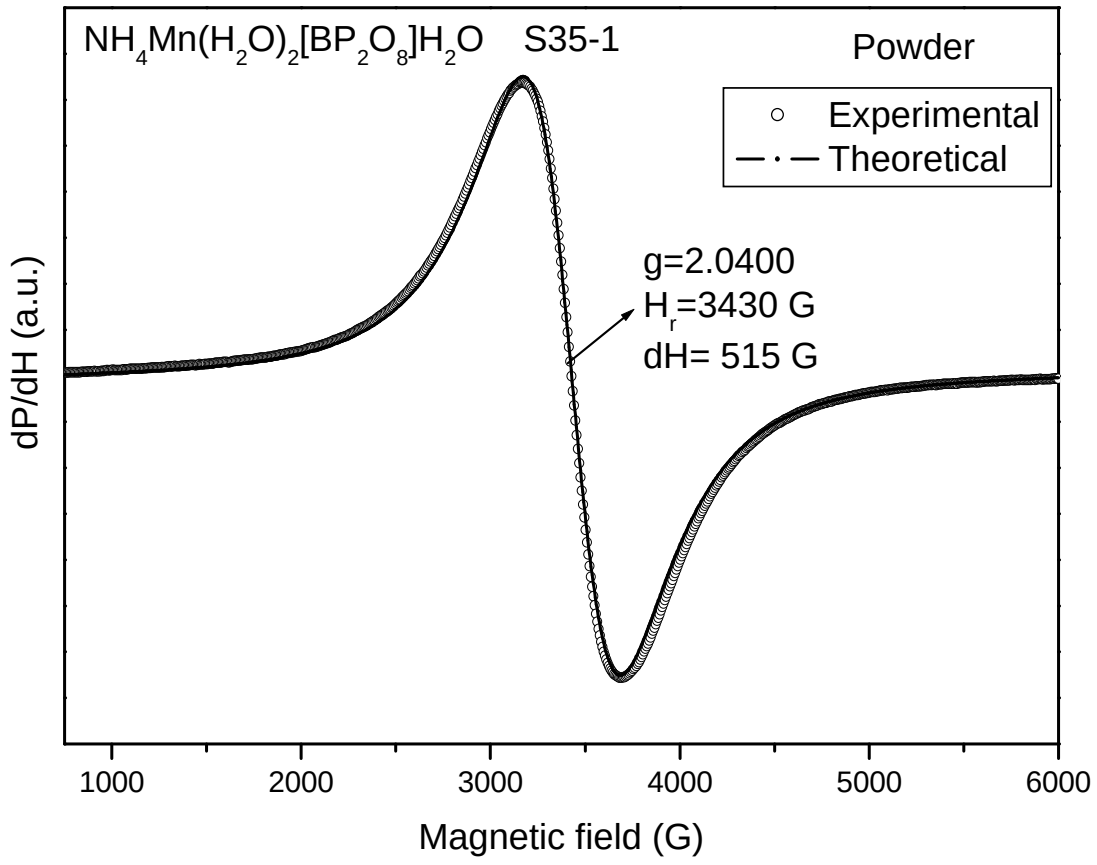

Figure 3.9 Room temperature ESR spectrum and computer simulation of Exp.35.

Normally, one should expect any electron paramagnetic (EPR) spectrum, coming from the transitions between the electronic magnetic states (|Ms>_|Ms_1>), to split into 6 hyperfine components separated about 90– 110G in field from each other. Since paramagnetic Mn^{2+} spins sees their own nuclear spins distributed randomly between 6 nuclear states from one ion to another, then each individual Mn^{2+} electronic spin in the sample would resonate independently from each other. If the intrinsic line width is larger than this splitting, then the six components overlap giving broader (at least 500-600 G) single line [97].

3.2.2 SEM Analysis

Morphology and microstructure of the product was investigated by SEM and micrographs are presented in Figure 3.10. There are highly faceted crystals in the form of elongated hexagonal bipyramids, Figure 3.10(a). These crystals have length in the range 2-5 μm and width in the range 1-2.5 μm. Overall, micrographs show the same polygon crystal form with different sizes, mostly as intergrown twins. In some parts spherical particles in the range 100-150 nm were observed that were beginning to sinter and probably fuse to already existing crystals, Figure 3.10(b). Since the growth takes place via the formation of these polygonic crystals it is hard to estimate a grain size for this system.

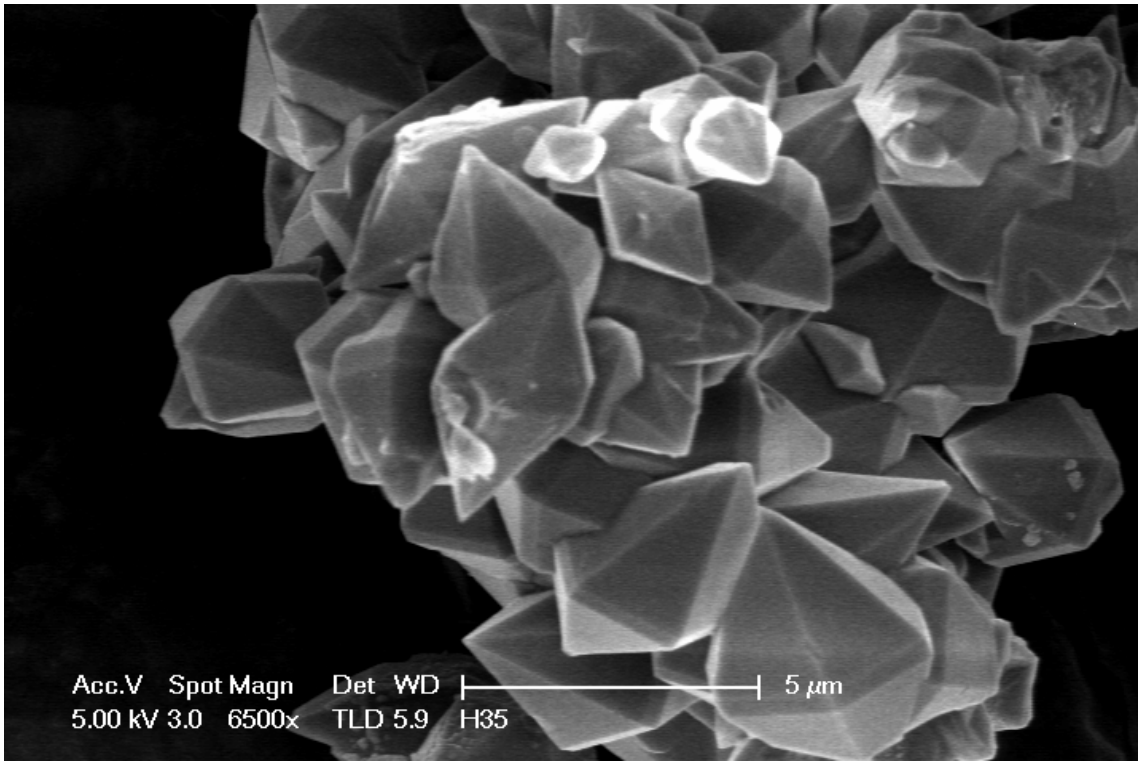

Figure 3.10a SEM photograph of the compound $(NH_4)_{0.5}Mn_{1.25}(H_2O)_2[BP_2O_8].0.5H_2O$ showing hexagonal unit cell by 6500 magnification.

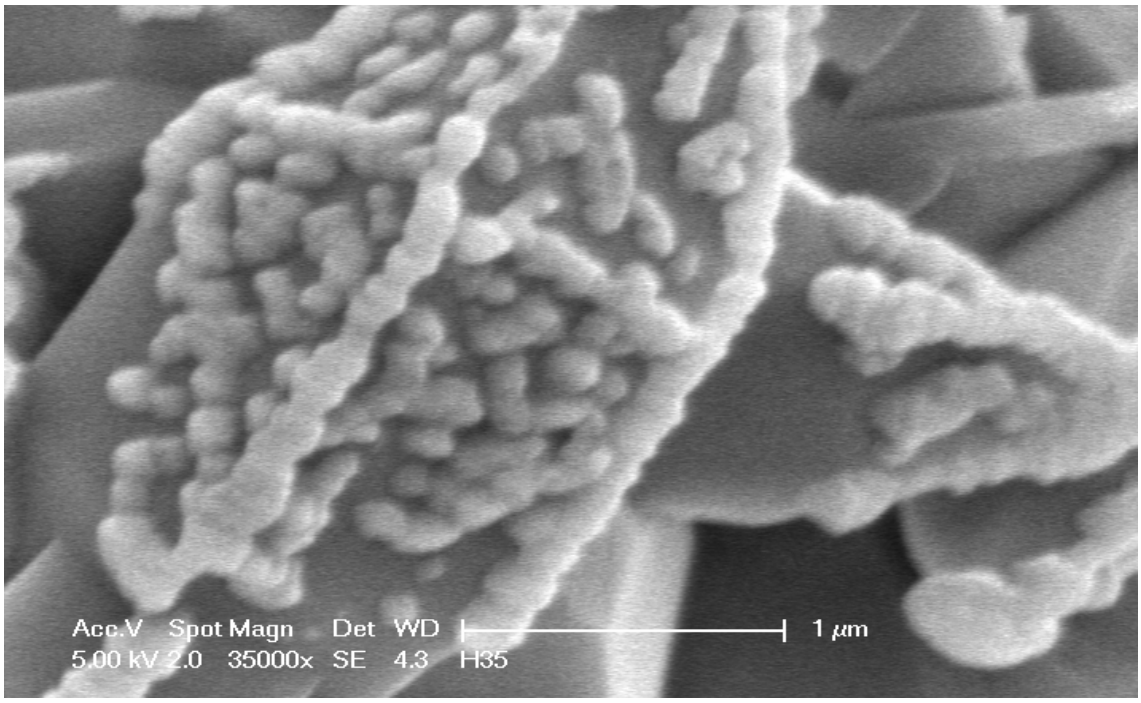

Figure 3.10b SEM photograph of the compound $(NH_4)_{0.5}Mn_{1.25}(H_2O)_2[BP_2O_8].0.5H_2O$ showing hexagonal unit cell by 35000 magnification.

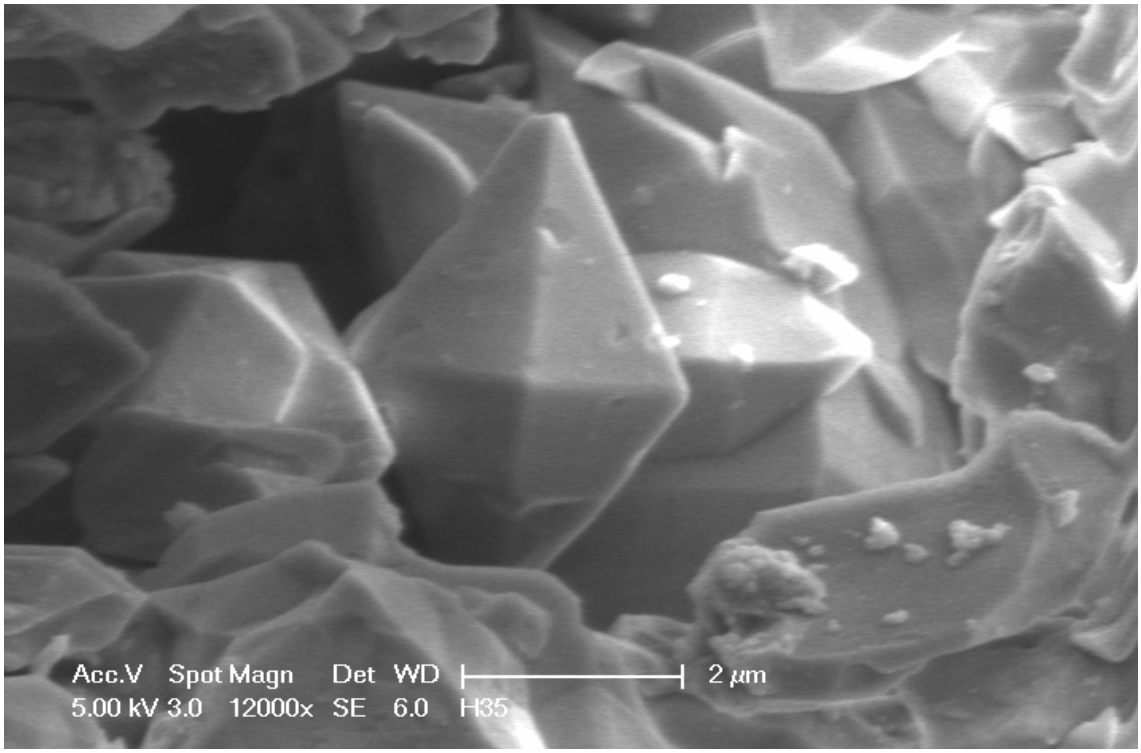

Figure 3.10c SEM photograph of the compound $(NH_4)_{0.5}Mn_{1.25}(H_2O)_2[BP_2O_8].0.5H_2O$ showing hexagonal unit cell by 12000 magnification.

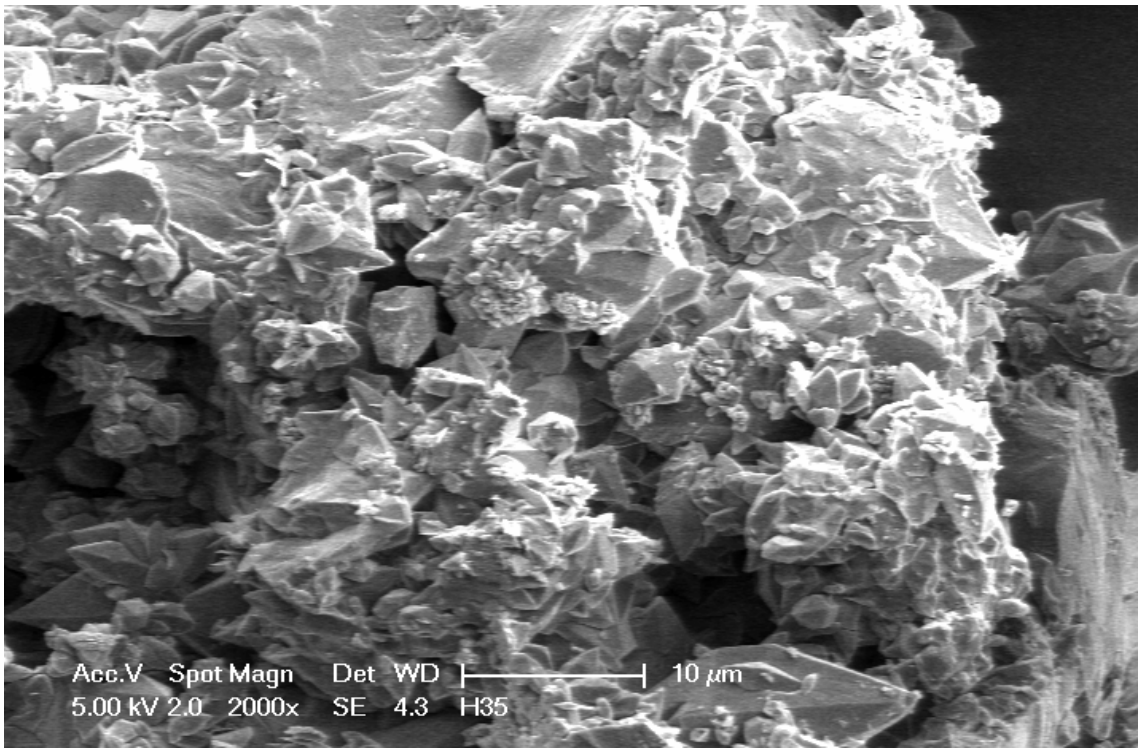

Figure 3.10d SEM photograph of the compound $(NH_4)_{0.5}Mn_{1.25}(H_2O)_2[BP_2O_8].0.5H_2O$ showing the structure with 2000 magnification.

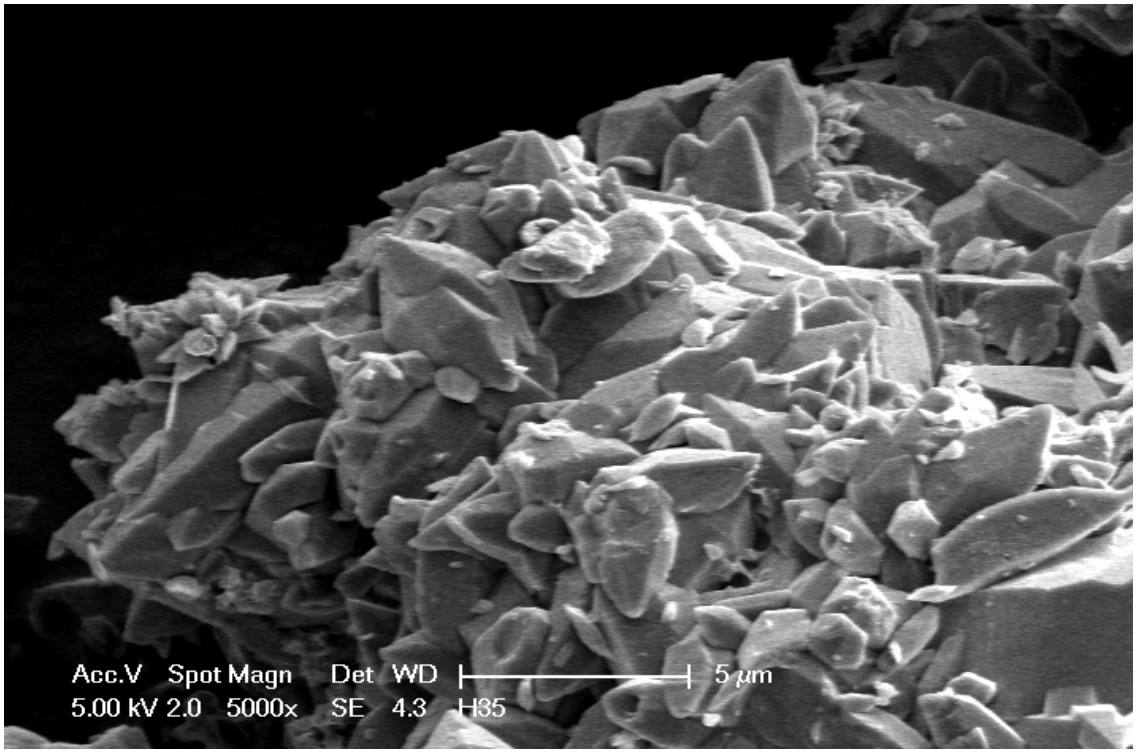

Figure 3.10e SEM photograph of the compound $(NH_4)_{0.5}Mn_{1.25}(H_2O)_2[BP_2O_8].0.5H_2O$ showing a nice morphology of hexagonal structures with 5000 magnification.

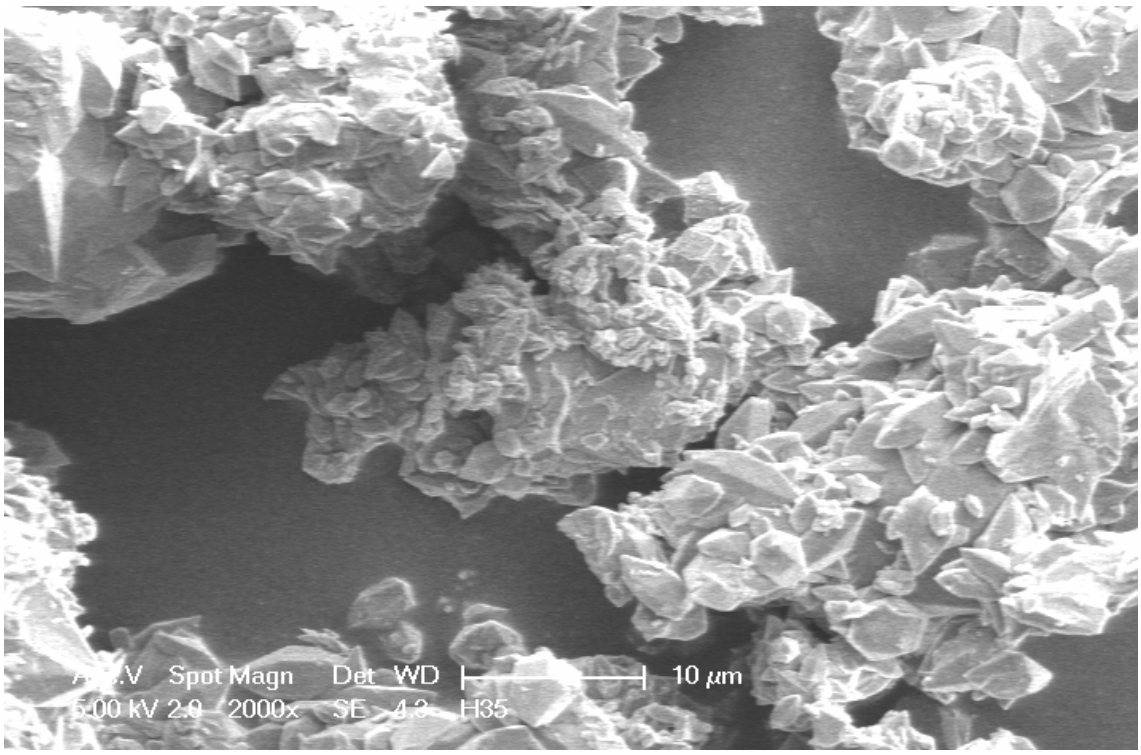

Figure 3.10f SEM photograph of the compound $(NH_4)_{0.5}Mn_{1.25}(H_2O)_2[BP_2O_8].0.5H_2O$ with 2000 magnification.

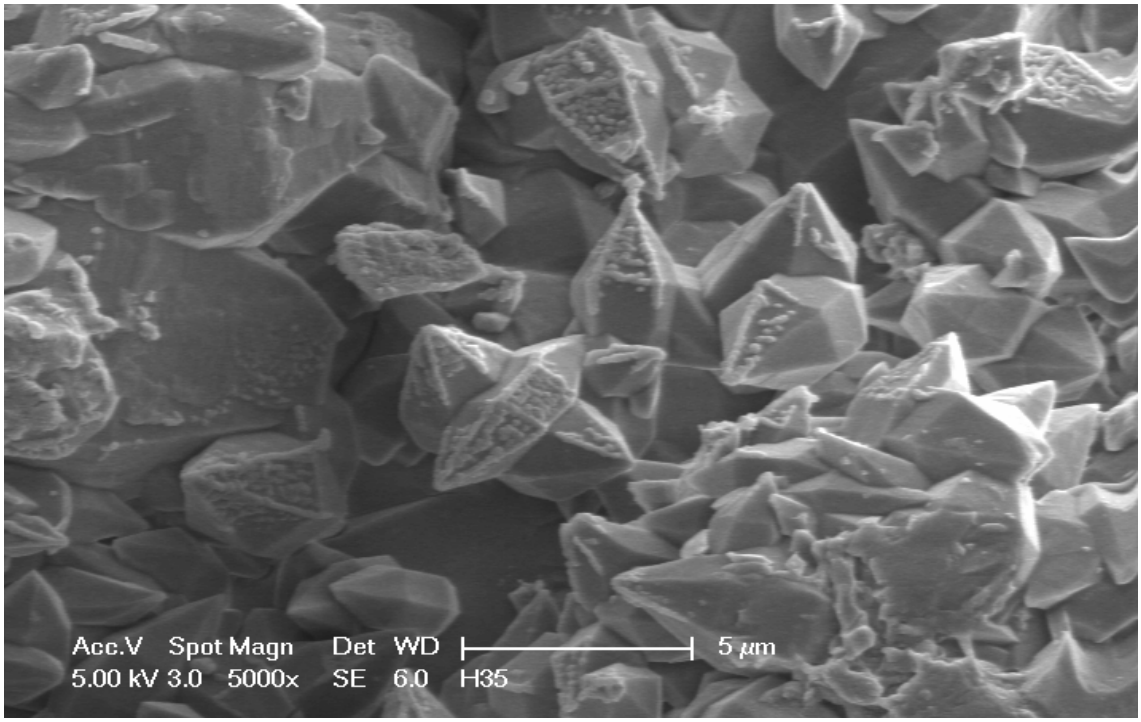

Figure 3.10g SEM photograph of the compound $(NH_4)_{0.5}Mn_{1.25}(H_2O)_2[BP_2O_8].0.5H_2O$ with 5000 magnification.

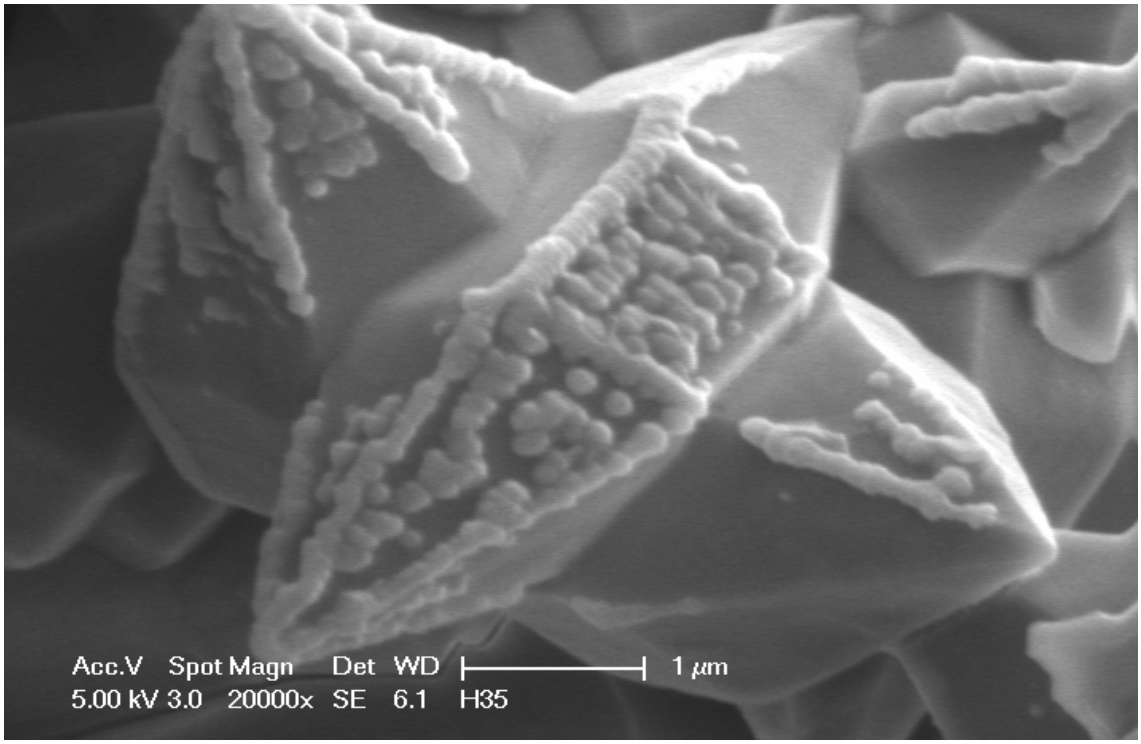

Figure 3.10h SEM photograph of the compound $(NH_4)_{0.5}Mn_{1.25}(H_2O)_2[BP_2O_8].0.5H_2O$ showing hexagonal structure with nanoparticles.

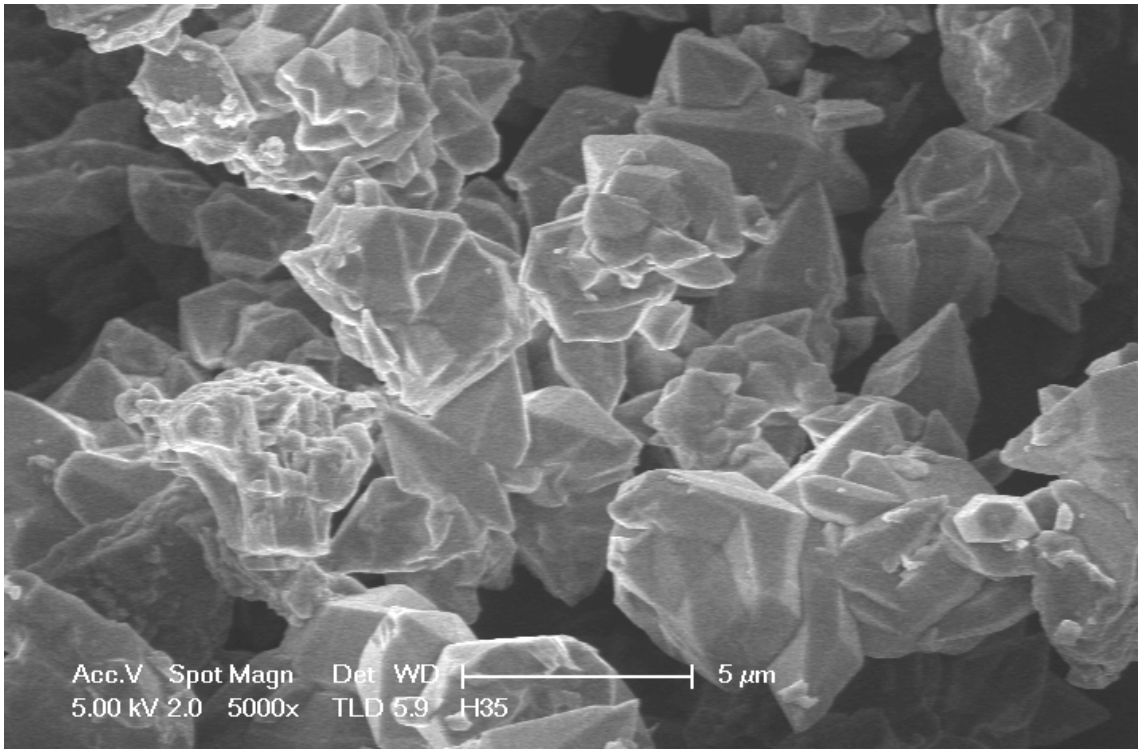

Figure 3.10i SEM photograph of the compound $(NH_4)_{0.5}Mn_{1.25}(H_2O)_2[BP_2O_8].0.5H_2O$ with 5000 magnification.

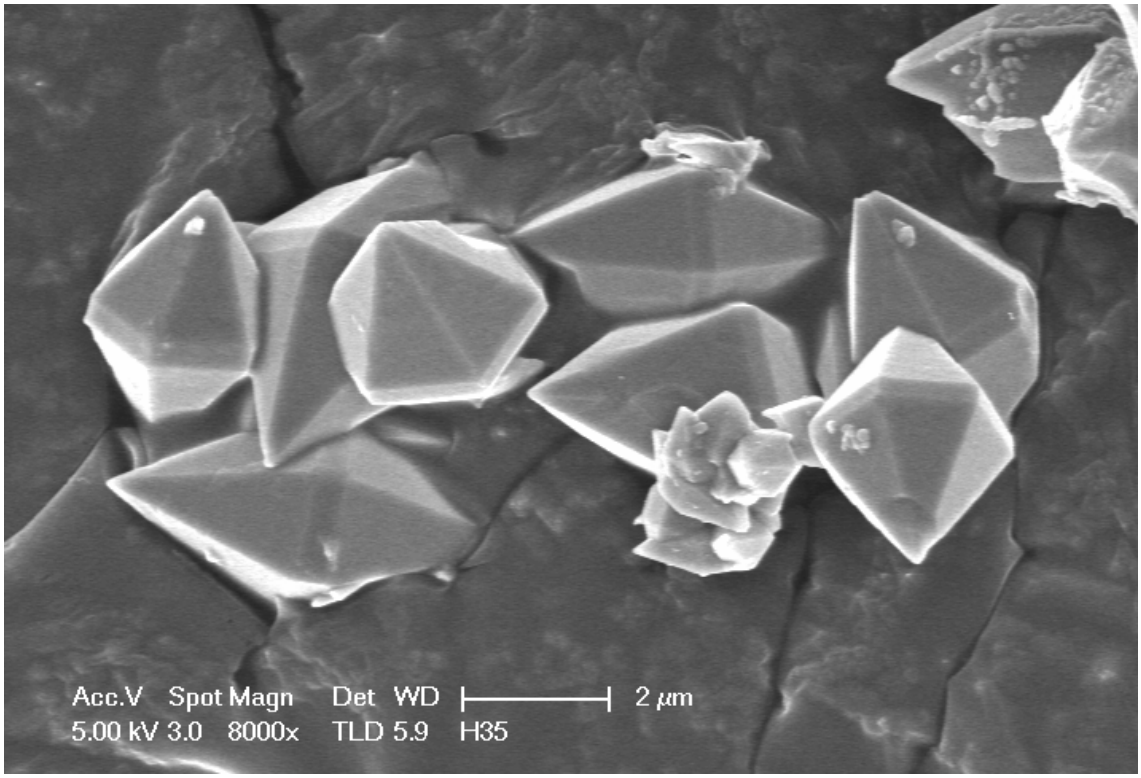

Figure 3.10j SEM photograph of the compound $(NH_4)_{0.5}Mn_{1.25}(H_2O)_2[BP_2O_8].0.5H_2O$ with 8000 magnification.

3.2.3 Thermal Gravimetric Analysis

The thermal stabilities of compounds were analyzed with thermogravimetric analysis (TGA) and is shown in Figure 3.11. Thermal dehydrations of the compound takes place in several steps. In the first step evaporation of adsorbed water is observed around 100 ^{o}C. Around 270 ^{o}C crystalline water and 1 mol water coordinated to metal center were released, thereafter the last mole of water in the coordination was lost at 360 ^{o}C. The final loss around 560 ^{o}C is assigned to the decomposition of ammonia in the structure.

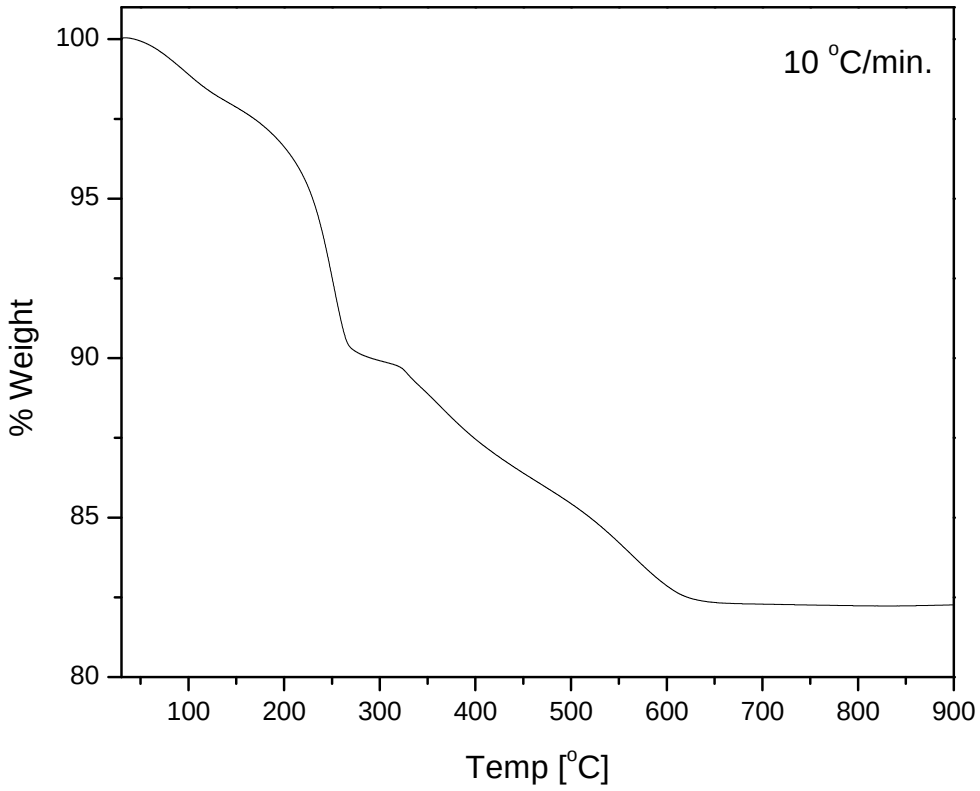

Figure 3.11 TGA analysis showing the thermal behavior of $(NH_4)_{0.5}Mn_{1.25}(H_2O)_2[BP_2O_8]\cdot 0.5H_2O$.

3.3 Na–Mn-As–B–O-H CONTAINING COMPOUND

The products of Exp.73 and 73a are summarized in Table 3.7.

Table 3.7 Products of Exp.73, 73a.

Exp. No	Product
73	$NaMnB_xAs_yO_z$
73a	$BAsO_4$ (03-0314)

The presence of Na and Mn in the product of Exp.73 was confirmed qualitatively. The results of ICP analysis showed that the product of Exp.73 contains B, As and Mn (Table 3.8) also. In order to perform ICP analysis the sample was dissolved in aqua regia. By using these results the closed formula of the product of Exp.73 can be written as $NaMnB_xAs_yO_z$.

The XRD powder pattern of the product of Exp.73 is given in Figure 3.12. According to the XRD powder pattern the characterization studies were done. The XRD pattern verifies that the parameters of the product do not match with any known compound in the literature. FTIR spectrum of product of Exp.73 is given in Figure 3.13. FTIR spectrum shows the presence of peaks around 471 cm^{-1} $\nu_2(BO_4)$, 554 cm^{-1} $\upsilon_4(BO_4)$, 724 cm^{-1} υ_3 $(BAsO_4)$, 816 cm^{-1} $\upsilon_1(AsO_4)$, 850 (B-O-As), 1035 υ_3 (BO_4).

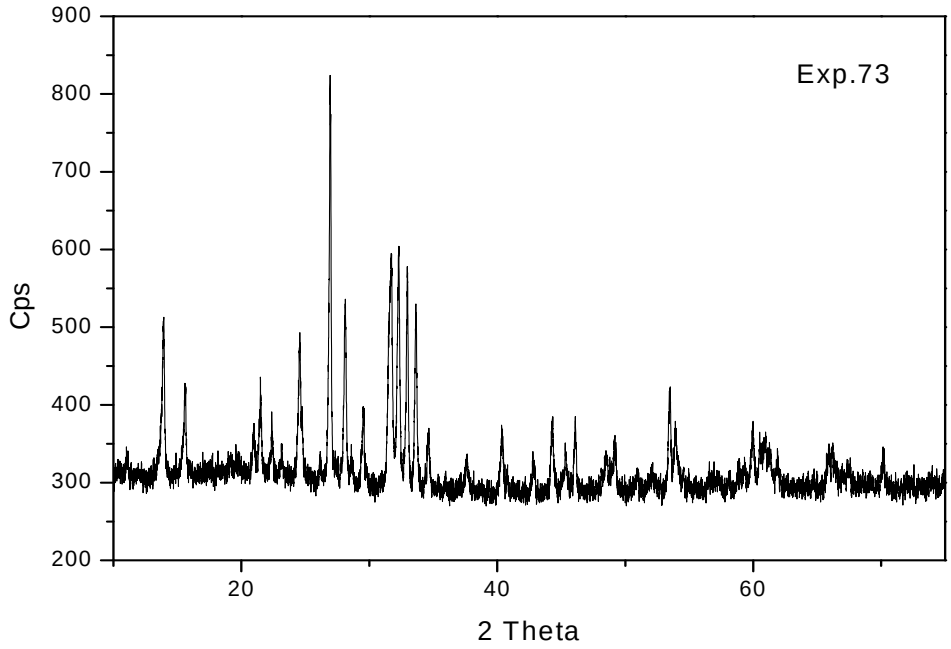

Figure 3.12 The XRD powder pattern of the product of Exp.73.

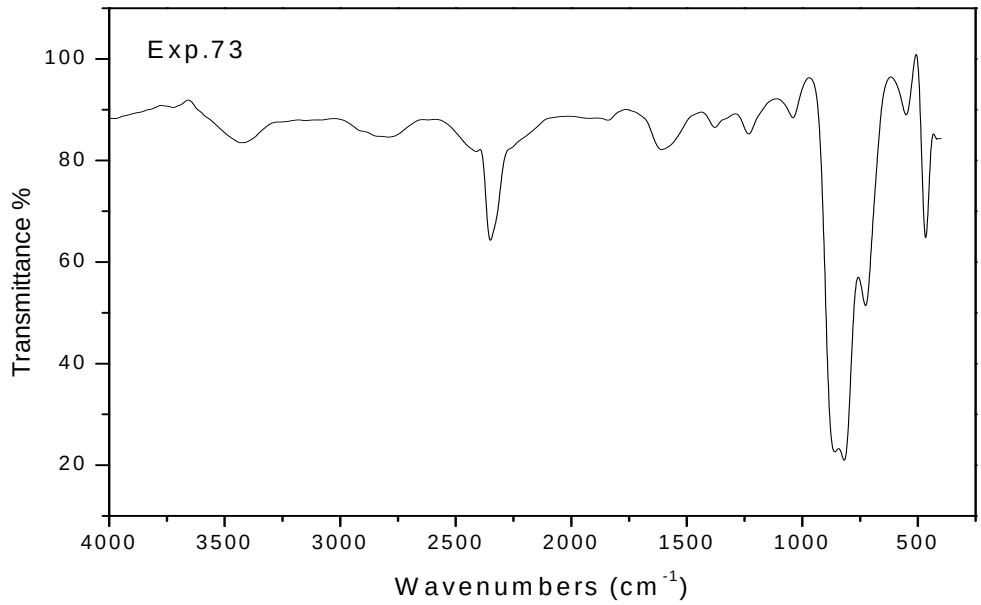

Figure 3.13 The FTIR spectrum of the product of Exp.73.

Table 3.8 ICP results of the product of Exp.73.

Manganese %	**Arsenic %**	**Boron %**
9.3	5	0.13

3.4 Na–Co-As–B–O-H CONTAINING COMPOUND

For the synthesis of $NaCo(H_2O)_2[BAs_2O_8].H_2O$ compound, five experiments were done at different conditions as given in section 2.3.8. The products of these experiments (Exp. 61, 61a, 71, 71a and 71b) are given in below table (Table 3.9).

Table 3.9 Products of Exp.61, 61a.

Exp. No	**Product**
61	$BAsO_4$
61a	$BAsO_4$
71	$NaCoB_xAs_yO_z$
71a	$NaCoB_xAs_yO_z$
71b	$NaCoB_xAs_yO_z$

For the product of Exp.61, qualitative cobalt analysis was showed the presence of Co in it. XRD powder pattern of Exp.61 (Figure 3.14) showed that the major product was $BAsO_4$ (denoted by black point) and minor product was Co containing compound (denoted by arrow).

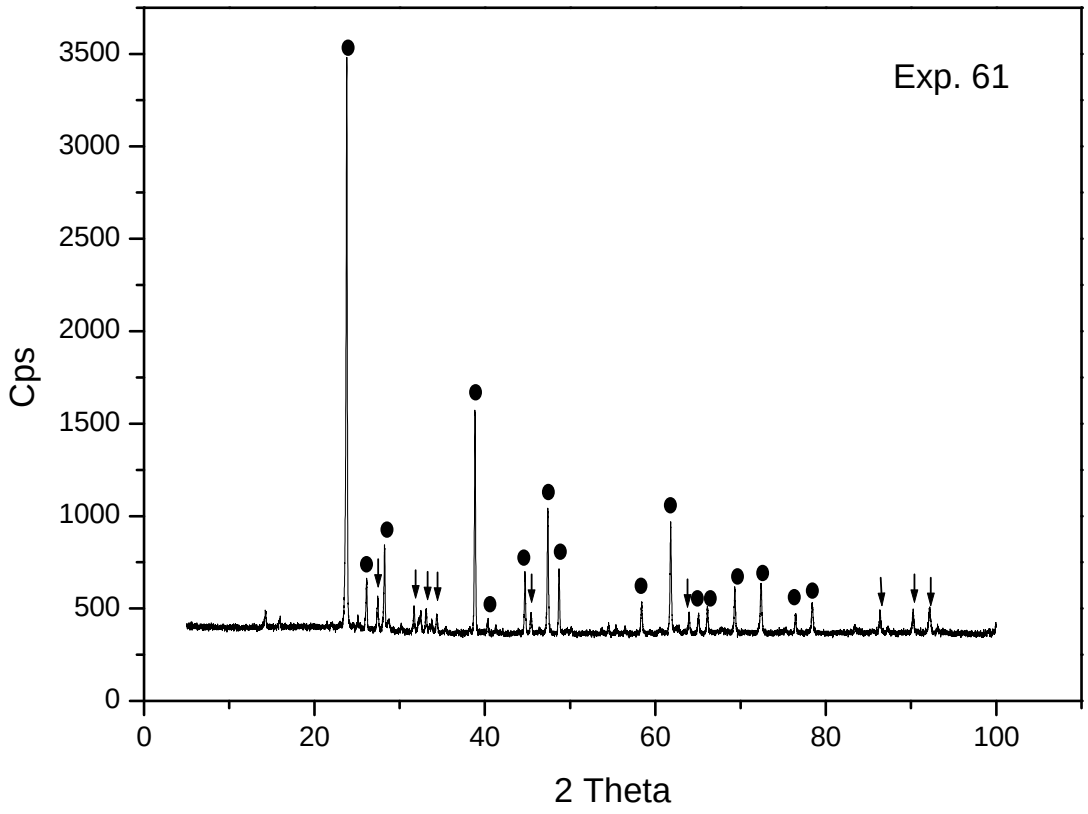

Figure 3.14 The XRD powder pattern of the product of Exp.61.

The XRD powder patterns of Exp.71, 71a, 71b were given in Figure 3.15. According to these XRD powder patterns, products of Exp.71, 71a, 71b are exactly the same. Unfortunately crystal structure investigation of this product was failed due to the lack of single crystal product. But our investigations on the single crystal synthesis of these compounds are going on.

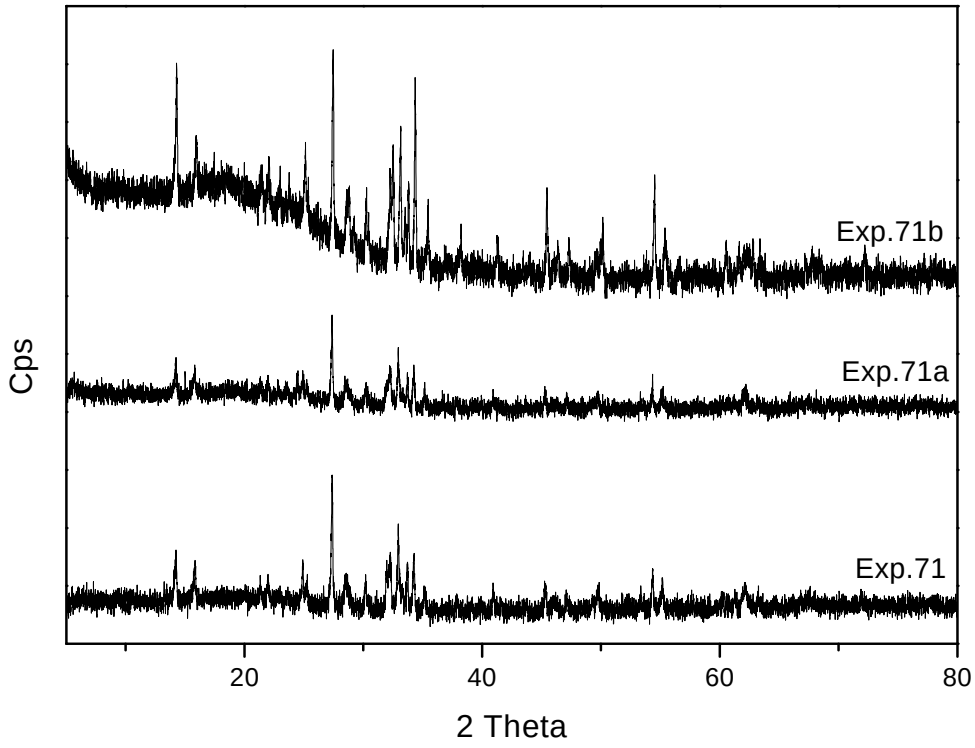

Figure 3.15 The comparison of XRD powder patterns of the products of Exp.71, 71a, 71b.

The product of Exp.71 was analyzed by ICP. This analysis showed the presence of Co, As, B in the product. Results are summarized in Table 3.10. In order to perform ICP analysis the sample was dissolved in aqua regia. The presence of Na in the product was proved qualitatively.

Table 3.10 ICP analysis results of the product of Exp.71.

Cobalt %	**Sodium %**	**Arsenic %**	**Boron %**
22.3	7.55	0.4	0.24

The FTIR spectra (Figure 3.16) of the reaction products were collected to confirm the presence of B-O and AsO_4^{-3}. Three spectra verify the presence of AsO_4^{-3} (ν_1= 808 cm^{-1}, ν_2= 737 cm^{-1}) [36] and BO_3^- (Table 3.11). The band around 3500 cm^{-1} is assigned as O-H stretching mode of water [14]. An unambiguous peak assignment of the modes in the lower range could not be made.

Table 3.11 The FTIR frequencies for Exp.71, 71a, 71b [98-100].

Assignments	**Frequency (cm^{-1})**
ν_3 (BO_3)	1232
ν_1 (BO_3)	1067
ν_2 (BO_3)	714

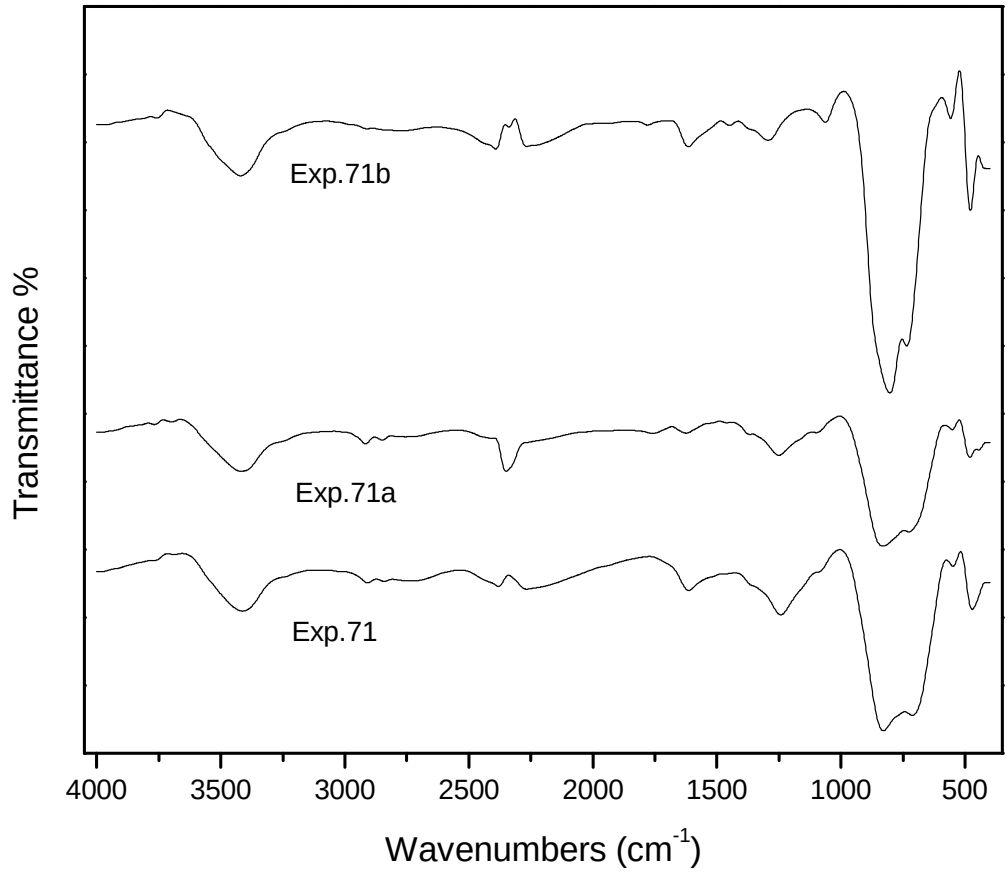

Figure 3.16 The comparison of FTIR spectra of the products of Exp.71, 71a, 71b.

According to the above explanations, closed formula of the products (Exp.71, 71a, 71b) can be given as $NaCoB_xAs_yO_z$.

3.5 Na–Zn-As–B–O-H CONTAINING COMPOUND

The results of the Exp. 64, 64a, 72, 72a, 72b are summarized in Table 3.12.

Table 3.12 Products of Exp.64, 64a, 72, 72a, 72b.

Exp. No	Product
64	$BAsO_4$
64a	$BAsO_4$
72	$NaZnB_xAs_yO_z$
72a	$NaZnB_xAs_yO_z$
72b	$NaZnB_xAs_yO_z$

Qualitative elemental analysis (Na, Zn) for Exp. 64 and 64a showed the absence of Zn and Na in the product. During washing process, compounds containing Na and Zn dissolved and discarded.

All lines in XRD pattern of product of Exp.64 and 64a match very well with the line of $BAsO_4$ (JCPDS Card No: 03-0314) (Figure 3.17).

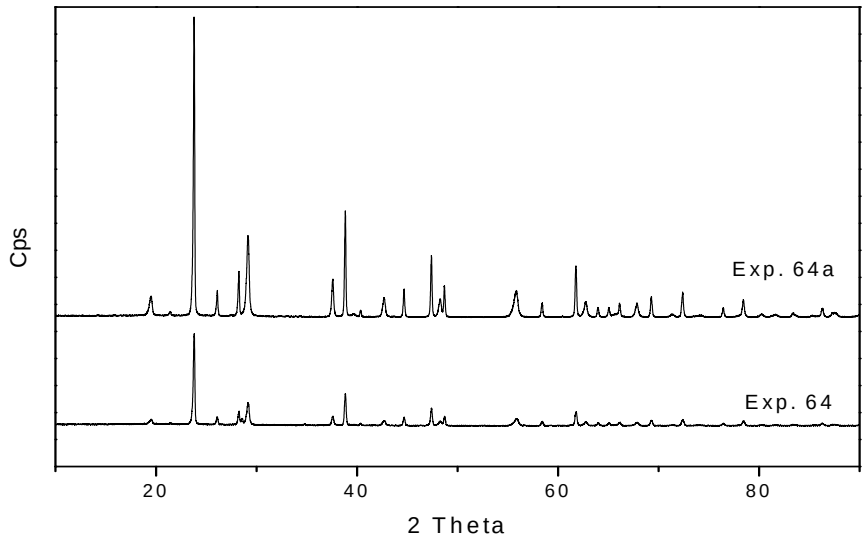

Figure 3.17 The comparison of XRD powder patterns of the products of Exp.64, 64a.

The ICP analysis result of Exp.73 is given in Table 3.13. In order to perform ICP analysis the sample was dissolved in aqua regia. By using these results the closed formula of the products can be written as $NaZnB_xAs_yO_z$.

Table 3.13 ICP analysis results of the product of Exp.73.

Zinc %	Arsenic %	Boron %
15	4.6	0.0076

Due to the lack of single product, assignment of correct chemical formula could not be done. But the experiments on the single crystal synthesis of this compound are continuing.

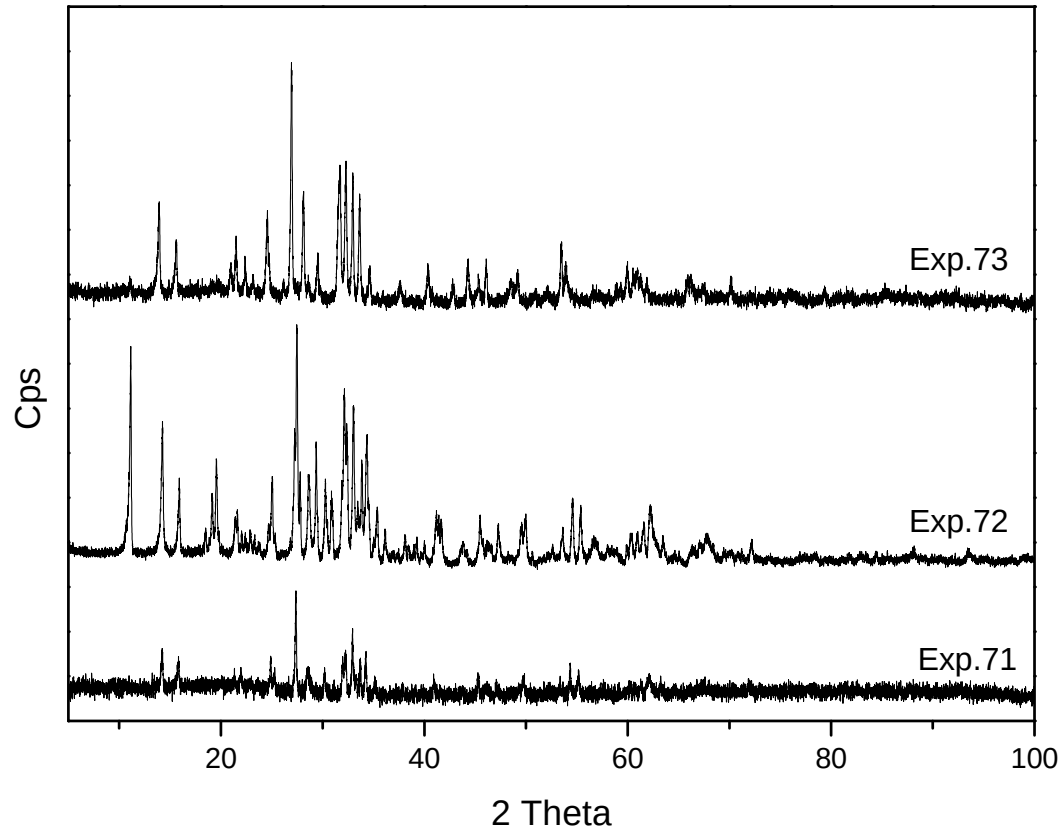

Figure 3.18 The comparison of XRD powder patterns of the products of Exp.71, 72, 73.

The FTIR investigation of product of Exp. 71, 72 and 73 revealed that in all FTIR spectra, BO_3 and AsO_4^{3-} functional groups are present.

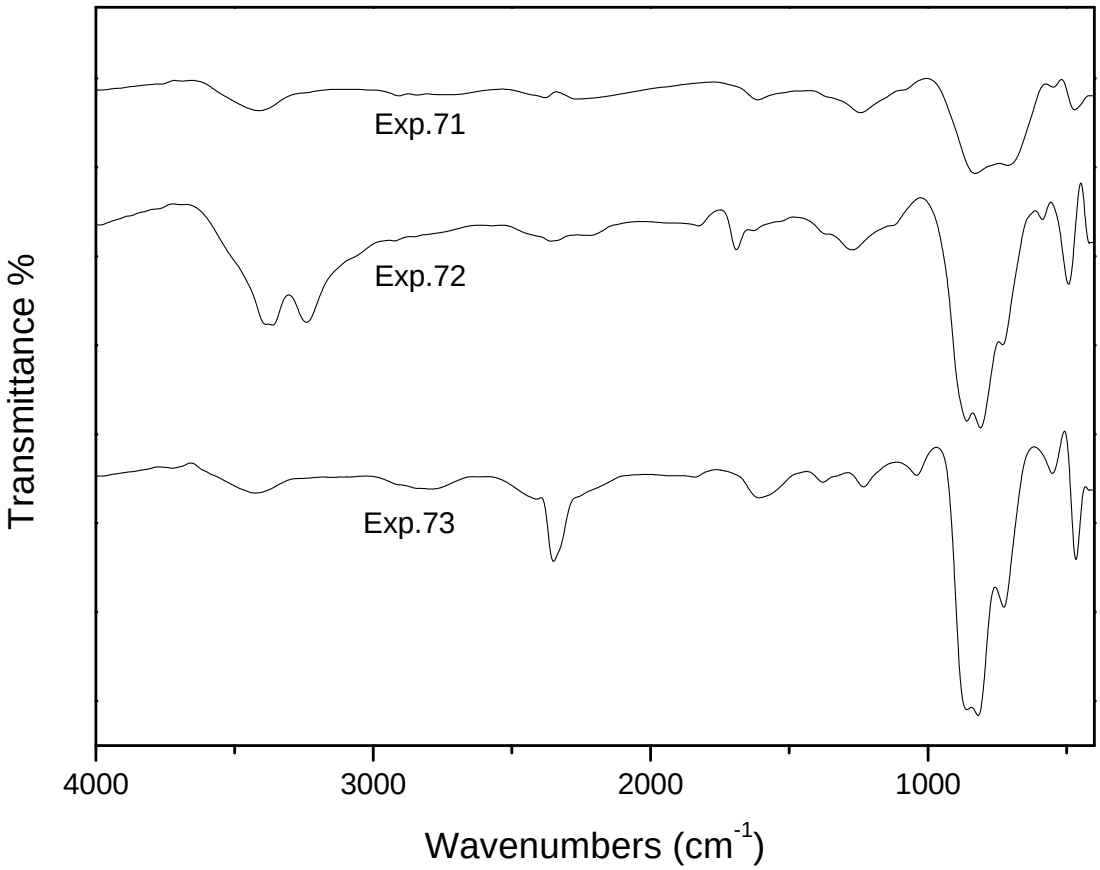

Figure 3.19 The comparison of FTIR spectra of the products of Exp.71, 72, 73.

In conclusion; according to the XRD and FTIR spectrums (Figure 3.18, Figure 3.19) the products of experiments 73, 71, 71a, 71b, 72, 72a, 72b are same. They all have the same formula of $NaMB_xAs_yO_z$ (M=Zn, Mn, Co).

3.6 H–Co-P–B–O CONTAINING COMPOUND

Actually, we tried to obtain $(NH_4)_{0.5}Co_{1.25}(H_2O)_{1.5}[BP_2O_8].H_2O$ other than Exp.26, 38, and 38a just by changing the reactants. But we obtained completely different product which was $(H)_{0.5}Co_{1.25}(H2O)_{1.5}[BP_2O_8].H_2O$. On the base of the literature survey, we understood that this titled compound was previously synthesized by Ayşen et al [81] through hydrothermal method. We just compared the d-values of our product (Figure 3.20) with that of Ayşen's product. Also, qualitative Co analysis was done and its presence was observed.

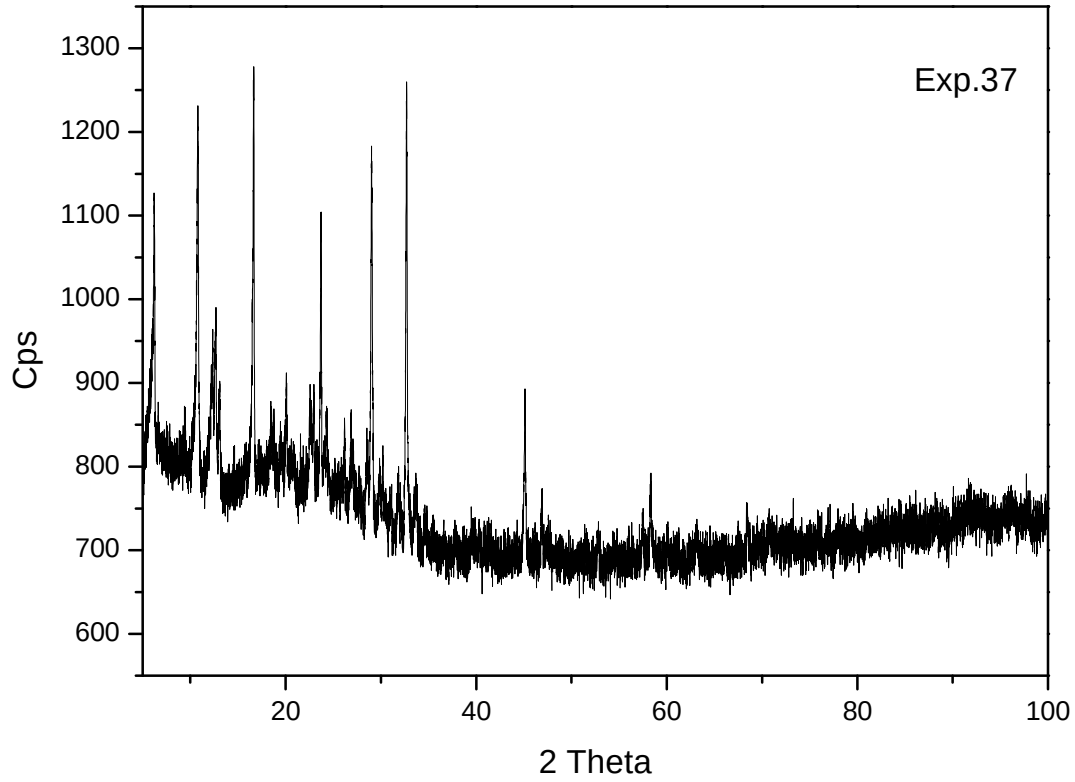

Figure 3.20 The XRD powder pattern of the product of Exp.37.

3.7 Li–Mn-P–B–O-H CONTAINING COMPOUND

Unfortunately, all experiments related with the synthesis of $LiMn(H_2O)_2[BP_2O_8].H_2O$ were failed (Table 3.14). All the products are only BPO_4 (JCPDS Card No: 34-0132) (Figure 3.21). Most probably metal ions were discarded during hot water washing treatment.

Table 3.14 Products of Exp.70, 70a, 70b, 59, 59a.

Exp. No	Product
70	BPO_4
70a	BPO_4
70b	BPO_4
59	BPO_4
59a	BPO_4

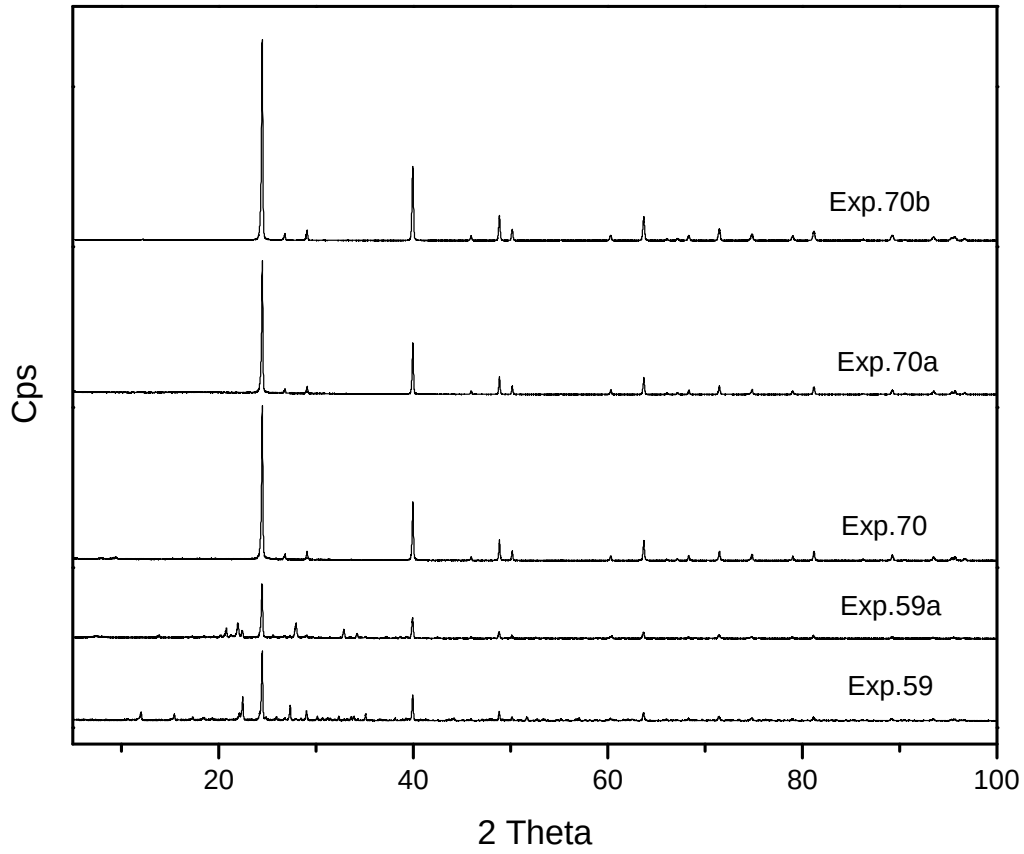

Figure 3.21 The comparison of XRD powder patterns of the products of Exp.59, 59a, 70, 70a, 70b.

3.8 Li-Cd-As-B-O-H CONTAINING COMPOUND

The products of Exp.75 and 75a are summarized in Table 3.15. Their XRD pattern (Figure 3.22) match completely with Li_3AsO_4 (JCPDS Card No: 13-432). The qualitative analysis proves us that there is no cadmium and boron in the products.

Table 3.15 Products of Exp.75, 75a.

Exp. No	Product
75	Li_3AsO_4
75a	Li_3AsO_4

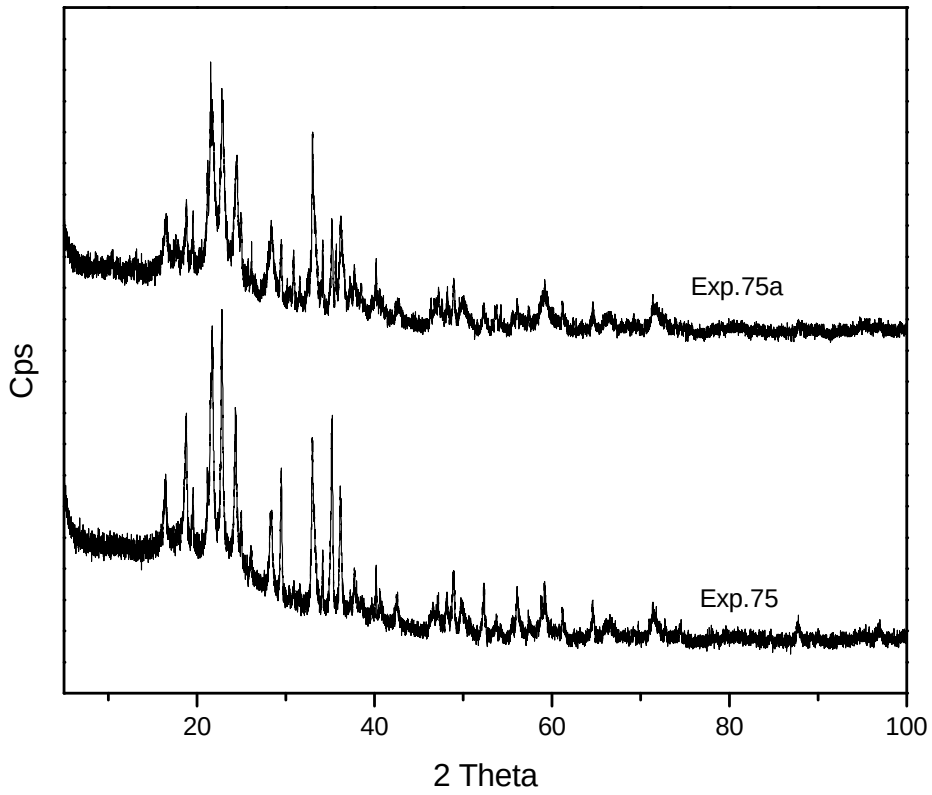

Figure 3.22 The comparison of XRD powder patterns of the products of Exp.75, 75a.

The FTIR spectra of Exp.75 and 75a are given in Figure 3.23. According to FTIR, the presence of AsO_4^{-3} (850 cm^{-1}) and OH^- (3588 cm^{-1}) in the sample was confirmed. In addition to this, the presence of Cadmium in the samples was also confirmed qualitatively.

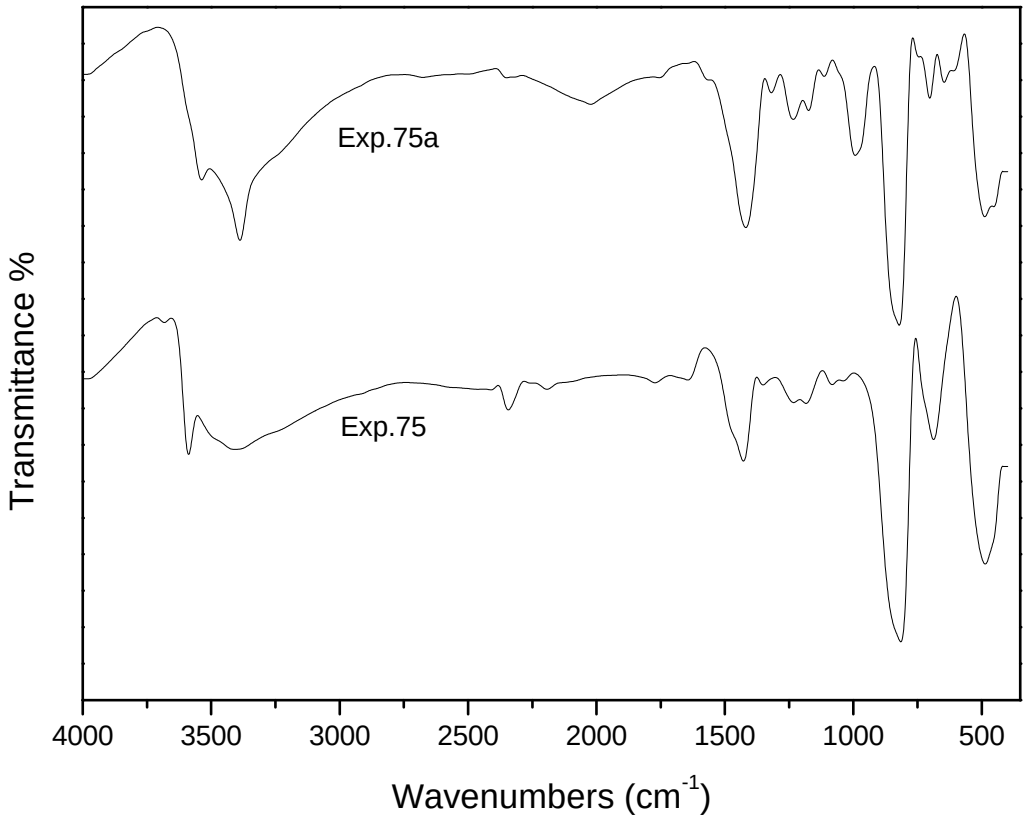

Figure 3.23 The comparison of FTIR spectra of the products of Exp.75, 75a.

3.9 Cr-B-P-O-H CONTAINING COMPOUND

$Cr(H_2O)_2[BP_2O_8].H_2O$ compound could not be synthesized although it was our main goal in this section. Instead of this compound, we obtained well-known borophosphate compound, BPO_4 (JCPDS Card No: 34-0132) (Figure 3.24).

The products of the compounds that were synthesized in Exp.50 and 51 are listed in Table 3.16.

Table 3.16 Products of Exp.50, 51.

Exp. No	Product
50	BPO_4
51	BPO_4

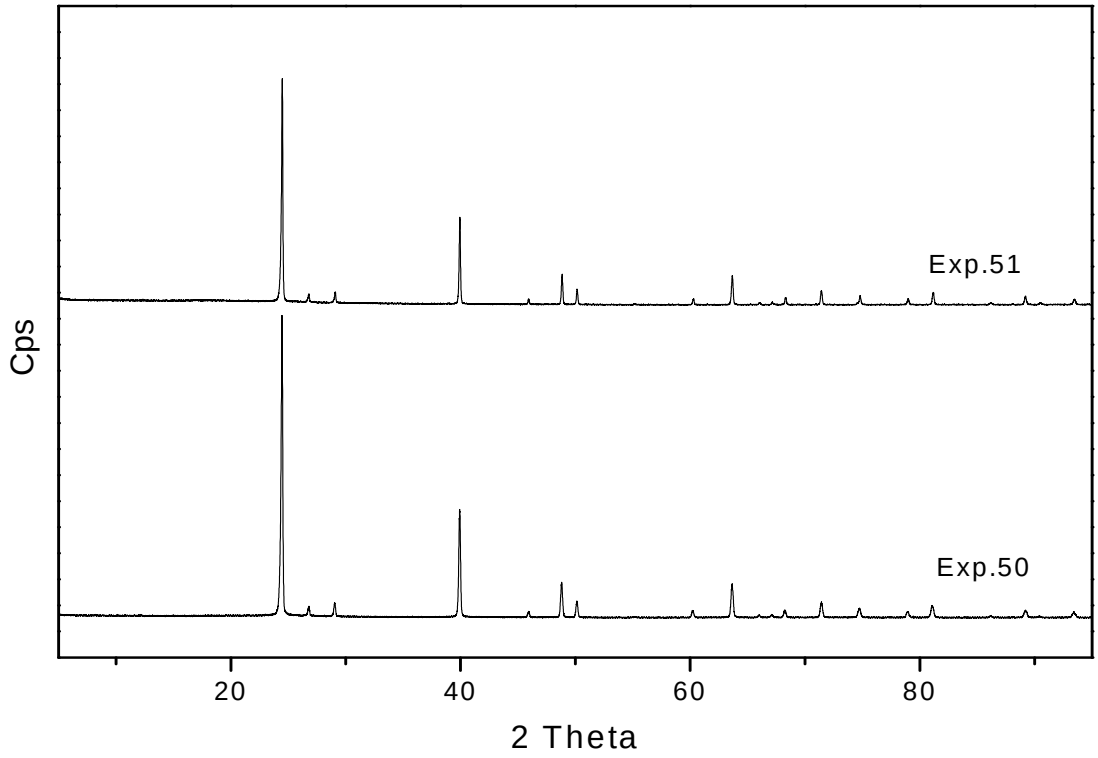

Figure 3.24 The comparison of XRD powder patterns of the products of Exp.50, 51.

3.10 Fe-B-P-O-H CONTAINING COMPOUND

Table 3.17 Products of Exp.53.

Exp. No	Product
53	$NH_4Fe(III)[BP_2O_8(OH)]$

The hydrothermal reaction of $FeCl_2.4H_2O$, H_3BO_3 and $(NH_4)_2HPO_4$ did not give the expected product $Fe(H_2O)_2[BP_2O_8].H_2O$ as given in the experimental section 2.3.10. According to the investigations that were done during this study, it was identified that the product of Exp.53 (Table 3.17) was isostructural with the compound, $NH_4Fe(III)[BP_2O_8(OH)]$, which has already been synthesized by M. Kritikos et. al. in 2001 [9].

The peaks in FTIR spectra (Figure 3.25) were observed at (cm^{-1}); 980, 1065, 1124, 1444, 3170, 3240. Stretching and bending frequencies of B-O and P-O groups are

observed up to 1445 cm^{-1}. The band at 3240 cm^{-1} was assigned as a O-H stretching mode. An unambiguous peak assignment of the modes in the lower range could not be made.

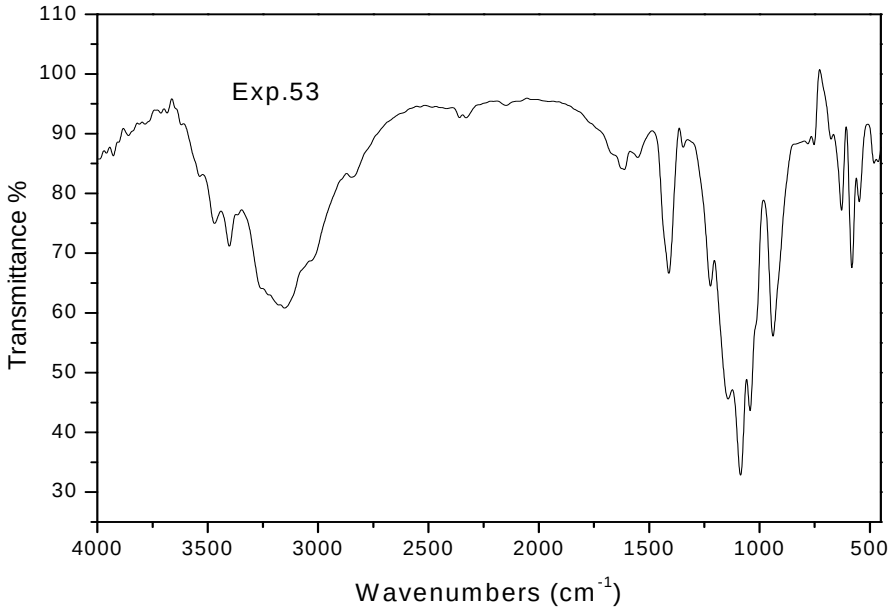

Figure 3.25 The FTIR spectrum of the product of Exp.53.

The XRD powder pattern of Exp.53 shows also similarity with that of the compound $NH_4Fe(III)[BP_2O_8(OH)]$ (Figure 3.26).

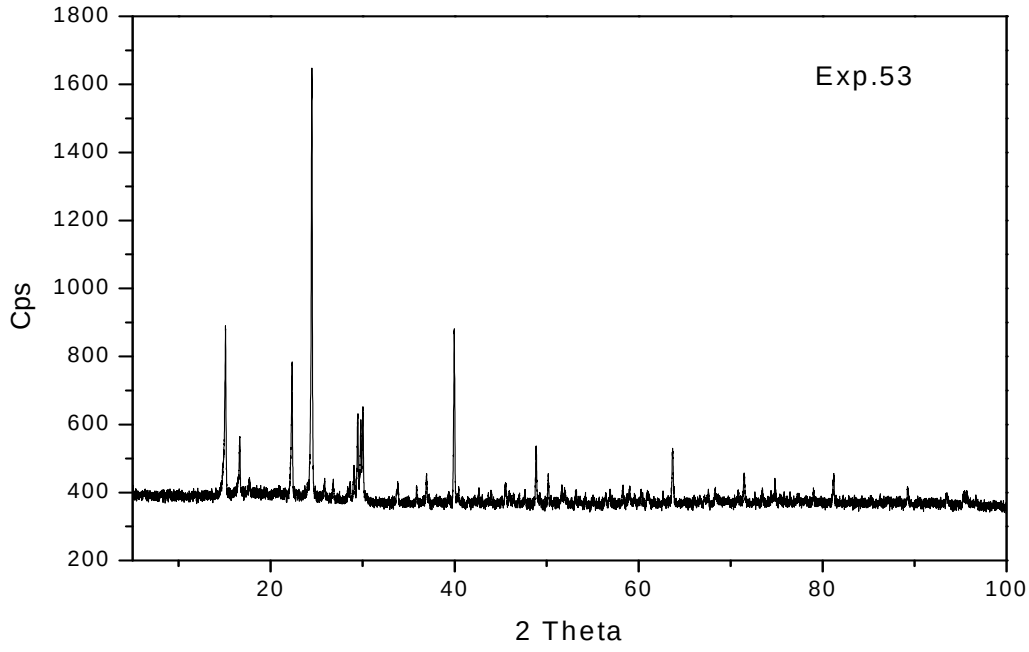

Figure 3.26 The XRD powder pattern of the product of Exp.53.

The products of experiments 48, 48-1, 48-2, 48-3 are listed in Table 3.18. $Fe_2BP_3O_{12}$ was synthesized by solid state method as explained in section 2.3.13.

Table 3.18 Products of Exp.48, 48-1, 48-2, 48-3.

Exp. No	Product
48	$Fe_2BP_3O_{12}$
48-1	$Fe_2BP_3O_{12}$
48-2	$Fe_2BP_3O_{12}$
48-3	$Fe_2BP_3O_{12}$

The FTIR band frequencies of $Fe_2BP_3O_{12}$ are as; 1427, 1386, 1193, 1081, 989, 898, 633, 600, 523 in cm^{-1} as shown in Figure 3.27.

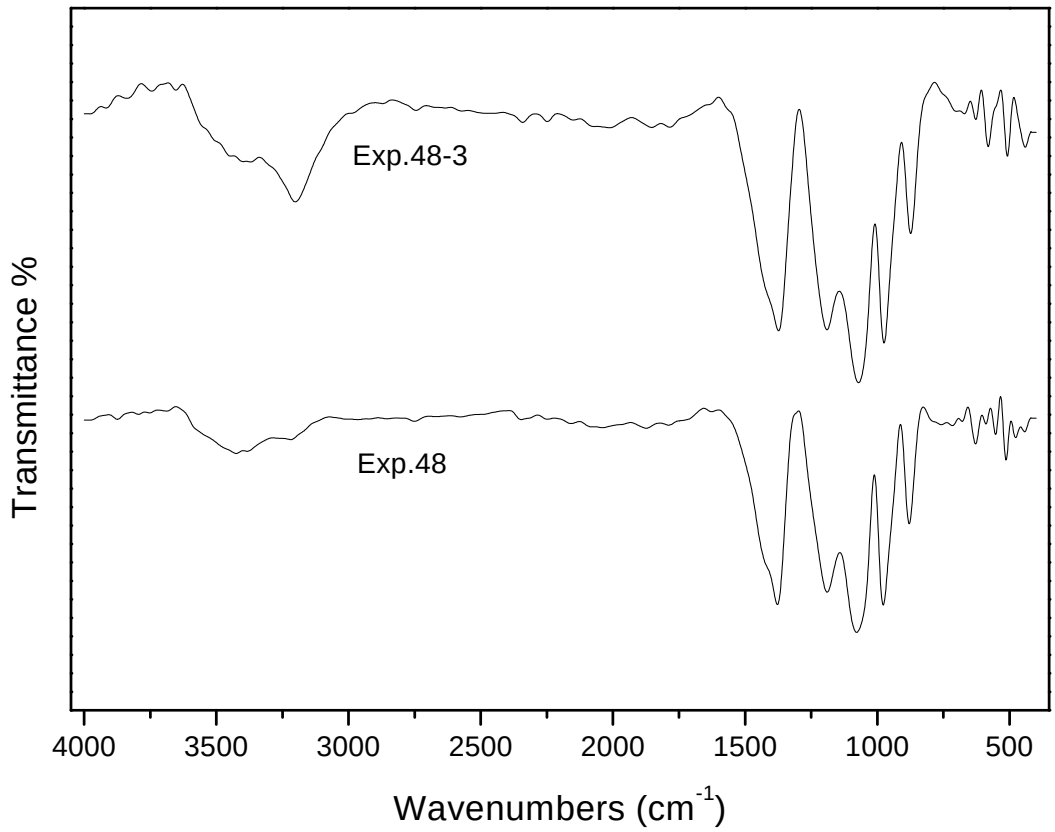

Figure 3.27 The comparison of FTIR spectra of the products of Exp.48, 48-3.

The XRD pattern of the product of Exp.48 and 48-3 are given in Figure 3.28.

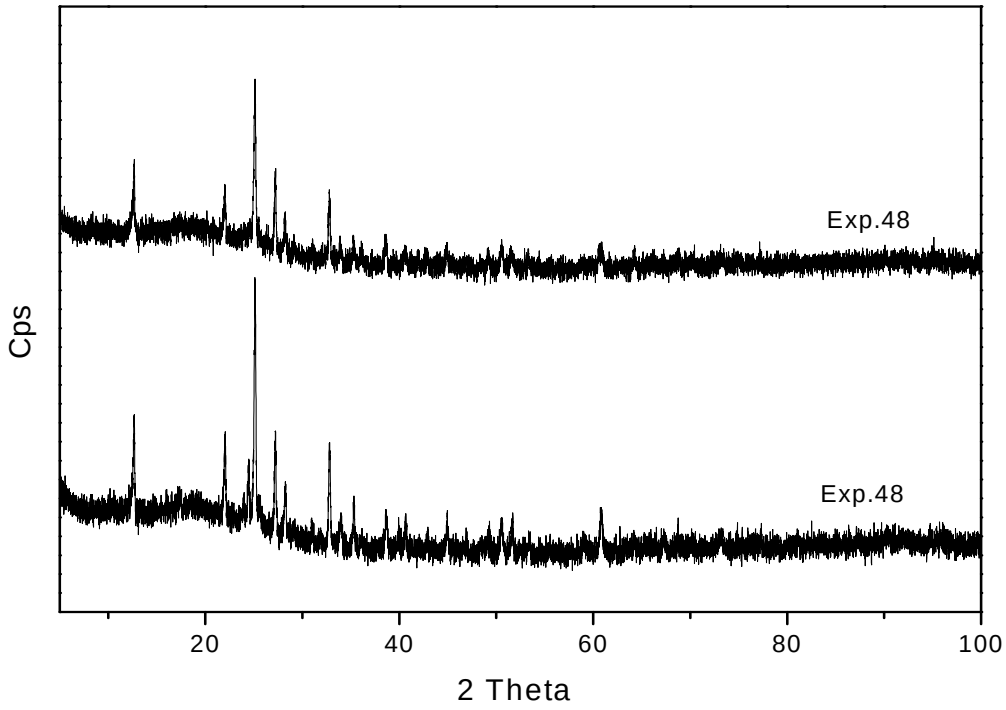

Figure 3.28 The comparison of XRD patterns of the products of Exp.48, 48-3.

The compounds $M_3BP_3O_{12}$ (such as $Ba_3[BP_3O_{12}]$ [98], $Pb_3[BP_3O_{12}]$ [101] and $Sr_3[BP_3O_{12}]$ [98]) in which cation was alkaline metal, has corner shared BO_4 and PO_4 tetrahedra in orthorhombic crystal structure. For $Fe_2BP_3O_{12}$, $[BP_3O_{12}]$ is built up by central trigonal planar BO_3 group sharing common corners with three phosphate tetrahedral in trigonal crystal structure.

Compound $Fe_2BP_3O_{12}$, which has also been synthesized by S.Tuncel, is isostructural with $Cr_2BP_3O_{12}$ which was synthesized by Mi et al [102]. Cell parameters of $Fe_2BP_3O_{12}$, $Cr_2BP_3O_{12}$, and $Ba_3[BP_3O_{12}]$, $Pb_3[BP_3O_{12}]$, $Sr_3[BP_3O_{12}]$ are summarized in Table 3.19 and 3.20 respectively.

Table 3.19 The comparison of cell parameters of $M_2[BP_3O_{12}]$ (M=Cr and Fe).

Parameters	**$Fe_2BP_3O_{12}$ [99]**	**$Cr_2BP_3O_{12}$ [102]**	**$Fe_2BP_3O_{12}$ (This Study)**
a (Å)	8.0881	7.95419(6)	8.002
c (Å)	7.4334	7.36130(1)	74.144
Space Group	P3 (143)	P3 (143)	P3 (143)

Table 3.20 The comparison of cell parameters of $M_3[BP_3O_{12}]$ (M=Ba, Pb and Sr).

Parameters	**$Ba_3[BP_3O_{12}]$**	**$Pb_3[BP_3O_{12}]$**	**$Sr_3[BP_3O_{12}]$**
a (Å)	22.211	69.460	22.25
b (Å)	14.285	14.990	14.32
c (Å)	7.102	21.116	39.393
Space Group	Ibca (No:73)	Pbca (No:61)	Ibca (No:73)

$Fe_2BP_3O_{12}$ was indexed, Table 3.21, in the trigonal system with unit cell parameters of a = 8.002(2) Á, c = 7.4144(5) and space group is P3.

Table 3.21 The X-ray powder diffraction data of Exp.48.

Intensity	**2Th(obs.)**	**2Th(Calc.)**	**d**	**h**	**k**	**l**
38	12.730	12.639	6.948	0	1	0
8	17.400	17.400	5.092	0	1	1
31	21.990	21.982	4.038	1	1	0
5	23.960	23.952	3.711	0	0	2
100	25.120	25.073	3.542	1	1	1
38	27.180	27.170	3.278	0	1	2
20	28.140	28.171	3.168	0	2	1
45	32.750	32.734	2.732	1	1	2
11	33.830	33.863	2.647	1	2	0
18	35.250	35.219	2.544	0	2	2
6	36.350	36.270	2.469	0	0	3
15	38.600	38.565	2.330	0	3	0
11	40.460	40.503	2.227	0	3	1
6	42.780	42.816	2.112	1	1	3
14	44.860	44.830	2.018	2	2	0
5	46.500	46.554	1.951	2	2	1
8	49.070	49.039	1.855	0	0	4
14	50.400	50.461	1.809	1	2	3
13	52.090	52.246	1.754	0	4	0
6	53.860	53.975	1.701	0	3	3
3	59.020	58.973	1.563	2	2	3
18	60.950	60.928	1.518	1	2	4

3.11 Al-B-P-O-H CONTAINING COMPOUND

Actually, our purpose was to synthesize the titled compound of $Al(H_2O)_2[BP_2O_8].H_2O$. But products of experiment were completely different as it is given in Table 3.22. If we could success on this synthesis, it would be the first Aluminum borophosphate compound with microporous structure.

Table 3.22 Products of Exp.56.

Exp. No	Product
56	$BPO_4 + NH_4AlP_2O_7$

The XRD powder pattern of product (Figure 3.29) matches very well with BPO_4 (JCPDS Card No: 34-0132) and $NH_4AlP_2O_7$ (JCPDS Card No: 49-0557). The presence of $NH_4AlP_2O_7$ was also proved with FTIR spectra (Figure 3.30); NH_4^+ (υ= 1414 cm^{-1}, 3170 cm^{-1}), P_2O_7 (υ=740 cm^{-1}). In addition to these observations, the presence of Al in the product was also confirmed qualitatively.

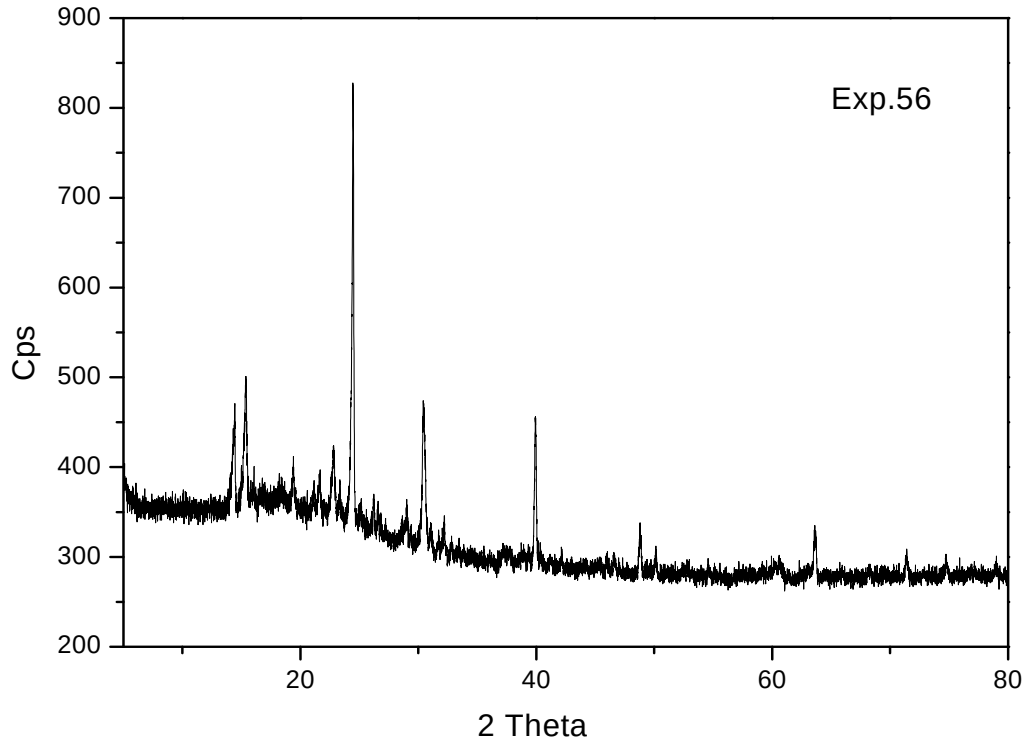

Figure 3.29 The XRD powder pattern of the product of Exp.56.

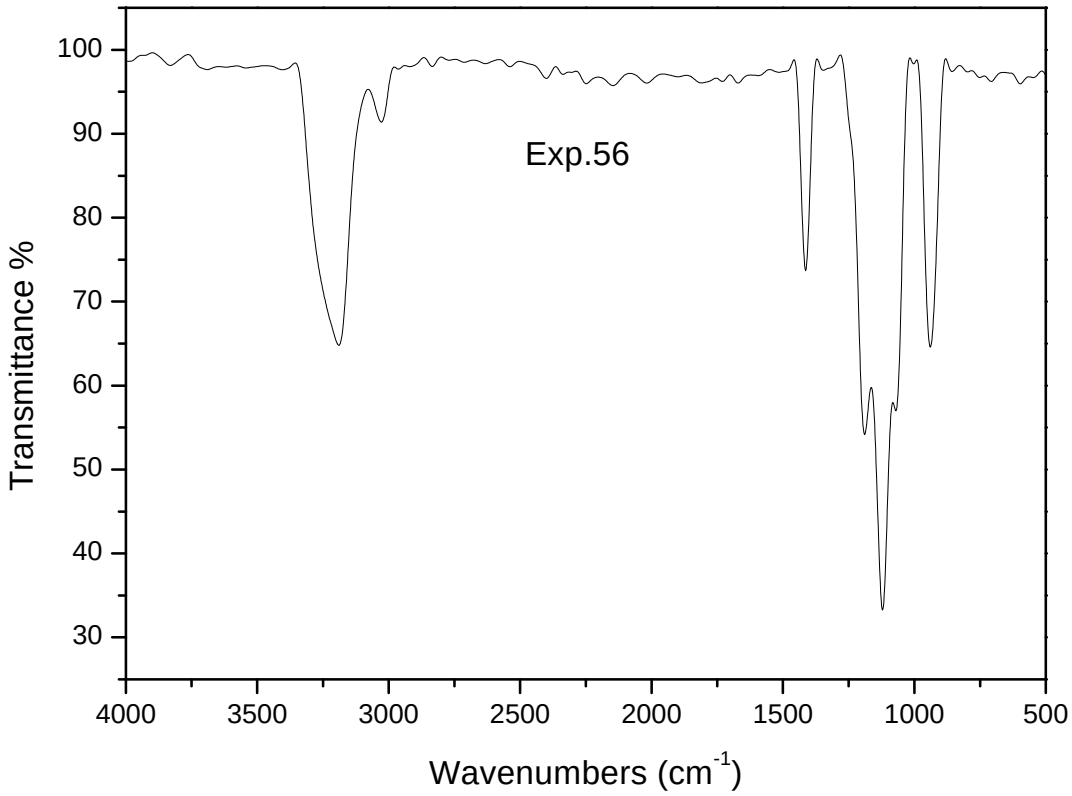

Figure 3.30 The FTIR spectrum of the product of Exp.56.

3.12 Al–As–B–O-H CONTAINING COMPOUND

The results of the Exp. 65a, 65b, 65b.1 are summarized in Table 3.23. The products of Exp. 65a, 65b, 65b.1 were highly crystalline and the new compound containing minor amount of $Al_2(OOH)_2$ (JCPDS Card No: 05-0190).

Table 3.23 Products of Exp.65, 65a, 65b, 65b.1, 65c, 65d, 65e, 65f.

Exp. No	Product
65a	New Compound
65b	New Compound
65b.1	New Compound

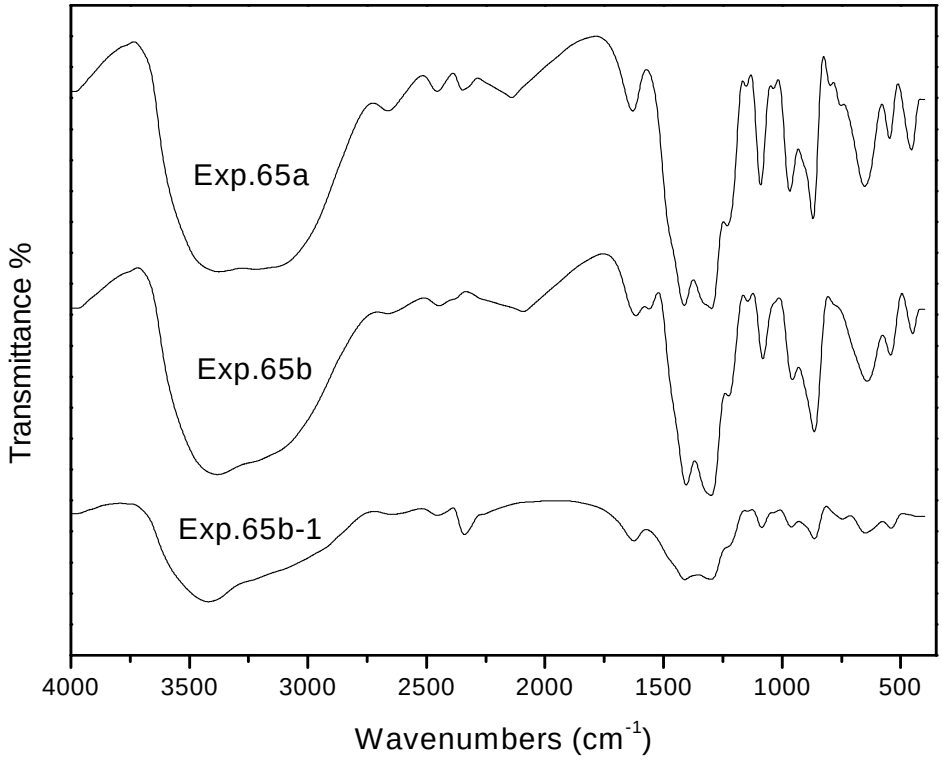

Figure 3.31 The comparison of FTIR spectra of the products of Exp.65a, 65b, 65b.1.

Figure 3.31 gives the FTIR spectrum of the products of the same experiments. The FTIR studies exhibit the presence of water and the lack of hydroxyl bands are common in most of the hydrothermally synthesized boroarsenate compounds. A large number of bands observed in the region 1300-400 cm^{-1} where B-O, As-O stretching and bending modes are expected. Bands of AsO_4^{-3} are given in Table 3.24.

Table 3.24 Vibrational spectra of AsO_4^{3-}.

Vibrational Spectra of AsO_4^{3-} [36-37]
υ_1 = 818 (A_1) - 858
υ_3 = 786 (F-stretching) - 744
υ_4 = 405 (F-bending)
υ_2 = 350 (E)

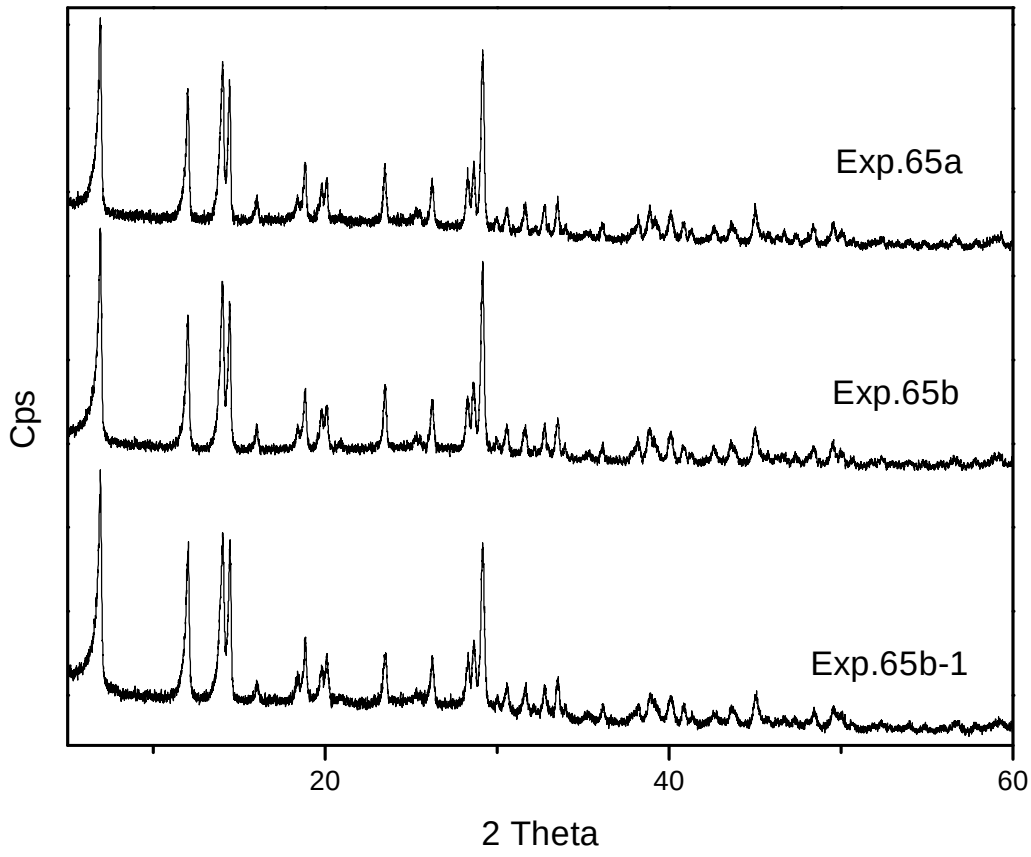

Figure 3.32 The comparison of XRD powder patterns of the products of Exp.65a, 65b, 65b.1.

The X-ray powder diffraction pattern of the products of Experiment 65a, 65b and 65b.1 are given in Figure 3.32. The crystals are very small to do single crystal structural analysis. The lines of powder X-ray diffraction data do not match with the any known Al, B, As, Cl and O containing compounds.

As it is seen in Figure 3.31 and Figure 3.32, the product of Experiment 65a, 65b and 65b.1 are exactly the same. The results of ICP analysis of products of Exp. 65a are summarized in Table 3.25. In order to perform ICP analysis the sample was dissolved in aqua regia.

Table 3.25 ICP analysis results of the products of Exp.65a.

Aluminium %	**Boron %**	**Arsenic %**
11.83	7.54	10.75

3.13 K–P–B–O CONTAINING COMPOUND

3.13.1 Hydrothermal Synthesis

In this study $K_5B_2P_3O_{13}$ was tried to be synthesized by hydrothermal method as explained in section 2.3.14.1. According to the investigations that were done for the products of Exp.67 and Exp.67a, it was proved that the structure of the products was not in the form of target compound. The products are listed in Table 3.26.

Table 3.26 Products of Exp.67, 67a.

Exp. No	Product
67	BPO_4 + $K_3H_5(P_2O_7)_2$ (JCPDS card No: 25-0638)
67a	BPO_4 + $K_3H_5(P_2O_7)_2$ (JCPDS card No: 25-0638)

The XRD powder patterns and FTIR spectra of Exp.67 and 67a are compared in Figure 3.33 and Figure 3.34 respectively.

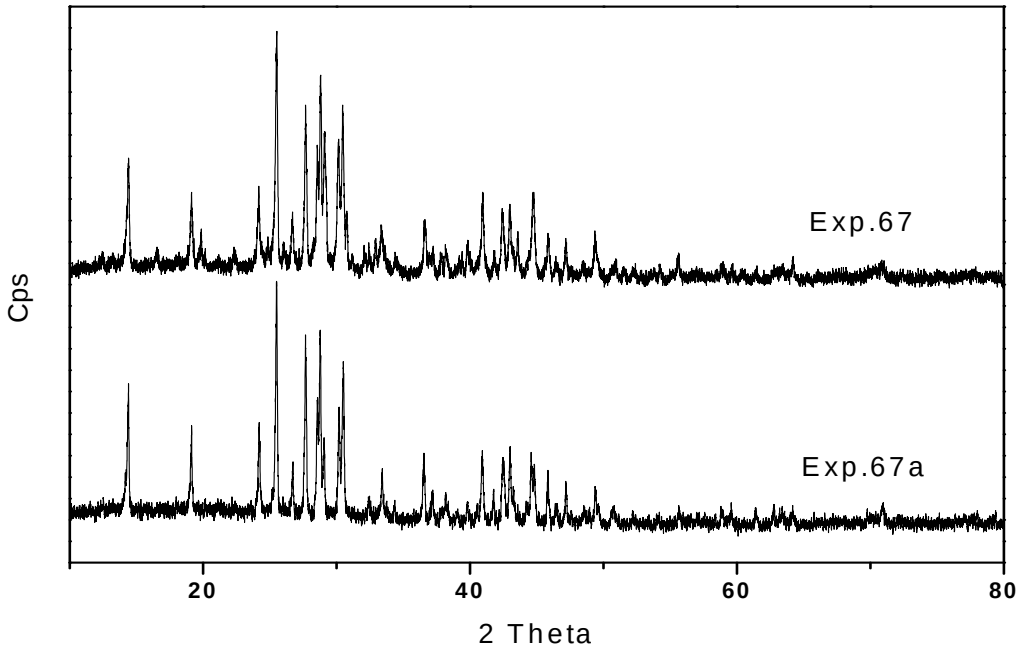

Figure 3.33 The comparison of XRD powder patterns of the products of Exp.67, 67a.

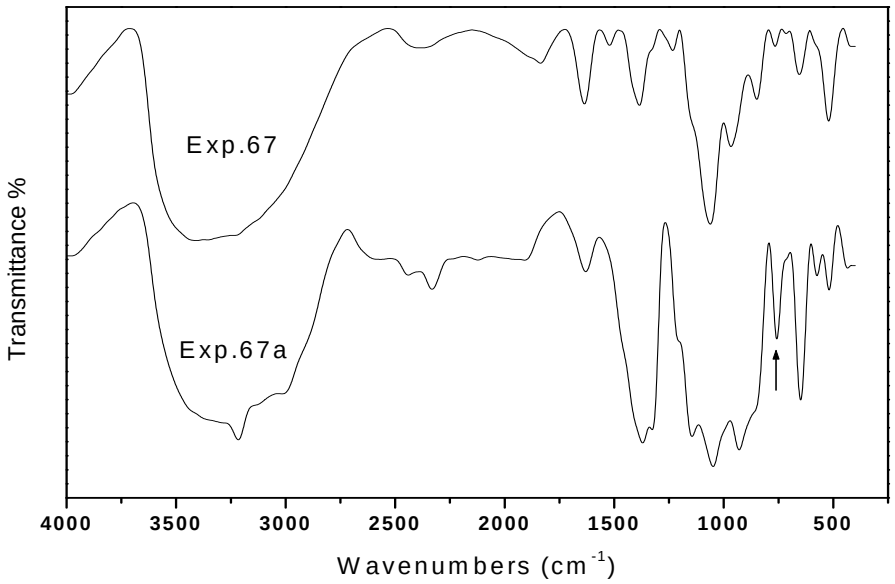

Figure 3.34 The comparison of FTIR spectra of the products of Exp.67, 67a. The peak denoted by an arrow corresponds to $(P_2O_7)^{-4}$.

3.13.2 Solid State Synthesis

In this study $K_5B_2P_3O_{13}$ was tried to be synthesized by solid state method as explained in section 2.3.14.2. But the synthesis of $K_5B_2P_3O_{13}$ was failed, the obtained product was identified as KPO_3 (JCPDS Card No: 35-0819) according to its XRD powder pattern (Figure 3.35).

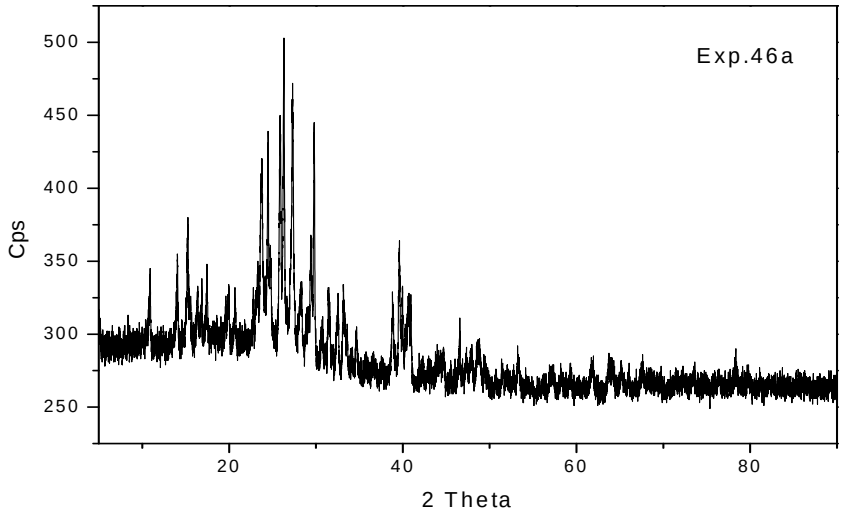

Figure 3.35 The XRD powder pattern of the product of Exp.46a.

3.14 Na–As–B–O-H CONTAINING COMPOUND

3.14.1 Hydrothermal Synthesis

The synthesis of $Na_5(B_2As_3O_{13})$ was tried hydrothermally by using the chemicals $NaBO_2.4H_2O$, $Na_2HAsO_4.7H_2O$ and As_2O_5 as given in section 2.3.15.1. The XRD analysis for these products were also failed. The XRD pattern given in Figure 3.37 do not matched with any known Na-As-O-B-H containing compound (Table 3.27). Due to the lack of single crystal product for these experiments, only possible way to identify the crystal structure is Rietveld analysis. This process is continuing.

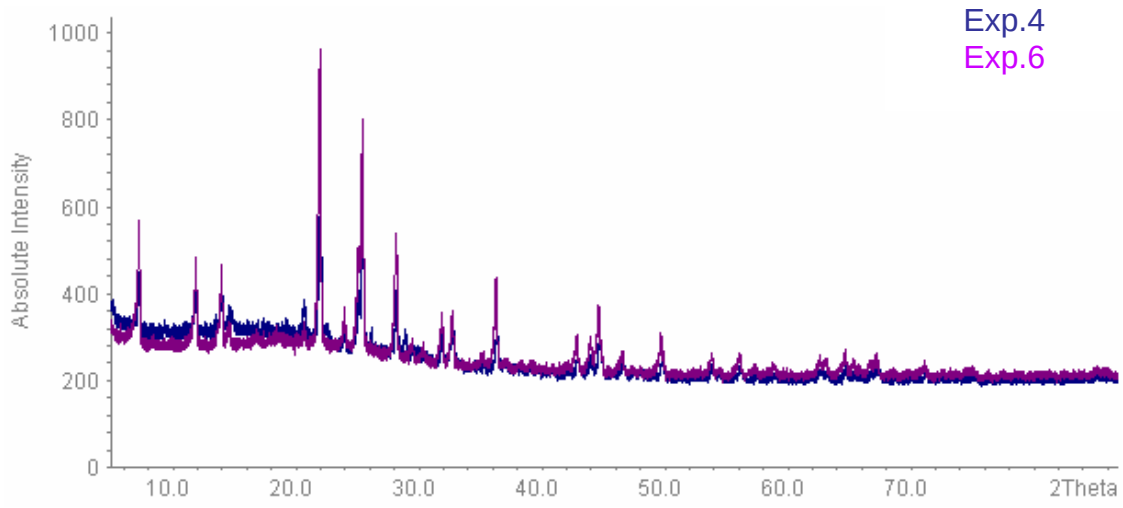

Figure 3.36 The comparison of XRD powder pattern of the products of Exp.4, 6.

Table 3.27 Products of Exp.4 and 6.

Exp. No	Product
4	New Compound
6	New Compound

The FTIR spectra of products (Figure 3.37) were found to be in good agreement with the bands of AsO_4^{-3}, B-O-As, and BO_4 groups given in the literature. The weak band at 1211 cm^{-1} is characteristic peak of tetrahedral BO_4 (850 -1200 cm^{-1}) and the band at 948 cm^{-1} is assigned to B-O-As asymmetric and symmetric vibrations [103]. And the characteristic band of tetrahedral AsO_4 (υ_s, υ_{as}) are at 800 cm^{-1}. Other bands

around 1640, 3450 cm^{-1} are the OH vibrations of absorbed water and H-bond between H_2O and AsO_4^{-3}.

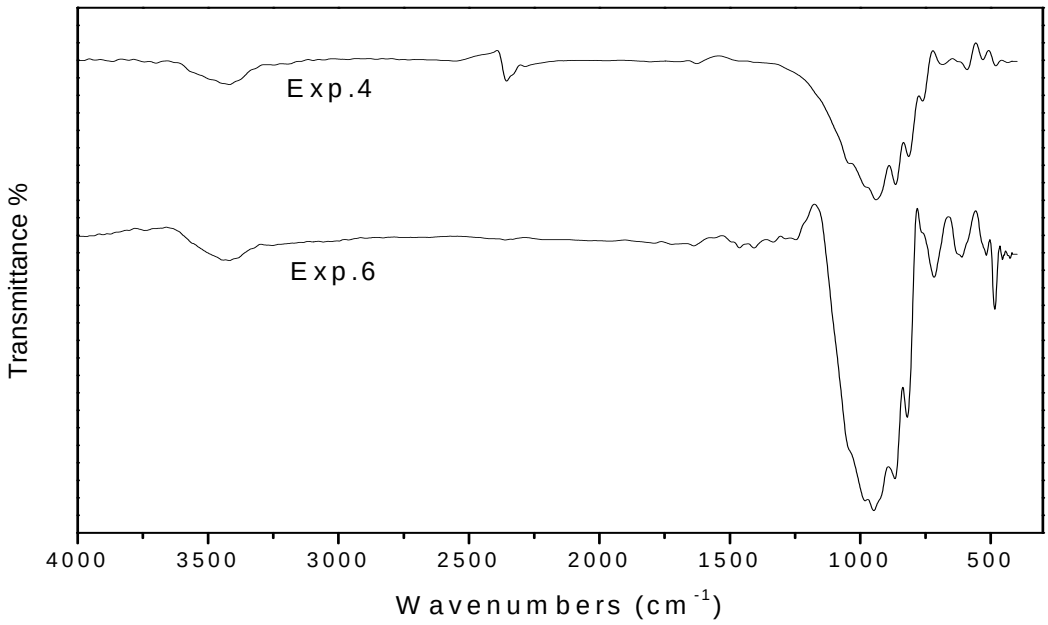

Figure 3.37 The comparison of FTIR spectra of the products of Exp.4, 6.

3.14.2 Microwave-Assisted Synthesis

The XRD pattern of Exp.2 given in Figure 3.38 is exactly the same with the XRD pattern of Exp.4 and 6. The only difference between them is the low crystallinity of Exp.2. This showed that annealing must be done for the product of Exp.2 for the exact formation of crystal. At the same time their FTIR spectra (Figure 3.37 and Figure 3.39) are also matching to each other. As a result same unknown compound was obtained both by hydrothermal and microwave methods.

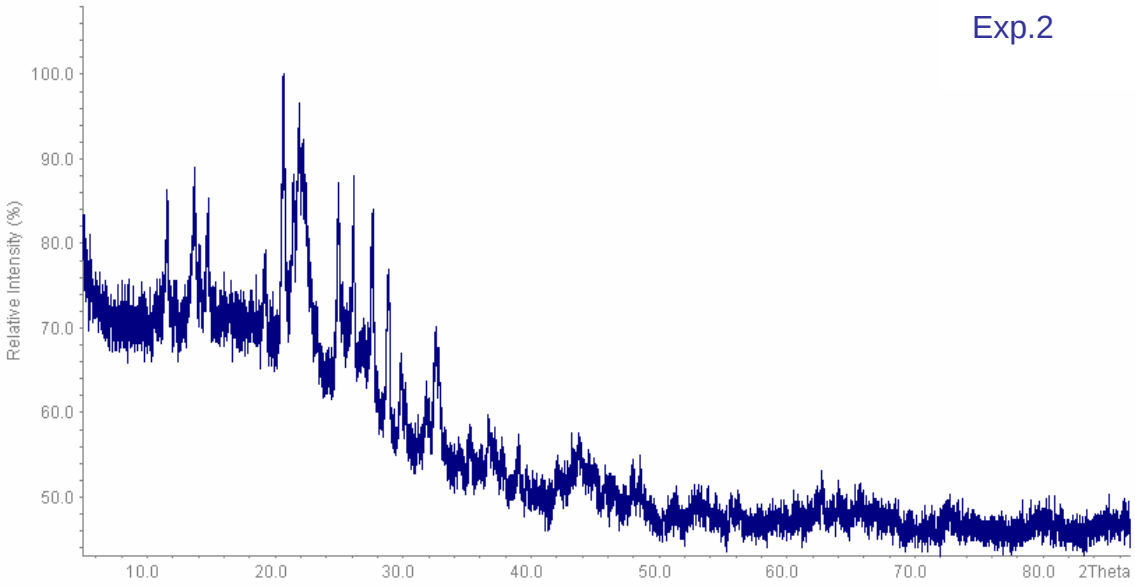

Figure 3.38 The XRD powder pattern of the product of Exp.2.

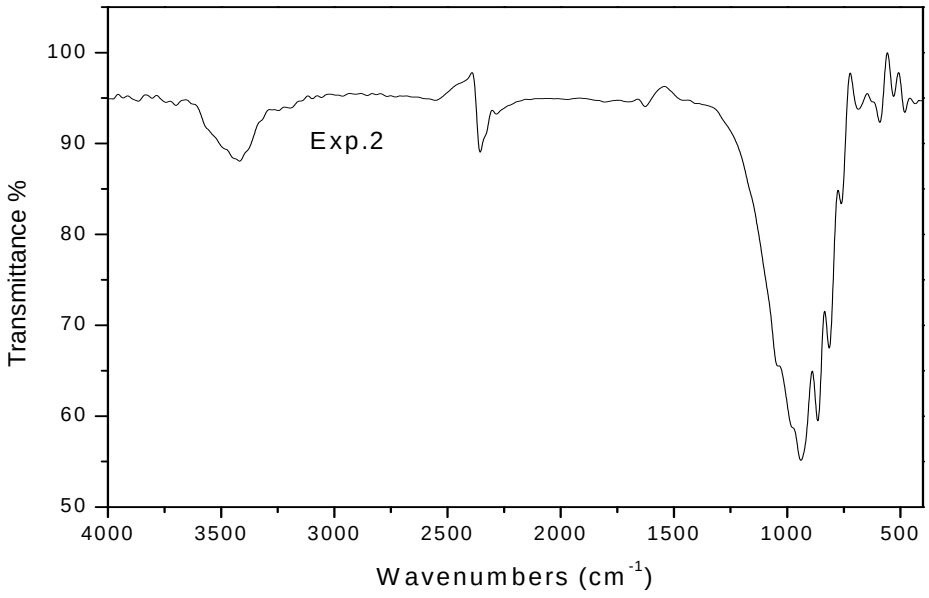

Figure 3.39 The FTIR spectrum of the product of Exp.2.

CHAPTER 4

CONCLUSION

In this work several borophosphate compounds which contain BO_3, BO_4 and PO_4 complex anionic structures were synthesized by a) solid state reactions, b) hydrothermal methods, c) micro-wave assisted synthesis and identified.

a) Solid State Reactions

As a part of systematic investigation of borophosphate structures of transition metal, first some of the known compounds were prepared using the conventional and the new solid state methods such as $Fe_2[BP_3O_{12}]$. An X-ray powder diffraction analysis was undertaken. The unit cell parameters are refined and compared with the previous data if available.

In addition the functional complex anions such as BO_3, BO_4 and PO_4 in the form of isolated triangle, unbranched, loop branched or open branched chains are investigated by IR spectroscopy.

b) Hydrothermal Reactions

A new borophosphate compound with the composition $(NH_4)_xMn_{((3-x)/2)}(H_2O)_2[BP_2O_8].(1-x)H_2O$ was prepared under mild hydrothermal conditions and characterized by X-ray powder diffraction (XRD) and Fourier Transform Infrared Spectroscopy (FTIR) methods. The title compound was synthesized from $MnCl_2.2H_2O$, H_3BO_3, $(NH_4)_2HPO_4$ with variable molar ratios by heating at 180 ^oC for 7 days in an autoclave. The X-ray diffraction data of water insoluble polycrystalline powder was indexed by TREOR program in hexagonal system with the unit cell parameters of a = 9.5104, c = 15.7108 Å, Z = 6 and the space group $P6_5$ (No.176). $(NH_4)_xMn_{((3-x)/2)}(H_2O)_2[BP_2O_8].(1-x)H_2O$ is isostructural with $(NH_4)_xM^{II}_{((3-x)/2)}(H_2O)_2[BP_2O_8].(1-x)H_2O$ (M^{II} = Co, Cd, Mg; x = 0.5-1). Its unit cell parameters and hkl values were in

good agreement with the other isostructural compounds. This is the first report presenting on the synthesis details and indexed X-ray powder diffraction pattern of this compound as well as analysis results using several techniques as FTIR, TGA (Thermal Gravimetric Analysis), SEM (Scanning Electron Microscopy) and EPR (Electron Paramagnetic Resonance).

$(NH_4)_xCo_{(3-x)/2)}(H_2O)_2(BP_2O_8)(1-x)H_2O$ (x=0.5) was also synthesized by hydrothermal method. For this synthesis, HNO_3 and H_3PO_4 are used respectively. The powder XRD data of the product was indexed by Checkcell program in the hexagonal crystal system with the unit cell parameters a = 9.4920(±2), c= 15.5820(±3). This titled compound was synthesized before by Schafer et.al. in 2001 as single crystal. In order to check the reproducibility of the product, two additional experiments were done. SEM analysis showed that both $(NH_4)_xCo_{(3-x)/2)}(H_2O)_2(BP_2O_8).(1-x)H_2O$ and $(NH_4)_xMn_{((3-x)/2)}(H_2O)_2[BP_2O_8].(1-x)H_2O$ where x=0.5, have the hexagonal shape.

Open framework $(H)_{0.5}Co_{1.25}(H_2O)_{1.5}[BP_2O_8].H_2O$ compound was synthesized hydrothermally by using the chemical compounds; $CoCl_2.6H_2O$, H_3BO_3, $(NH_4)_2HPO_4$. The structure of compound was characterized by X-ray powder diffractometer. The compound is in the hexagonal crystal system, and its unit cell parameters are a = 9.4960(6) Å, c = 15.6230(13) Å, Z=1. FTIR spectroscopy was also used for characterization. Stretching and bending frequencies of B-O and P-O groups are observed up to 1400 cm^{-1} and the band around 3500 cm^{-1} was assigned as O-H stretching mode.

$NH_4Fe(III)[BP_2O_8(OH)]$ was synthesized in this study. Compound represents new members of the hydrated phosphate rich borophosphates. Characteristic structural features are infinite one dimensional branched anions consisting of alternating corner sharing tetrahedral $BO_3(OH)$ borate and PO_4 phosphate groups with an additional branched phosphate group linked to the borate tetrahedron. Octhahedrally coordinated transition metal ions connect the anionic chains. Moreover, ammonium ions or alkali ions occupy interchain cavities.

New Al–As–B–O containing compound was also synthesized with unknown composition. Unfortunately it was not possible to solve the crystal structure of this

compound in the powder form. Attempt on the synthesis of single crystal of this compound is going on.

$NaM(H_2O)_2[BAs_2O_8].H_2O$ where M = Mn, Co, Zn was tried to be synthesized in this study. The powder patterns of obtained products indicate that the structures are not identical with the compound $NaMg(H_2O)_2[BP_2O_8].H_2O$ that had already been synthesized before. Crystal investigation of Na–M-As–B–O containing compound where M = Mn, Co, Zn haven't completed yet. According to the FTIR spectrum the presence of AsO_4^{-3} and BO_3 units were confirmed.

c) Microwave Assisted Reactions

$Na_5(B_2As_3O_{13})$ was proposed to be synthesized with microwave-assisted method by using $NaBO_2.4H_2O$, As_2O_5 and $Na_2HAsO_4.7H_2O$ according to the following chemical reaction;

$$4NaBO_2.4H_2O\,(s) + 3/2As_2O_5\,(s) + 3Na_2HAsO_4.7H_2O\,(s) \longrightarrow 2Na_5(B_2As_3O_{13})\,(s) + 77/2\,H_2O(g)$$

An unknown compound was obtained but its X-ray powder diffraction data could not be indexed. Its IR data suggested that the structure is composed of AsO_4 and BO_4 tetrahedra alternatively.

REFERENCES

[1] E. L. Muetterties, The Chemistry of Boron and Its Compounds, John Wiley publ., New York, 1967.

[2] J. D. Lee, Concice Inorganic Chemistry, Blackwell Publishing Limited, 1999.

[3] http://134.68.135.1/jitt/sampler/chemistry/goodfors/goodforBNCT.html.

[4] P. A. Cox, The Elements On Earth, Oxford University Press, New York, 1995.

[5] A. F. Wells, Structural Inorganic Chemistry, Oxford, Clarendon Press, 1975.

[6] K. Byrappa, D. Y. Pushcharovky, Prog. Cryst. Grow. Charact., 24, 1992, 269.

[7] R. Kniep, H. Engelhardt, C. Hauf, Chem. Mater., 10, 1998, 2930.

[8] C. J. Duan, W. F. Li, X. Y. Wu, H. H. Chen, X. X. Yang, J. T. Zhao, J. Lumin., 117, 2006, 83.

[9] M. Kritikos, E. Wikstad, K. Wallden, Sol. Stat. Scien., 3, 2001, 649.

[10] Y. Shi, J. Liang, H. Zhang, J. Yang, W. Zhuang, G. Rao, J. Sol. Stat. Chem., 129, 1997, 45.

[11] S. C. Sevov, Angew. Chem. Int. Ed., 35, 1996, 2630.

[12] R. Bontchev, J. Do, A. J. Jacobson, Inorg. Chem., 38, 1999, 2231.

[13] R. Bontchev, J. Do, A. J. Jacobson, Angew. Chem. Int. Ed., 38, 1999, 1937.

[14] A. Yilmaz, L. Tatar Yildirim, X. Bu, M. Kizilyalli, G. D. Stucky, Cryst. Res. Technol., 40(6), 2005, 579.

[15] M. H. Ge, W. Lei, H. H. Chen, M. R. Li, X. X. Yang, J. T. Zhao, Z. Anorg. Allg. Chem., 631, 2005, 1213.

[16] G. Schafer, W. Carillo-Caberra, W. Schenelle, H. Borrmann, R. Kniep, Z. Anorg. Allg. Chem., 628, 2002, 289.

[17] M. H. Ge, J. X. Mi, Y. X. Huang, J. T. Zhao, R. Kniep, Z. Kristallogr. NCS, 218, 2003, 273.

[18] D. Y. Pushcharovsky, E. R. Gobetchia, M. Pasero, S. Merlino, O. V. Dimitrova, J. Alloys Compd., 339, 2002, 70.

[19] A. Baykal, G. Gözel, M. Kızılyallı, M. Toprak, R. Kniep, Turk J. Chem., 24, 2000, 381.

[20] M. Li, W. Liu, M. Ge, H. Chen, X. Yang, J. Zhao, Chem. Commun., 11, 2004, 1272-1273.

[21] S. Sao, M. Hasegawa, T. Sodesawa, F. Nozake, Bull. Chem. Soc. Jpn., 64, 1991, 516.

[22] K. Ahmed, C. Geisert, L. Vac. Sci. Technol. A, 10(2), 1992, 313.

[23] S. Imamura, K. Imakuba, S. Furuyoshi, H. Jindai, Ind. Eng. Chem. Res., 30, 1991, 2355.

[24] R. P. Bontchev, S. C. Sevov, Inorg. Chem., 35, 1996, 6910.

[25] S. C. Sevov, Angew. Chem., Int. Ed. Engl., 35, 1996, 3641.

[26] C. Hauf, R. Kniep, Z. Kristallogr. NCS, 212, 1997, 313.

[27] R. P. Bontchev, J. Do, A. J. Jacobson, Angew. Chem. Int. Ed., 38, 1999, 1937.

[28] R. Kniep, G. Schäfer, H. Engelhardt, I. Boy, Angew. Chem. Int. Ed., 38, 1999, 3641.

[29] R. P. Bontchev, J. Do, A. J. Jacobson, Inorg. Chem., 39, 2000, 4179.

[30] J. Do, A. J. Jacobson, Chem. Mater., 13, 2001, 2436.

[31] G. Y. Yang, S. C. Sevov, Inorg. Chem., 13, 2001, 2436.

[32] I. Boy, F. Stowasser, G. Schäfer, R. Kniep, Chem. Eur. J., 7, 2001, 834.

[33] G. Schäfer, H. Borrmann, R. Kniep, Micropor. Mesopor. Mater., 41, 2002, 161.

[34] Y. X. Huang, G. Schäfer, H. Borrmann, J. T. Zhao, R. Kniep, Z. Anorg. Allg. Chem, 629, 2003, 3.

[35] S. M. J. Zaidi, Electrochimica Acta, 50, 2005, 4771-4777.

[36] S. C. B. Myneni, S. J. Traina, G. A. Waychunas, T. J. Logan, Geochim. Cosmochim. Acta, 62(19/20), 1998, 3285-3300.

[37] S. C. B. Myneni, S. J. Traina, G. A. Waychunas, T. J. Logan, Geochim. Cosmochim. Acta, 62(21/22), 1998, 3499-3514.

[38] http://en.wikipedia.org/wiki/Chromated_copper_arsenate.

[39] http://gsa.confex.com/gsa/2002AM/finalprogram/abstract_38997.htm.

[40] Pollution Prevention and Abatement Handbook World Bank Group Effective, July 1998.

[41] A. K. Cheetham, G. Férey, T. Loiseau, Angew. Chem., 1999, 111, 3466; Angew. Chem. Int. Ed. 1999, 38, 3269.

[42] R. Rajic, N. J. Serb, Chem. Soc., 2005, 70, 371.

[43] T. Wakihara, T. Okubo, Chem. Lett., 2005, 34, 276.

[44] N. Guillou, Q. Gao, P. M. Forster, J. S. Chang, M. Nogues, S. E. Park, G. Ferey, A. K. Cheetham, Angew. Chem. Int. Ed., 2001, 40, 2831.

[45] P. F. Henry, M. T. Weller, R. W. Hughes, Inorg Chem., 2000, 39, 5420.

[46] A. M. Healy, M. T. Weller, Inorg. Chem., 38, 1999, 455.

[47] R. W. Hughes, L. A. Gerrard, D. J. Price, M. T. Weller, Inorg. Chem., 42, 2003, 4160.

[48] J. L. C. Rowsell, N. J. Taylor, L. F. Nazar, J. Am. Chem. Soc., 2002, 124, 6522.

[49] I. D. Williams, M. Wu, H. H. Y. Sung, X. X. Zhang, J. Yu, Chem. Commun., 1998, 2463.

[50] J. Ju, T. Yang, G. Li, F. Liao, Y. Wang, L. You, J. Lin, Chem. Eur. J., 2004, 10, 3901.

[51] J. Haines, O. Cambon, R. Astier, P. Fertey, C. Chateau, Z. Krystallogr., 219, 2004, 32.

[52] C. H. Park, K. Bluhm, Z. Naturforsch., 1997, 52b, 102.

[53] P. B. Moore, S. S. Ghose, Am. Mineral., 56, 1971, 1527.

[54] R. Kniep, G. Gözel, B. Eisenmann, C. Röhr, M. Asbrand, M. Kizilyalli, Angew. Chem. Int. Ed. Engl., 34, 1994, 749.

[55] S. C. Sevov, Angew. Chem., 1996, 108, 2814.

[56] S. B. Wiggin, M. T. Weller, J. Am. Chem. Soc., 127(49), 2005, 17172.

[57] M. Rozman, M. Drofenik, J.Am. Chem.Soc., 78, 1995, 2449.

[58] G. B. Ji, S. L. Tang, S. K. Ren, F. M. Zhang, B. X. Gu, Y. W. Du, J. Cryst Growth, 270, 2004, 156.

[59] R. A. Laudise, Chem. Engineer. News, 9, 1987, 30.

[60] W. J. Dawson, Ceram. Bulletin, 67(10), 1988, 1673.

[61] P. Lidström, J. Tierney, B. Wathey, J. Westman, Tetrahedron, 57, 2001, 9225.

[62] D. D. Vosaic, D. R. Stojakovic, Mater. Res. Bull., 32, 1997, 779.

[63] B. Vaidhyanathan, K. J. Rao, J. Solid State Chem., 132, 1997, 349.

[64] H. Guler, F. Kurtuluş, J. Mater. Science, 40, 2005, 6565.

[65] J. Rao, B. Vaidhyanathan, M. Ganguli, P. A. Ramakrishnan, Chem. Mater., 11, 1999, 882.

[66] D. M. P. Mingos and D. R. Baghurst, Chem. Soc. Rev. 20**,** 1991, 1-48.

[67] A. Baykal, A. Evren, Turk J. Chem., 30, 2006, 723-730.

[68] R. Roy, S. Komarneni, L. J.Yang, J. Am. Cer. Soc. 68**,** 1985**,** 392-396.

[69] C. Hauf, A. Yılmaz, M. Kızılyallı and R. Kniep, J. Solid State Chem. 140, 1998, 154-156.

[70] A. Baykal, M. Kızılyallı, M.Toprak, R. Kniep, Turk. J. Chem. 25, 2001, 425-432.

[71] T. Seip, E. E. Carpenter, C.J. O'Conner, V.T. John, S. Li, IEE Trans. Magn. 34, 1998, 111.

[72] R. West, Basic Solid State Chemistry, Wiley Publ., New York, 1999.

[73] U. Scubert, N. Hüsing, Synthesis of Inorganic Materials, Wiley Publ., New York, 2005.

[74] J. Rouquerol, D. Avnir, C. W. Fairbridge, D. H. Everett, J. H. Haynes, N. Pernicone, J. D. F. Ramsay, K. S. W. Sing and K. K. Unger, Pure Appl. Chem. 66, 1994, 1739.

[75] B. McCusker, F. Liebau, G. Engelhardt, Pure Appl. Chem., 73, 2001, 381.

[76] T. J. Barton, L. M. Bull, W. G. Klemperer, D. A. Loy, B. McEnaney, M. Misono, P. A. Monson, G. Pez, B. Scherer, J. C. Vartuli, O. M. Yaghi, Chem. Mater., 11, 1999, 2633.

[77] J. Weitkamp, Solid State Ionics, 131, 2000, 175.

[78] J. V. Smith, Zeolites, 4, 1984, 309.

[79] P. Yang, The Chemistry of Nanostructured Materials, World Scientific Publ., London, 2003, 1-10.

[80] http://www.gracedavison.com/eusilica/Adsorbents/product/zeolite_molecular_sieve.htm.

[81] A. Yılmaz, Synthesis and Characterizations of Alkaline, Alkaline Earth and Transition Metal Borophosphates Compounds, D. Thesis, The Middle East Technical University, Ankara, 2000.

[82] Z. Logar, L. Golič, V. Kaučič, Croatica Chemica Acta, 72 (2-3), 1999, 187.

[83] S. Borman, R. Dagani, R. L. Rawls, P. S. Zurer, Chemical & Engineering News, January 12, 1998.

[84] S. H. Park, P. Daniels, -H. Gies, Microporous Mater., 37, 2000, 129.

[85] Q. Song, Size And Shape Controlled Synthesis And Superparamagnetic Properties Of Spinel Ferrites Nanocrystals, Ph.D. Thesis, Georgia Institute of Technology, Georgia, 2005

[86] F. Settle, Handbook of Instrumental Techniques for Analytical Chemistry, Prentice Hall PTR, 1997, New Jersoy.

[87] Y. Huang, G. Schafer, W. Carillo-Cabrera, R. Cardoso, W. Schenelle, J. Zhao, R. Kniep, Chem. Mater. 13 (2001) 4348;

[88] W. H. Flanke, T. E. Whyte, Perspectives in Molecular Sieve Science, American Chemical Society, Washington, 1998.

[89] A. Baykal, M. Kızılyallı, J. Mater. Science, 35, 2000, 4621-6426.

[90] W. E. Klee, G. Engel, J. Inorg. Nucl. Chem., 32, 1970, 1837-1843.

[91] K. Nakamoto, Infrared Spectra of Inorganic and Coordination Compounds, Plenum Press, New York, 1971.

[92] S. D. Ross, Inorganic Infrared and Raman Spectra, McGraw-Hill Press, London, 1972.

[93] A. Baykal, M. Kizilyalli, Turk. J. Chem., 21(4), 1997, 394-400.

[94] G. J. Hutchings, I. D. Hudson, D. G. Timms, J. Chem. Soc. Chem. Communic., 23, 1994, 2717-2718.

[95] J. C. Vedrine, F. Delennay (Ed.), Characterization of Heterogeneous Catalysts, Dekker, New York, 1994.

[96] W. S. Kijlstra, E. K. Poels, A. Bliek, B. M. Weckhuysen, R. A. Schoonheyd, J. Phys. Chem. B, 101, 1997, 309-316.

[97] Y. Köseoğlu, F. Yıldız, J. V. Yakhmi, J. Qin, X. Chen, B. Aktas, J. Magn. Magn. Mater. 416-418, 2003, 258-259.

[98] A. Baykal, in PhD Thesis, Middle East Technical University, Ankara, 1999.

[99] S. Tuncel, M. Thesis, Middle East Technical University, Ankara, 2004.

[100] G. Gözel, A. Baykal, M. Kızılyallı, R. Kniep, J. Europ. Ceramic Soc., 18, 1998, 2241-2246.

[101] H. Park, K. Bluhm, Z. Naturforsch., 50B, 1995, 1617.

[102] J. X. Mi, J. T. Zhao, S. Y. Mao, Y. X. Huang, H. Engelhardt, R. Kniep, Z. Kristallogr. NCS 215, 2001, 201-202.

[103] R. A. Nyquist, R. O. Keyel, Infrared Spectra of Inorganic Compounds, Chemical Physics Research Laboratory, The Dow Chemical Company Midland, Michigan, Academic Press, New York and London, 1971.